

THESIS FOR THE DEGREE OF DOCTOR OF PHILOSOPHY

Environmentally friendly approaches for recycling of CIGS solar cells

IOANNA TEKNETZI

Department of Chemistry and Chemical Engineering

CHALMERS UNIVERSITY OF TECHNOLOGY

Gothenburg, Sweden 2025

Environmentally friendly approaches for recycling of CIGS solar cells
IOANNA TEKNETZI

© Ioanna Teknetzi, 2025.
ISBN: 978-91-8103-196-6

Doktorsavhandlingar vid Chalmers Tekniska Högskola
Ny serie nr: 5654
ISSN: 0346-718X
Nuclear Chemistry and Industrial Materials Recycling
Department of Chemistry and Chemical Engineering
Chalmers University of Technology
SE-412 96 Gothenburg, Sweden
Telephone + 46 (0)76-230 4609

Cover:
Developed process for complete separation and recovery of valuable materials from CIGS solar cells

Printed by:
Chalmers Digitaltryck
Gothenburg, Sweden 2025

Environmentally friendly approaches for recycling of CIGS solar cells

IOANNA TEKNETZI

Industrial Materials Recycling
Department of Chemistry and Chemical Engineering
Chalmers University of Technology

Abstract

The expected huge increase in photovoltaics (PV) deployment is going to be accompanied by a considerable volume of PV waste. Recycling of this waste is still at a primitive stage though. Among the current PV types, the Copper Indium Gallium diSelenide (CIGS) thin-film technology can achieve high energy conversion efficiencies, while consuming small amounts of materials. However, the presence of critical, precious and toxic elements in this PV technology demands its waste to receive proper treatment, in order to address resource scarcity, safety and economic issues. The existing limited literature on waste recycling of two of the most important elements present in a CIGS solar cell, namely indium (In) and silver (Ag), suggests their separation from the waste mainly through acid leaching, using high chemicals concentrations and often high temperatures. However, such conditions are not environmentally friendly and can also be costly for the industry. Another challenge in their recycling is the demand for highly selective recovery processes, since only highly pure recovered materials can replace virgin materials. In this work, these issues are addressed by exploring alternative methods for efficient and selective recovery of materials from CIGS solar cells, characterized by low environmental impact, in terms of chemicals and energy consumption. For this purpose, different conditions for Ag and In recovery were tested and two different recovery processes were developed: first, a high efficiency acid leaching of Ag and In and, later, a selective recovery of solid Ag and In-compounds. The prior method achieved a complete leaching of Ag and an about 85 wt% leaching of In in 24 h using 2 M HNO₃. The same leachate proved to be able to be used for at least 10 leaching cycles, without losing its leaching efficiency per cycle for these two metals. However, a considerable amount of many other elements present in the solar cell leached as well. In the latter recycling approach, complete dissolution of Zn and liberation of Indium Tin oxide (ITO) particles were achieved in a first step, using only 0.1 M HNO₃ and low ultrasonic (US) power. In a second step, the Ag grid was recovered, using 0.1 M HNO₃ and high US power. The remaining material was then leached with a solution of pH=11 at 50 °C, with the aim to selectively dissolve Mo and subsequently liberate the CIGS material on top of it. As a result, separate fractions of solid Ag, ITO and CIGS, dissolved Mo (with or without W and Ti) and Zn and the solid stainless-steel substrate were recovered. The developed methods are simple and can be attractive for the recycling industry.

Keywords: Silver, indium, ITO recovery, CIGS recycling, acid leaching, ultrasonic-leaching, alkaline leaching, molybdenum

List of publications and Manuscripts

This thesis is based on the following papers and manuscript:

Paper I

I. Teknetzi, S. Holgersson and B. Ebin, Valuable metal recycling from thin film CIGS solar cells by leaching under mild conditions, *Solar Energy Materials & Solar Cells* 252 (2023) 112178, <https://doi.org/10.1016/j.solmat.2022.112178>

Contribution: Main author and all experimental work and analysis of data.

Paper II

I. Teknetzi, N. Click, S. Holgersson and B. Ebin, An environmentally friendly method for selective recovery of silver and ITO particles from flexible CIGS solar cells, *Sustainable Materials and Technologies* 39 (2024) e00844, <https://doi.org/10.1016/j.susmat.2024.e00844>

Contribution: Main author and all experimental work and analysis of data.

Paper III

I. Teknetzi, H. C. Nguyen and B. Ebin, A simple step-by-step guide to the design and analysis of unreplicated split-plot experiments through a case study on molybdenum recycling from CIGS solar cells, *Applied Sciences* 15(1) (2025) 415, <https://doi.org/10.3390/app15010415>

Contribution: Main author, design and analysis of experiments, supervision of experiments.

Manuscript

I. Teknetzi, H. C. Nguyen, S. Holgersson and B. Ebin, A simple step-by-step guide to the design and analysis of unreplicated split-plot experiments through a case study on molybdenum recycling from CIGS solar cells

Contribution: Main author, part of the experimental work and analysis of all data, supervision of experiments.

Contents

1. Introduction	1
2. Background	3
2.1. Basic information on solar cells and PV technologies	3
2.2. The CIGS solar cell	3
2.3. Current methods for recycling of materials present in CIGS solar cells	4
2.3.1. Commercial recycling methods of CIGS-containing waste	5
2.3.2. Laboratory scale recycling methods of CIGS-containing waste	7
2.3.3. Commercial and laboratory scale recycling of Ag	10
2.3.4. Commercial and laboratory scale recycling of ITO	12
2.4. Issues with the current methods	13
3. Theory	15
3.1. Leaching	15
3.1.1. Chemical equilibrium	15
3.1.2. Thermodynamics	16
3.1.3. Kinetics	17
3.2. Predicted reactions	20
3.2.1. Acid leaching	20
3.2.2. Alkaline leaching	23
3.3. Considerations regarding the processes developed in this work	25
4. Materials and methods	27
4.1. CIGS solar cell samples	27
4.2. Chemicals	27
4.3. Experimental	28
4.3.1. Experimental procedures and setups	29
4.3.1.1. Digestion of the untreated solar cell for characterization purposes	29
4.3.1.2. Acid leaching targeting the dissolution of Ag and In	29
4.3.1.3. US-leaching targeting the recovery of Ag and ITO in solid form	30
4.3.1.4. Alkaline leaching investigating the possibility of direct Mo dissolution	31
4.3.1.5. Split-plot factorial experiments on factors affecting the alkaline leaching of Mo	32
4.3.1.6. Alkaline leaching of Mo targeting the recovery of CIGS in solid form	33

4.3.2. Characterization methods	34
5. Results and Discussion	35
5.1. Characterization of the untreated solar cells	35
5.2. Results and discussion of leaching experiments	38
5.2.1. Results of acid leaching targeting the dissolution of Ag and In.....	38
5.2.1.1. Results of the investigation of different HNO ₃ concentrations and A:L.....	38
5.2.1.2. Results of the experiment using a fresh leaching solution for a second leaching cycle.....	44
5.2.1.3. Results of multiple leaching cycle experiments using the same solution.....	45
5.2.2. Discussion on the results of acid leaching targeting the dissolution of Ag and In	47
5.2.3. Results of US-leaching targeting the recovery of Ag and ITO in solid form.....	52
5.2.3.1. Results for the selection of the optimum US-leaching times	52
5.2.3.2. Results of the highly efficient and selective 2-step US-leaching process	53
5.2.4. Discussion on the results of US-leaching	59
5.2.5. Results of alkaline leaching investigating the possibility of direct Mo dissolution	60
5.2.6. Discussion on the results of alkaline leaching investigating the possibility of direct Mo dissolution.....	61
5.2.7. Results of split-plot factorial experiment on factors affecting the leaching of Mo	62
5.2.8. Discussion on the results of the split-plot factorial on factors affecting the alkaline leaching of Mo.....	66
5.2.9. Results of alkaline leaching targeting the recovery of CIGS in solid form.....	66
5.2.9.1. Composition of unleached CIGS	67
5.2.9.2. Alkaline leaching at pH=11 at 50 °C using only NaOH	67
5.2.9.3. Alkaline leaching at pH=11 at 50 °C using NaOH and sodium tartrate.....	72
5.2.10. Discussion on the results of alkaline leaching targeting the recovery of CIGS in solid form.....	75
6. Conclusions.....	77
7. Future work.....	79
Acknowledgements	81
Reference	83
Appendix.....	93

Abbreviations and definitions

5N	Purity of five nines (99.999%)
A:L	Geometrical surface to liquid ratio
c-Si	Crystalline silicon
CI(G)S	Copper Indium diSelenide with or without Gallium doping
CIGS	Copper Indium Gallium diSelenide
EDS	Energy Dispersive X-ray Spectroscopy
EoL	End of Life
Eq.	Equation
EU	European Union
GW _p	Gigawatt peak (“peak” refers to ideal conditions)
ICP-OES	Inductively Coupled Plasma-Optical Emission Spectroscopy
IEA	International Energy Agency
ITO	Indium Tin Oxide
LCD	Liquid Crystal Displays
MQ	Milli-Q (trademark of Merck company for high purity water)
ORP	Oxidation-Reduction Potential
PCB	Printed Circuit Board(s)
PV	Photovoltaic(s)
R.	Reaction
S:L	Solid to liquid ratio
SC-CPSM	Shrinking Core-Constant Particle Size Model for leaching processes
SCM	Shrinking Core Model for leaching processes
SC-SPM	Shrinking Core-Shrinking Particle Model for leaching processes
SEM	Scanning Electron Microscopy
SP	Sub-plot
SPM	Shrinking Particle Model
SS	Sum of Squares
TCO	Transparent Conductive Oxide
US	Ultrasounds/Ultrasonic
WP	Whole-plot
WEEE	Waste of Electrical and Electronic Equipment
XRD	X-ray Diffraction
Zn(Mg)O	Manganese-doped zinc oxide
Zn(Al)O	Aluminium-doped zinc oxide
Zn(S, O, OH)	Zinc sulphide, oxide, hydroxide or mixed compound

1. Introduction

Solar energy is one of the most important forms of renewable energy today. In 2022, the global electricity generated by solar PV systems reached 1300 TWh, accounting for 4.5% of the total global electricity generation. Alignment with the International Energy Agency's (IEA) "Net Zero Emissions Scenario by 2050" demands this number to increase even more, to about 8300 TWh, in 2030 [1]. Since every product produces some amount of waste, the already considerable installed PV capacity (1.6 TW in 2023 [2]) and its expected tremendous increase are going to be accompanied by an equally considerable amount of waste, produced throughout the whole life cycle of a PV, i.e. manufacturing (e.g. defective PV or process waste), transportation, installation and use (e.g. damaged PV) and, finally, end of life [3, 4]. In European Union (EU), end-of-life (EoL) PV are considered as Waste of Electrical and Electronic Equipment (WEEE) and their disposal is regulated, requiring PV producers to ensure their proper treatment [5], but, outside EU, there are no equally strict regulations yet [3, 6-7]. Given that the lifetime of a PV is about 20-30 years [6], the volume of EoL PV waste is still relatively small [8]. However, the volumes of the other PV waste streams are being produced continuously and are increasing fast.

The PV technology dominant in the market today is the crystalline silicon (c-Si) PV, with a 27.3 % conversion efficiency at cell level and in lab-scale in 2023 [2]. A PV technology with comparably high conversion efficiency (23.4 %) and, at the same time, considerably lower material consumption is the one based on a thin-film semiconductor made of CIGS [2]. The specific technology owes its high efficiency to its inclusion of several valuable and critical materials like Ag, In and Ga [9-10]. Elements which can have toxic effects on human if not treated properly, like Se, are also contained in CIGS solar cells [11]. The CIGS compound may also be used in more modern technologies, like the tandem [12]. Therefore, recycling of CIGS PV waste is of great economic, safety and environmental importance.

The main interest for this thesis was the recycling of Ag and In from CIGS solar cells. The selection of Ag as one of the two elements of interest was due to the high demand in Ag for industrial applications in combination with its low recycling rates. More specifically, in 2022, the global Ag reserves were estimated at 610 ktons [13], while the total global Ag supply was about 28.5 ktons [14]. Only about 18% of this Ag supplied to the market came from recycling activities [14]. Industrial applications of Ag contributed to about 50% of its demand, with only the PV sector demanding about 11% [14], due to the metal's exceptional conductivity [13]. Those numbers, in combination with the expected future surge in PV deployment, the rise of other electronic technologies using Ag and the limited reserves [14], evidently show that there is a high demand for the metal and increasing its recycling rates is important. Regarding In, the element was selected for this study due to its listing in "the critical minerals list" of IEA [9]. Its criticality relates to its great economic importance, as it is used in the electronics industry mainly in the form of ITO in Liquid Crystal Displays (LCD), in combination with abundancy issues, since its global reserves are mainly located in China. In addition, there are challenges

in In production, since it is present in low concentrations in the Earth's crust and a by-product of Zn ore mining mainly [13, 15]. Interestingly, official quantitative estimates of the global In reserves are not available [13]. It is known though that the total global refinery production of In in 2022 was 999 ton [13]. Regarding recycling of In from EoL products, some In from ITO scrap is recycled in Japan and the Republic of Korea, however, there is no official data on the recovered quantities [13].

Currently, commercial scale PV recycling is under development. The existing literature on recycling mainly focuses on lab-scale recycling of the dominant in the market c-Si PV technology [16]. As a result, the recycling of materials coming from other PV technologies, like the CIGS, has greatly been neglected so far. More specifically, the very few research works available on the recycling of CIGS-containing waste, mainly concern the recovery of the constituent elements of the CIGS compound from process waste, like sputtering targets and chamber waste, not from waste CIGS solar cells and cell-containing products. However, the former type of waste is much simpler than the latter, which contains a plethora of different elements and materials. This simpler composition renders the recycling and the achievement of purities of 99.999% (5N), required for semiconductors used in PV manufacturing [17], in case the recovered materials are to be reused in new solar cells, less challenging. The recycling methods proposed so far also have the disadvantage of using rather harsh recovery conditions, with concentrated acids, high temperatures etc, which increase the environmental impact of recycling and may render it too costly for the industry. Thus, exploring more sustainable options is necessary. Knowledge on the recycling of waste coming from the CIGS thin-film PV technology is important not only for the proper treatment of the waste this specific technology produces, but also as a reference for the future treatment of new and developing PV technologies containing materials found in the CIGS thin-film PV technology today. For instance, the tandem solar cell technology can contain a CIGS layer and the heterojunction solar cell technology usually contains ITO and an Ag grid [18-19, 12]. Similarly, development of PV waste management strategies today cannot only ensure the proper treatment of the existing PV waste which are already present in considerable volumes (e.g. process waste), but also guarantee a smooth management of the future EoL PV waste volumes, when they become large enough to consider for treatment.

This PhD thesis explores the possibilities of selective and efficient recovery of materials from CIGS solar cells, with a main focus on Ag and In (however, possible recycling of other metals was also investigated), using mild recovery conditions. Different leaching conditions and processing methods were tested and the concentrations of all metals detected in the untreated solar cells after their characterization were measured in the recovered fractions, to assess the achieved purities. The main result is the development of a recycling process for a complete recovery of Ag and In under mild conditions. This process starts with two steps of US-leaching for the recovery of ITO and Ag as solids as the Zn-containing layer underneath them dissolves and, then, the process continues with an alkaline leaching step that targets the dissolution of Mo, followed by brushing or US treatment for the liberation and recovery of the CIGS material as solid particles.

2. Background

Solar cells convert sun light into electricity, by the photoelectric effect, using semi-conductive materials. Several PV technologies are available today. This section describes the materials used for the manufacturing of the solar cells used in the CIGS thin-film PV technology and the available methods for recycling the Ag, CIGS and ITO found in them.

2.1. Basic information on solar cells and PV technologies

A solar or PV cell is a device which can convert sun light directly into electricity by using semi-conductive materials. When multiple solar cells are connected electrically in circuits, more power can be generated. Solar cell circuits sealed in an environmentally protective laminate constitute PV modules. One or more PV modules assembled as a pre-wired, field-installable unit constitute PV panels. Finally, the complete power-generating unit is called a PV array and consists of any number of PV modules and panels [20].

The dominant PV technology, with a global annual production of about 95%, is based on crystalline Si cells. The remaining market share is occupied by the so-called thin-film technologies, nowadays mainly based on CdTe and CIGS semiconductors. The most recent (June 2024) record cell efficiencies in lab scale are 27.3%, 24.4%, 23.4% and 21.0% for monocrystalline-Si, polycrystalline-Si, CIGS and CdTe technologies, respectively [2]. Except for these well-established in the market PV technologies, there are also new emerging ones, like those using organic and perovskite-based cells (alone or in tandem), heterojunction cells and highly efficient III-V multi-junction cells, with the latter ones achieving impressive efficiencies up to about 47% [2].

2.2. The CIGS solar cell

The CIGS thin-film PV technology occupies only about 1% of the PV market share, corresponding to about 1.5 GWp in 2021 [2]. However, the great advantage of this PV technology is the fact that it exhibits efficiencies close to the ones of the dominant c-Si PV, but, for the same efficiency, uses a very much smaller amount of materials, since all the layers of the solar cell have thicknesses smaller than a few μm [21]. These small layer thicknesses also give the advantage of low weight and flexibility to the CIGS solar cells, rendering this technology suitable for building integration [22].

A CIGS solar cell usually comprises several very thin layers (functional layers), deposited on a stainless-steel, glass or plastic substrate [21], as shown in Fig. 1. More specifically, on the top of the substrate, a film of Mo is deposited as the back contact and the CIGS absorber film follows [21, 23]. The buffer layer, which is commonly CdS or one of the ZnS, ZnSe, In_2S_3 , Zn(S, O, OH) and Zn(Mg)O, is deposited on top of the CIGS film [21, 24-27] and then the window layer, usually ZnO, follows [24, 26]. The film layer deposited the last is the Transparent Conductive Oxide (TCO), made of ITO or Zn(Al)O [21, 28]. As soon as the

deposition of all film layers is completed, the conductive Ag or Al/Ni grid is finally created on top of the cell [21, 29]. Regarding their thicknesses, the thickest layer is the CIGS, which is still only 1-3 μm [21] (about 2 orders of magnitude thinner than a typical c-Si PV absorber layer [30-31]). The Mo back contact layer has a similar thickness of 1.5-2 μm , while any other functional layer is even thinner, from a few tens to a few hundreds of nm [21]. It should be clarified here that the discussed layers and materials are the most basic and common ones for CIGS solar cells, however, extra layers or alternative materials have been developed for improving the performance or sustainability of the cell.

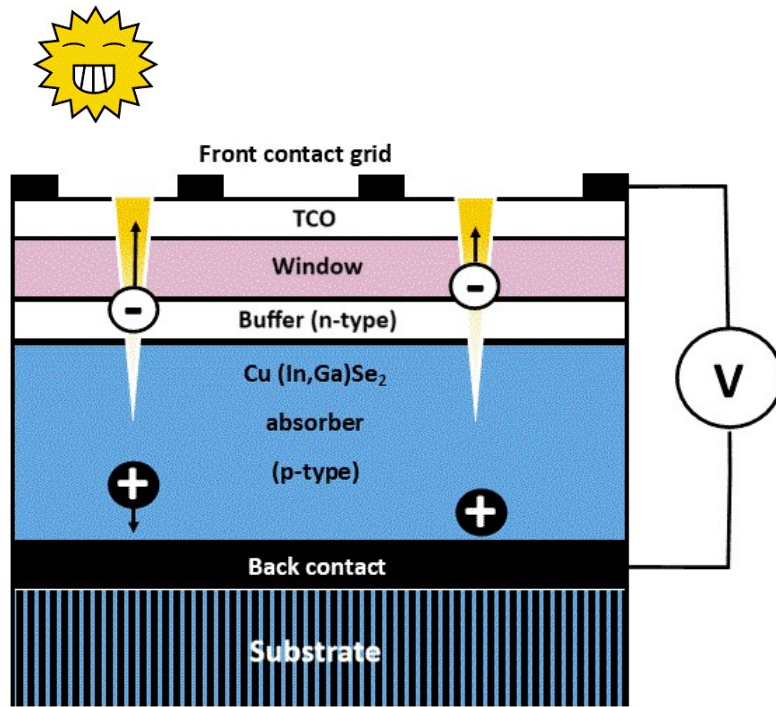


Fig. 1: Graphical representation of the basic structure of a CIGS solar cell (not to scale).
(Figure created by Stellan Holgersson)

2.3. Current methods for recycling of materials present in CIGS solar cells

Recycling processes are distinguished in this section between commercial and laboratory scale ones. Recycling methods used and/or proposed in both scales are presented in this section for CIGS, Ag and ITO. It should be clarified here that, since this thesis primarily focuses on recycling of metals from the actual PV cells, any separation techniques of accessory bulk materials and components of PV modules and panels (e.g. glass, plastics, encapsulation material, etc) are only briefly described when necessary.

2.3.1. Commercial recycling methods of CIGS-containing waste

The recycling of CIGS-containing materials in general (i.e. PV cells, modules, panels, spent sputtering targets and chamber waste) is still limited and any information of recycling activities is not easily accessible. The situation is illustrated very vividly in an IEA's report on commercially available recycling technologies for PV waste published in 2024 [16]. The authors identified 177 recyclers and PV recycling equipment manufacturers (regardless of the PV technology) globally, but only 24 of them applied what can be considered the best available or modern recycling technologies in industrial or even pilot scale. Although all these 24 businesses were invited to participate in the IEA's research by sharing data about their recycling practices, only 7 of them responded. Only one of these companies (LuxChemtech GmbH in Germany successor of Loser Chemie) was active in recycling of waste related to the CIGS PV technology.

More specifically, according to the same report, the LuxChemtech GmbH company seems to perform R&D for the recycling of different PV technologies and is currently building a demonstration plant for treating both c-Si as well as thin-film PV panels. The information which the company provided on their recycling activities referred to the latter facility and the process comprises the following stages: first, the frame and junction box of the PV panel are removed and recovered. Then, a high-pressure waterjet (or, alternatively, light pulse technology for thin-film PV waste specifically) is applied, in order to separate the remaining glass plate from the polymers, cells and any other metals contained in the module. The glass plate is recovered and filtration of the water with separation of the rest of the solids follows. These solids are later further separated into organic polymers and non-ferrous metals, but the separation method is not specified. Until this stage, the process is applicable to both c-Si and thin-film PV. After this step, different chemical treatments can be expected to follow, depending on the PV technology of the waste used as feed. Details of the chemical treatment step, however, are not disclosed. It is only clarified that any Ag present in the solar cell fragments dissolves in acid and then is recovered by electrolysis. NaOH, CH₃SO₃H (methanesulfonic acid), HCl and H₂O₂ are mentioned as the main chemicals used in the chemical treatment, but it is not clear from the report if this is the case for both c-Si and thin-film PV panel waste.

Although information on commercial scale recycling activities of CIGS-containing waste is difficult to find, an idea of recycling solutions which could have potential for up-scaling can be taken from the few available patents on the topic. Unless the solar cells are production solar cell waste (i.e. defective cells before the encapsulation/lamination stage), encapsulation materials keep the cells sealed and sandwiched between layers made of various materials. If the latter is the case, recycling of PV waste modules starts with a step in which the sandwiched structure is opened (assuming that frames, cables etc have already been removed), so that the metals contained in the cells can be accessed and recovered. Patents filed on delamination for specifically thin-film or CI(G)S PV describe different approaches. One method is to shred the panel first in order to assist the exposure of the metal-containing layers to leaching agents and

thus liberation of them from the encapsulation materials too [32-33]. Another method separates the substrate and cover layers by taking advantage of the different thermal expansion coefficients of the different materials after cooling the panel to very low temperatures (e.g. liquid N₂, i.e. 77 K) [34]. Further methods describe the design of a recyclable CI(G)S PV, which includes the insertion of a non-adhesive resin sheet between the top part of the cell and the encapsulant, so that the cells can be recovered easily after cutting along their periphery [35]. Another approach, suitable, however, only for cells with a substrate transparent to lasers, is the scanning of the back contact, through the substrate, with a laser, which causes the partial evaporation of the back contact and its detachment from the substrate. This is followed by heating of the areas which do not include the solar cells, until the softening temperature of the encapsulant is reached, so that the lamination can be peeled off and the bottom area of the cell is then left exposed for further treatment [36].

As soon as the structure is opened and the metals of the cell are exposed, they can be recovered in various ways. Drinkard [32] and Palitzsch [33] describe the direct recovery of the metals contained in the solar cell from the shattered glass and plastic fractions through leaching with oxidizing acid solutions. Kushiya et al. [35] on the other hand suggest dry mechanical separation of the exposed functional layers of the cell using e.g. a metal blade or sandblasting, so that further treatment of the recovered metal-rich fraction becomes possible. In the patent by Lai et al. [34] (stating that treatment of CIGS PV with liquid N₂ resulted in opening the PV structure at the interface between the CIGS and Mo layers), rinsing the part containing the CIGS with a dilute acid solution enables the peeling off and selective recovery of the CIGS layer, so that it can be further treated.

If the CIGS layer is leached (like in the patents of Drinkard and Palitzsch [32-33]), separation and purification of the metals follow. Drinkard [32] suggested electrolysis of the leachate to obtain a mix of solid Cu and Se in elemental form at the cathode and with In and Zn dissolved in the leachate. The Se and Cu were claimed to be separable after their oxidation with concentrated acid followed by crystallization of the oxides and finally a roasting step for distilling off the formed SeO₂. The In- and Zn-rich leachate is proposed to undergo evaporation so that salts of In and Zn form. These salts should then be subjected to high temperatures, in order to decompose and form a mix of oxides. The oxide mix was suggested to be sold to a refinery, which could separate the metals further. The fate of Mo, however, is not addressed in these patents. If the recovered CIGS material is not leached directly, an option is to first employ a thermal treatment for recovering the volatile Se, like in the patent of Lai et al. [34]. In the same patent, it is also suggested that the resulting In, Ga and Cu oxides are then leached in acid and that a following solvent extraction in two steps can separate In first, and then Ga. The three resulting aqueous solutions, each enriched in one of the metals, may then undergo precipitation to form the metal hydroxides. Each of the resulting hydroxide fraction is then suggested to undergo roasting, so that the respective oxides can be obtained. However, since in the patent by Lai et al. [34] the Mo layer is assumed to already have been separated from the CIGS layer during a previous step, it is not certain that the method could be applied directly in CIGS-rich fractions contaminated with other elements, like for example the CIGS powders obtained with

the dry mechanical separation method described in the patent by Kushiya et al. [35], which contain Mo contamination.

More patents can be found on recycling of CIGS (or even just In and Ga)-containing waste which do not come from solar cells. More specifically, one of them [37] describes the recycling of CIGS powder through oxidative roasting in a first step, aiming to remove the Se, leaching of the oxidized waste with HCl and then electrodeposition of Cu, In and Ga, one metal at a time, using different cathodes and suitable conditions for their selective recovery. In another patent [38], CIGS waste (no source specified) is used as the anode, in order to electrolytically recover In at the cathode, Ga dissolved in the electrolyte and insoluble Cu and Se in the anode slime. The Ga in the leachate is separated by precipitation as hydroxide and then leached again, so that it can be purified further by electrolysis. The anode slime dissolves completely and a reducing agent is added after the proper pH adjustment, in order to precipitate elemental Se. According to the patent, Cu remains in the leachate and can be recovered by cementation or electrolysis. A further patent [39] suggests the selective recovery of In and Ga from mixtures of solid materials containing both metals. The patented method comprises an optional size reduction first step, followed by acid leaching using oxidizing agents and then solvent extraction in two steps, first of In and then of Ga. In the case Se and Cu are also present in the waste, Se can be recovered, according to the patent, either before the leaching step as SeO_2 , through an oxidative thermal treatment, or after the separation of In and Ga, through precipitation. Cu is also suggested to be recovered after the separation of In and Ga, either through precipitation or solvent extraction.

It is worth noticing that none of the patents for recycling of thin-film or CIGS PV material cited above addresses the issue of Ag recovery. Moreover, although patents usually avoid to state specific recovery conditions, and they claim a wide range instead, it is clear from the descriptions of the cited patents that they use highly oxidizing and acidic conditions and/or high temperatures for metals recovery, which are known for having a negative impact on both the environment and the equipment and for contributing to the cost of the process.

2.3.2. Laboratory scale recycling methods of CIGS-containing waste

Just like the recycling methods for CIGS waste in industrial scale, the published research at laboratory scale is also limited. However, there is more detailed information available on the actual recovery of metals from CIGS waste, compared to the case of commercial scale. Again, if the cells to be recycled are encapsulated, the sandwiched structure should be opened up first, to enable the recovery of the metals from the solar cells. Different methods have been proposed in the literature for this purpose. Kushiya et al. [40] first removed the frame and junction box of a panel with glass substrate and then manually peeled off the back sheet layer, assisted by a wire brush. The encapsulant was then heated so that it softens and the cover glass was simultaneously pushed away mechanically. The remaining glass substrate with the functional layers and the remaining encapsulant on top of them, was immersed in concentrated acetic acid for 24 h, which resulted in the dissolution of the Zn-containing layer and thus the removal of

the encapsulant deposited on top of it. The remaining glass substrate with the Mo and CIGS layers on top was then treated with a metal blade, aiming to the recovery of the CIGS in powder form. Some of the inventors of the patent of Lai et al. [34], published one of the examples presented in the patent as a research paper by Liu et al. [41]. The authors claimed that splitting of a CIGS solar module with a glass substrate in two parts, at the interface of the CIGS and Mo layers, was successful, after cooling the module with liquid N₂. The CIGS layer was then easily recovered by peeling off after rinsing the upper part of the module with 1 M HCl. In a different approach, Amato et al. [42] crushed CIGS panels to a smaller size, in order to expose the CIGS layer. It seems that no treatment for recovery of the CIGS in powder form followed. It is worth noting that the discussed methods for opening the CIGS modules in order to expose the functional layers at lab scale are very similar to the ones described in the patents.

More references can be found on the recycling of the compositional elements of the CIGS layer for lab scale research. One suggested option is to directly leach the CIGS panels, if they were crushed in a previous stage [42], i.e. without recovering the CIGS as powder first. If the CIGS material has been recovered as a powder though, this could be treated following a variety of different processing routes. Liu et al. [41] suggested the oxidative high-temperature treatment (900 °C) of the CIGS powder recovered from panels, in order to remove the Se and S (in case the latter is contained in the CIGS powder too), then acid leaching of the solid residues using 5 M HNO₃ at 80 °C, followed by two solvent extraction steps for separation of In, Ga and Cu. In their suggested route, each of the metals was later stripped from the organic phase and then precipitated as hydroxide. Finally, the authors claimed that the metals were recovered as oxides, after subjecting their hydroxides to high-temperature treatment in a CO₂ atmosphere.

The remaining available literature deals with the recycling of CIGS powders which originated from pure CIGS-containing waste, i.e. CIGS material coming from process waste, not from solar cells. As this waste is purer and usually in powder form already, they might not be directly applicable to the recovery of the CIGS material which is still attached to a substrate (e.g. ground cells) or CIGS powders recovered from solar cells and containing a considerable amount of impurities (e.g. recovery of the CIGS using a metal blade). However, a review of these methods is still important, as they can be used as a starting point for the development of recycling processes suitable for CIGS waste coming from solar cells. One of the earliest works on the topic was the high-temperature recycling methods investigated by Gustafsson et al. [17, 43-44]. More specifically, the authors used crushed CIGS spent sputtering targets and subjected them to oxidative roasting, so that Se forms gaseous SeO₂, which was recovered after sublimation [17]. The rest of the metals remained in solid form, as a mix of oxides. Recovery of high purity Se could be achieved after reducing the SeO₂ separated at 800 °C, using either SO₂ or the organic reactant deoxybenzoin. The recovery of In, Ga and Cu from the mix of the oxides was suggested to be performed using high-temperature chlorination and for this purpose chlorine gas, hydrogen chloride gas and ammonium chloride were tested as chlorination agents [43]. After the researchers concluded that ammonium chloride was the most promising reagent for various reasons, they proceeded with optimization of the process [44]. More specifically, two high-temperature chlorination steps were applied, the first for recovering the Ga as GaCl₃

and the second for recovering the In as InCl_3 , while the Cu remained mainly in the form of solid chlorides. The optimization concluded recovery of the Ga and In chlorides at 260 °C and 340 °C, respectively.

A few other studies used the same or a similar thermal treatment approach as the one suggested by Gustafsson et al. [17] for recovery of Se, however, they recovered In, Ga and Cu by mainly using hydrometallurgical processes. More specifically, Lv et al. [45] subjected ground CIGS chamber waste to roasting at 1000 °C for the removal of Se as SeO_2 . The resulting mix of Cu, Ga and In oxides was then leached with H_2SO_4 . As soon as high leaching efficiencies were achieved for all metals (4 M H_2SO_4 , 90 °C), precipitation of In and Ga followed, resulting in a mix of their hydroxides, which was later subjected to roasting in order to form a mix of oxides of the metals. Cu mainly remained in the leachate as CuSO_4 after the precipitation step, and its recovery was achieved through solvent extraction with LIX984 in kerosene, stripping with H_2SO_4 and finally crystallization as CuSO_4 . Li et al. [46] continued this work by separating the In from Ga in the oxides mix resulted after roasting. In order to achieve this, they leached the oxides mixed with an alkaline solution (7 M NaOH , 60 °C), so that In precipitated mainly as $\text{In}(\text{OH})_3$, while Ga mainly remained in the leachate. Purification of the recovered In-rich fraction followed using a subsequent acid leaching step (2 M H_2SO_4 , 60 °C) and then a second precipitation step for formation of purified indium hydroxide powder. Finally, In was recovered in the form of In_2O_3 after roasting of its hydroxide. The Ga remaining in the leachate was recovered by precipitation as hydroxide, which was then subjected to roasting for recovering Ga as Ga_2O_3 . Ma et al. [47] used a two-step sulphation roasting approach for crushed CIGS chamber waste. In this approach, the waste was first subjected to sulphation roasting, in order to recover SeO_2 . In a second step, the Cu, In and Ga sulphates which were formed in the first step were roasted (without sulphation this time) under such conditions so that a mix of In and Ga oxides was formed, while Cu remained as CuSO_4 . The temperatures which were finally selected for the two thermal treatment steps were 600 °C and 710 °C, respectively. A water leaching step followed, in order to dissolve the soluble CuSO_4 and separate it from the non-soluble In and Ga oxides. Separation of the In and Ga from their oxides mix was proposed to take place through alkaline leaching and precipitation. Hu et al. [48] studied an inversed approach compared to the previous works for separating spent CIGS materials (of unspecified source), in the sense that the leaching step was applied first, using HNO_3 , and, then, the roasting step for the recovery of Se followed. More specifically, during the leaching step, Cu, Ga and some of the Se ended up in the leachate. In and the remaining Se did not dissolve but formed $\text{In}_2(\text{SeO}_3)_3 \cdot 6\text{H}_2\text{O}$ as the dominant crystalline phase. This solid was roasted, in order to recover Se as SeO_2 and to separate it from In, which ended up as In_2O_3 . Regarding the leachate, the elements which were present in it were first precipitated mainly as selenites (and a small amount of copper hydroxide), using MgO . The resulted solid fraction was then subjected to roasting as well, in order to recover Se as SeO_2 and separate it from the Cu and Ga which gave a mix of solid oxides. The recommended conditions were 3.2 M HNO_3 at 90 °C for the leaching step and 800-900 °C for the roasting steps.

Other researchers preferred to omit completely the high-temperature thermal treatment step for Se recovery and explore instead different routes for the recovery of the compositional elements of the CIGS material coming from spent sputtering targets: Hsiang et al. [49] subjected crushed targets to autoclave leaching with 3 M H₂SO₄ and a small amount of H₂O₂ at 140 °C, in order to dissolve Ga, In and Cu and to convert Se into its elemental form. The conditions were sufficient for almost complete leaching of the metals, while the addition of H₂O₂ as an oxidizing agent proved necessary for the decomposition of Cu-Se compounds. After drying the leachate, the latter was reacted with Se powder in oleylamine at elevated temperatures (250 °C), in order to produce new CIGS nanoparticles. On the other hand, Gu et al. [50] implemented a variety of wet chemistry separation methods, starting by an almost complete leaching of crushed CIGS targets using HCl (5 M and 40 °C were suggested as the most efficient conditions) mixed with H₂O₂ and continuing with separation of Cu and Se from leachate by electrodeposition. The remaining solution was then evaporated under vacuum and any left-over water was later removed by refluxing with SOCl₂, through a dehydration process. The different solubilities in the SOCl₂ of the previously formed indium and gallium chlorides, enabled their separation, as InCl₃ remained insoluble while GaCl₃ was solubilized in SOCl₂. The authors claimed that distillation of the latter fraction could achieve a recovery of Ga as solid GaCl₃. In most of the cases discussed in this section, metal recovery was stated to have exceeded 90 wt%, however, it is noticeable that high leaching agent concentrations (usually at least 3 M) and/or high temperatures (from 80 °C to 1000 °C) were employed.

2.3.3. Commercial and laboratory scale recycling of Ag

In 2022, 18% of the Ag supplied to the market came from recycling activities, with the main secondary sources of Ag being spent catalysts, e-waste, old X-rays, jewelry, silverware and coins [14]. Recycling of jewelry, silverware and coins usually involves pyrometallurgical processes, apparently due to the high concentrations of the metal. Low-grade jewelry scrap and processing waste, as well as used jewelry, silverware and coins are smelted first to form an impure silver, which is finally electrorefined, while high-grade jewelry scrap is usually realloyed on-site, rather than being refined [51-52]. On the other hand, photography-related waste (X-ray film, photographic paper and film, processing solutions) contain much smaller amounts of Ag. Therefore, hydrometallurgical treatments, like leaching (following a thermal treatment step for removal of organics if necessary) and electrolysis, are more suitable for this type of waste [51]. Similar is the case for spent catalysts, which are commonly leached using HNO₃ and then the dissolved Ag is recovered from the leachate either by precipitation at increased pH as Ag₂O or via electrolysis [53]. Industrial recycling of e-waste is more complex, as it starts with the removal of parts which can pose a threat during recycling (e.g. batteries, as they can explode) and then continues with size reduction of the waste. Mechanical and physical separations follow, in order to separate the main categories of materials, like ferrous metals, copper, aluminium, Printed Circuit Boards (PCB) and plastics. PCB are usually the parts which contain the precious metals and are sent to other companies for further processing. Although the information regarding the further processing of this fraction is not easily available, it is known that pyrometallurgical and hydrometallurgical processes can be applied [54-56]. Some

patents state though that pyrometallurgical treatment is not very suitable for PCB, as they contain toxic flame retardants [55-56]. A common alternative hydrometallurgical route used often starts with the leaching of the non-precious metals and then, in a subsequent step, the remaining precious metals are leached using aqua regia. Various chemical treatments of the solutions can be employed [56]. The patents which claimed the inappropriateness of the pyrometallurgical methods, for PCB treatment employ alkaline leaching instead. One of them [55] uses a system of ammonia-ammonium salt in the presence of an oxidizing agent in order to leach the waste and complex the Ag and other metals. Then cementation of Ag and any metal more noble than Cu follows, by adding Cu powder. The other patent [56] suggests crushing of the PCB, separation of their metal fraction and, then, its autoclave leaching. An alkaline solution under oxygen pressure is used for the leaching step, in order to dissolve Al and Sn first. The remaining solid is leached with H₂SO₄, in order to dissolve the Cu, while Ag, Pb and precious metals remain undissolved and are suggested to be treated with pyrometallurgical processes.

PV recycling does not seem to play an important role in Ag recycling yet, as the volume of EoL PV is still relatively low and there are also problems with their collection rates [14]. Given the small amounts of Ag present in solar cells, however, pyrometallurgical processes do not seem suitable for its recovery and application of hydrometallurgical treatments would be more expected. Indeed, two patents describe leaching c-Si PV or Ag-containing scrap using CH₃SO₃H (methanesulphonic acid) in the presence of an oxidizing agent for Ag dissolution [57-58]. One of these patents claims that Ag concentrations in the leachate of a few g/l can be achieved (the leaching efficiency is not mentioned though). The dissolved Ag is recovered as AgCl through precipitation. The other patent [57] suggests electrolysis of the resulting solution for recovering the Ag. Recovery rates higher than 90 % are claimed to be achievable with this method.

Recycling of Ag from PV at lab scale can be found in the literature for the case of c-Si PV. In these cases, as soon as the encapsulant (if present) is removed, employing a method of chemical treatment of the Ag contacts, aiming to the dissolution of Ag particles, is a common strategy. The use of HNO₃ seems very popular among the scientific literature for this purpose. The acid was often used in high concentrations, alone or (if other layers of the c-Si cell were also targeted) in mixtures with other acids, and elevated temperatures were also used sometimes, as reviewed by Wang et al. [59]. Despite the advantage of the high etching efficiency that the solutions described in these papers seemed to offer, it is worth noting that these etching conditions were not environmentally friendly. When less harsh conditions were studied, the reaction efficiencies were not specified, like in the case of Łazewska et al. [60] who investigated the etching of Ag using only 1–3 M HNO₃ at 30 °C and 50 °C. A less conventional leaching method was used by Wang et al. [61], who used US-leaching with different HNO₃ concentrations, temperature, time and US power for removing Ag and other elements from a c-Si cell. The Ag leaching efficiency was not specified, however, it seems that, for the tested conditions, Ag dissolution increased with the acid concentration, US power and temperature. The etching efficiency also increased with time up to 90 min, however, for longer times a

decrease was observed, which was not clear if it was a matter of error. The use of other acids, like HF, CH₃COOH, H₂SO₄ (as well as H₂O₂) in the presence or absence of HNO₃, is also vaguely described in some articles [62-64]. It is worth pointing out that in the majority of the reviewed cases the effect of the leaching parameters on the Ag leaching efficiency was not investigated and a reasonable explanation behind that is the fact that Ag was not the target element for recovery.

Despite the fact that most of the reviewed papers did not proceed with the recovery of the dissolved Ag, there were a few who did. One of them was the paper by Punathil et al. [65], who used 6 M HNO₃ at 70° C in order to etch Ag and Pb from c-Si wafers and then separated the Ag from the leachate by precipitation as AgCl. Jung et al. [66] took the recovery of Ag a step further. After leaching a recovered Si wafer and its Cu wires with 5 M HNO₃ at room temperature, Ag, Cu and Pb ended up in the leachate and Cu was separated first, using solvent extraction. Then, Ag was precipitated with HCl and the resulting AgCl was further converted into Ag₂O by 5 M NaOH at room temperature. A solution of hydrazine hydrate (N₂H₄·H₂O) in water and ethanol was then used to reduce the oxide into Ag powder. The powder was subsequently melted at 1100 °C and the product was used as an anode in an electrorefining step.

2.3.4. Commercial and laboratory scale recycling of ITO

ITO is a mixed oxide, consisting mainly of In₂O₃ and less than 10% wt SnO₂ [15]. Although some recycling of ITO scrap is taking place today in Japan and the Republic of Korea [13], any information on the recycling processes used could not be found. A few patents on recycling of ITO from spent ITO targets [67, 69] though describe the size reduction of the waste first (sometimes preceded by a polishing and cleaning pretreatment step for removal of superficial contamination), until it becomes fine powder. This powder is then mixed with a binder and in some cases with an extra amount of indium oxide. Calcination may follow, before the mix is pressed into a new target and then sintered. It is easily understandable that these methods require an already pure ITO material as their feed. There is also a number of patents, which describe the recycling or recovery of ITO or its In coming from LCD panels [70]. The review article by Amato et al. [70] on this topic shows that dismantling and/or crushing of the LCD panel is the first step, usually followed by classification of the different groups of materials. After the classification, the glass substrate on which the ITO is deposited is leached with acid or alkaline solutions, to dissolve the In. Different methods, like electrolysis and cementation, are then proposed to be used for In recovery. Some of the patents also describe thermal methods in which chlorination agents are used for formation and separation of the volatile indium chloride. Finally, a few patents describe the selective removal of the films deposited above the ITO layer, using chemical, mechanical or thermal methods, or a combination of them, to recover an ITO-coated glass.

Regarding recycling of ITO from PV, no commercial methods or patents could be found. In lab-scale, the topic has been investigated by some researchers for the cases of perovskite and

organic solar cells (all lab-fabricated). Interestingly, all available works are actually reuse strategies, as they targeted the dissolution of the layers placed above the ITO-coated substrate, so that latter can be reused. Some examples are: 1) the dissolution of all layers deposited above the ITO layer of a perovskite solar cell by a KOH solution [71], 2) the dissolution of Ag, MoO₃ and active layer of a polymer solar cell using chloroform and the subsequent removal of the ZnO layer with a lactic acid solution of 3% first and 1% afterwards [72] and, 3) the US dissolution of a vanadium oxide layer placed immediately above the ITO layer of an organic PV using 0.02 M NaOH [73].

2.4. Issues with the current methods

It is rather clear from this literature review that methods for recycling materials from CIGS solar cells are still under development. It becomes apparent though that leaching is in most cases an indispensable step. A trend of using harsh leaching conditions, i.e. high leaching agent concentrations and/or high temperatures, for achieving high leaching efficiencies for the CIGS compositional elements, was observed. Moreover, when high-temperature treatment methods were used, a high amount of toxic gases, like Se- and/or Cl-containing ones, was usually involved in the process. In the case of Ag recovery, similarly harsh leaching conditions were used for achieving high dissolution efficiency. In the few cases in which milder conditions were used, the recoveries achieved were not stated. At an industrial scale, these harsh conditions and/or presence of toxic gases can be challenging, due to corrosion, costly equipment, high cost for chemicals, regulations, safety and environmental concerns [74-76].

Regarding the recycling of ITO, the existing commercial methods are not suitable for its recycling from CIGS solar cells. One of the main reasons is that they focus on scrap ITO targets and LCD panels, which do not contain the plethora of metals found in solar cells. Thus, contamination of the recovered ITO with unwanted elements is expected to be much lower in the former type of waste and its refining (if needed) less challenging. Moreover, any methods proposed the recovery of the whole ITO-coated substrate and its reuse, are only suitable for specific arrangements of solar cells, i.e. the ones having the ITO deposited directly on a transparent substrate, which is usually not the case for CIGS solar cells. Additionally, reuse methods might be more challenging to apply in big scale, as they demand the careful handling and treatment of whole cells, since the ITO layer deposited on the substrate must remain in perfect condition in order to be reused again.

There is also a tendency in the literature to mainly focus on the measurement of the elements which were of interest to recover in each work. However, as mentioned previously, when whole solar cells are recycled, a plethora of elements is present, and, therefore, contamination of the recovered fractions with unwanted elements is very likely to happen. The purity requirements for materials used as semiconductors in the manufacturing of new solar cells are strict though. According to Gustafsson et al. [17], the purity of the recovered Cu, In, Ga and Se should be as high as 5N (i.e. 99.999) with regard to the impurities Sc, Ti, V, Cr, Mn, Fe, Co, Ni and Zn, if the recovered elements are going to be reused in the synthesis of the CIGS layer. Lower purities

with regard to these elements will compromise the efficiency of the solar cell. Therefore, measurement of impurities is of great importance, as recovered materials of high purity can achieve high value, increase the profit [77] and decrease the need for virgin materials.

As a result, it is concluded that there is a need for development of methods for recycling and recovery of materials from CIGS solar cells which are characterized by high efficiency, selectivity and flexibility. If this PV technology is going to expand further and simultaneously keep its green credentials, there is also a need for lowering the environmental impact of the new recycling methods, at least in terms of the type and consumption of reactants, as well as energy consumption. The need for development of recycling processes for CIGS solar cells which are easy to upscale, recover more types of and purer materials and consume lower amounts of chemicals has also been pointed out by Ravilla et al. [78]. All these issues have been attempted to be addressed by the current PhD thesis.

3. Theory

In this section, some basic theory of leaching is presented first. Then, discussion on the predicted reactions for acid and alkaline leaching follows.

3.1. Leaching

Leaching is considered as the very first step (and sometimes the most important one) of many hydrometallurgical processes. A leaching process is described by the reaction between a leaching agent A present in the liquid form with a reactant B present in the solid form, where A is (partially) dissolving B towards product formation [79]. The resulting solution is called leachate. As it becomes apparent, the leaching reaction is a heterogeneous solid-liquid reaction. The presence of the different phases adds some complexity to the system and the leaching process usually comprises several steps, assumed to be sequential. In order to understand and control the leaching reactions, knowledge of both thermodynamics and kinetics of the leaching system is important, since each can provide different information.

3.1.1. Chemical equilibrium

The reaction



denotes that, at any time, compounds A and B react towards formation of C and D and vice versa. The rates of these two reactions are not necessarily equal. When they become equal though, the system will be in a dynamic equilibrium, called chemical equilibrium.

The state of chemical equilibrium is described by the equilibrium constant K, defined as

$$K = \frac{[C]^c \cdot [D]^d}{[A]^a \cdot [B]^b} \quad (\text{Eq. 1})$$

where [X] is the concentration of substance X at equilibrium. Each chemical reaction is characterized by its own K, which depends on the temperature. It is worth noticing that if the coefficients of a specific reaction change, the value of its K will also change accordingly. Concentrations of pure solids and liquids are omitted from the right side of (Eq. 1), as they are constant and are, thus, considered on the left side (i.e. are considered as part of the K value). Low K values indicate that the equilibrium mixture mainly consists of reactants, while high K values indicate that the equilibrium mixture mainly consists of products [80].

In order to assess how close a reaction is to its equilibrium state, the reaction quotient, Q, is used. Q has the same expression as K, with the difference that the concentrations of the substances are the ones at any time t, not necessarily at equilibrium, if the system has not

reached it yet. When $Q=K$, the system has reached equilibrium. If $Q<K$, the formation of products proceeds faster than the formation of reactants, until equilibrium is reached. The opposite is true for $Q>K$ [80].

According to Le Chatelier's principle, *when a system in chemical equilibrium is disturbed by a change of temperature, pressure (if gasses participate in the reaction), or a concentration, the system shifts in equilibrium composition in a way that tends to counteract this change of variable*. For example, removal of a product will shift the reaction towards the products' side (until equilibrium is re-established), as the system will try to form again the removed product. Therefore, the yield of a product of a reaction can increase or decrease, by changing the reaction conditions [80].

As it becomes apparent, knowledge of the K of a reaction can provide many different types of information: i) based on its value, it can give an initial idea on whether the formation of products or reactants is favored at a specific temperature, ii) allow quantification of the composition of the equilibrium mixture and iii) allow the prediction of the direction the reaction is going to follow for a given composition of mixture (by comparing Q with K) [80].

3.1.2. Thermodynamics

Thermodynamics provides information about the ability of a reaction to take place [80] and species which are present in the system at equilibrium. If the concentrations of reactants and products are known, this can be used for telling how far the system is from its equilibrium state and in which direction the reaction is going [79].

The assessment of whether a reaction is spontaneous or not is based on the value of the Gibbs free energy change of the reaction in question (ΔG): a negative value of ΔG indicates a spontaneous reaction, while a positive value a non-spontaneous reaction. At equilibrium, $\Delta G=0$. ΔG relates to the standard Gibbs free energy change, ΔG° , and the reaction quotient, Q , through (Eq. 2) [80]:

$$\Delta G = \Delta G^\circ + RT \ln Q \quad (\text{Eq. 2})$$

For equilibrium conditions (i.e. $\Delta G=0$ and $Q=K$), a relation between ΔG° and the equilibrium constant, K , can be found:

$$\Delta G^\circ = -RT \ln K \quad (\text{Eq. 3})$$

(Eq. 2) and (Eq. 3) imply that whether a reaction will be spontaneous or not depends on the conditions under which it takes place. More specifically, the value of ΔG depends on the reaction temperature, as well as any factors which can affect the values of K and Q . For example, a reaction can be non-spontaneous up to a specific temperature, but spontaneous at

elevated temperatures. This knowledge is of great importance for choosing proper process conditions.

However, thermodynamics does not take the variable of time into account, meaning that it cannot answer to questions like whether a reaction will be completed in a few minutes or several years. Moreover, thermodynamics considers only the initial and final states of a process, while the path between the two states is irrelevant. Knowledge of the path though can be important for practical applications [79].

3.1.3. Kinetics

Kinetics provides information on the rate of chemical reactions, often also the underlying mechanisms (or fundamental reaction steps) describing an overall reaction process and the various factors affecting the mechanisms and the reaction rate [79]. Therefore, it complements thermodynamics by answering the time- and path-related questions for reactions. Since time is a significant parameter for real-world applications, kinetics is associated with chemical process feasibility, profitability and engineering design. Thus, its investigation for a process under development is essential.

Specifically for a leaching process, there are two to three steps which can control its rate [79]: In the first step, the leaching agent must diffuse from the bulk liquid phase through a liquid film, located between the bulk liquid and the solid particle. If there is an obstacle on the surface of the particle (e.g. the reaction may result in solid products which stick to the surface of the particle), the leaching agent should diffuse in the next step through this solid layer too. In the final step, the leaching agent reaches the unreacted surface of the particle and the reaction takes place. Depending on the reaction, some soluble products may form. These products must be evacuated by following the inverse path (i.e. diffusion through the solid product layer, if any, and then diffusion through the liquid film) until they end up into the bulk solution. As a result, three main mechanisms, namely liquid film diffusion, product layer diffusion and chemical reaction, can affect the kinetics of leaching. This means that both reaction and transport phenomena can play an important role in leaching processes. As the steps in leaching processes are assumed to be sequential, the rate controlling step is the slowest one. Depending on the system and leaching conditions, it is likely that there are more than one controlling steps, if those have rates of similar order of magnitude, or even that the controlling mechanism changes after some time [79].

Faraji et al. [79] distinguish between four basic models for describing the kinetics of leaching. The four models are actually all the possible combinations of a constant-size or shrinking particle with the existence or absence of a distinct unreacted core in the particle, as illustrated in Fig. 2. More specifically, if the size of the particle remains constant during leaching and its composition changes homogeneously throughout the entire volume of the particle as the reaction takes place, the model describing this situation is called Progressive Conversion Model (PCM). This is the case for highly porous particles where both the leaching reagent and product

can easily diffuse through the porosity without significant resistance. Since diffusion rate is fast, the chemical reaction is the rate controlling step. The other three models describe leaching of non-porous particles, where the reaction takes place only on the outer surface. The second model is the Shrinking Core-Constant Particle Size Model (SC-CPSM), which is a situation in which an insoluble solid product sticks to the surface of the unreacted particle. In this case, since the product sticks to the unreacted surface, the leaching reagent should diffuse through the product layer before it reaches the unreacted core. As soon as the reaction takes place, more insoluble product is formed and, thus, the solid product layer surrounding the particle becomes thicker with time, while the volume of the unreacted particle, looking like a “core”, shrinks. If any soluble products are formed, these should also diffuse back to the liquid. The third model described is the so-called Shrinking Core-Shrinking Particle Model (SC-SPM) and describes a very similar situation in terms of product layer and “core” formation with the SC-CPSM. However, in this case, the formed product layer remains only partly on the surface of the particle (due to various reasons). As a result, shrinkage of the whole particle with time is observed. The fourth and final simplified leaching model describes a situation in which no product layer is formed on the surface of the non-porous particle. As it can be easily understood, no “core” is formed and the particle shrinks with time. This model is simply called Shrinking Particle Model (SPM).

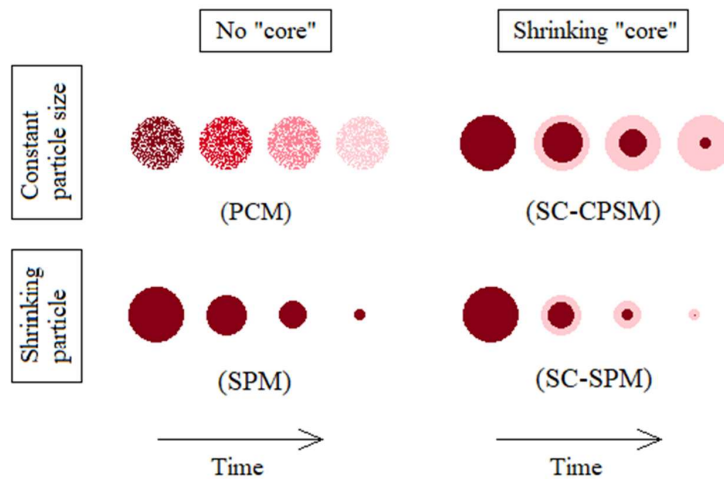


Fig. 2: The four basic models for describing the kinetics of leaching according to Faraji’s et al. [79] classification.

A plethora of factors can affect the leaching rate, however, their importance depends on the scale of view. Faraji et al. [79] mention four types of scale of view: i) grain, ii) particle, iii) cluster and iv) heap. Examples of factors that can play a significant role for each of these cases are given in their review paper [79]. At lab scale, due to the small sizes involved in the

experimentation, grain and particle scale view are considered suitable. The most important factors affecting a leaching process at these scales are the leaching agent, the leaching temperature, the size of the particles, agitation and solid to liquid ratio [79].

In more detail, different leaching agents can give different reaction mechanisms and, therefore, different kinetics of the leaching reactions. The concentration of the leaching agent is also an important parameter for the leaching rate, since the leaching rate is considered to be a function of the concentration of the reactant in the liquid phase. Usually, the leaching rate increases with an increase in the concentration of the leaching agent. Temperature can accelerate both the diffusion and reaction rates, as well as affect the solubility of both reactants and products. Chemical reactions, however, are in general more sensitive to temperature compared to diffusion [79]. The mixing conditions are another significant factor which affects the leaching rate. Generally, an increase in the mixing rate results in an increase of the leaching rate, through the reduction of the thickness of any liquid diffusive layer close to the surface of the particles. In addition, mixing gives a more efficient renewal of the leaching agent and removal of products at the surface of the solid. In some cases, harsh agitation can also cause detachment of any solid product layer covering the solid particles, thereby assisting the access of the reagent to the unreacted particle surface. Therefore, good mixing conditions are beneficial for both reaction and diffusion rates. However, as soon as a maximum leaching rate is achieved, a plateau or even decrease in the leaching rate is observed, if the mixing speed increases further. This trend is the result of poor mixing conditions due to flow problems (e.g. vortex and air bubble formation), which can hinder the access of reactants to the unreacted surface. As can be easily understood, leaching rates that depend on mixing are usually a sign of diffusion control. On the other hand, if the leaching rate is independent of the mixing conditions, that can be an indication of reaction control [79]. A special type of agitation is that using US [79]. The ultrasonic effect is the combination of two other effects: the cavitation effect (present at all frequencies) and the heating effect (greater at high frequencies; >100 kHz). In the cavitation effect, the US waves cause the formation of bubbles which go through the stages of inception, growth and implosion. During the implosion stage, a liquid jet emerges from the bubble, creating turbulence and, thus, enhancing mixing [81]. Locally, temperatures can reach 5500 °C and pressures 500 atm, during this stage. The high energy conditions can remove the external product layer (leaving the unreacted surface exposed), create microcracks in the particles and cause the formation of highly active species from the water molecules ($H\cdot$, $OH\cdot$, H_2O_2 , HO_2 , H_2 and $e^-_{(aq)}$) [79, 81]. Therefore, both mass transfer and chemical reactions can benefit.

The size of solid particles and the solid to liquid ratio (S:L, usually expressed in units of mass of solid per liquid volume) are two factors which affect the leaching rate inversely. Regarding the particles size, this is because (for a given mass of solid) smaller particles offer a larger surface area for reaction and any boundary layers between the particle and the liquid are thinner too [79]. Regarding the S:L, this ratio determines the molar ratio of the reactive chemical component in solid to the leaching agent in liquid [79]. For a given mass of solid, the larger the volume of the liquid (i.e. the lower the S:L), the higher the excess of the leaching agent is and thus the risk of running low of reactant is less. Another reason which can be responsible for the

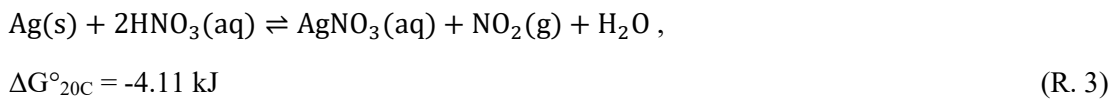
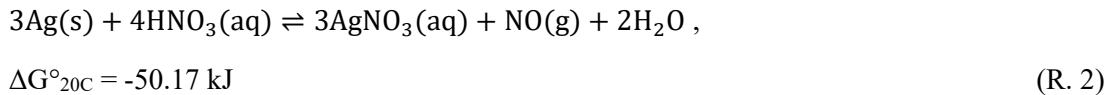
observed trend of the leaching rate with S:L is the increase in liquid's viscosity as the solution volume decreases (i.e. as S:L increases), which makes diffusion of species more difficult [79]. When S:L increases it is also likely that particles tend to clog together and thereby they become less accessible to leaching solution.

3.2. Predicted reactions

In this thesis, both acid and alkaline leaching were employed, depending on the target element. The expected reactions for each case, predicted based on thermodynamic data, are described below in detail. All reactions were simulated with the HSC Chemistry 10 software [82] and the predictions are based on the data for the standard states at 20 °C. Although it is true that the predictions may change to some extent if the conditions change, they were considered as a good starting point. It should also be clarified that, since no thermodynamic data for the CIGS compound were available in the HSC database or in the literature, the individual selenides were used instead, in order to simulate the behavior of the CIGS compound. Due to this simplification, some discrepancies between predicted and observed behavior of the CIGS compound and its elements can be expected. Finally, the species InOH^+ and $\text{HSO}_3(\text{aq})$ of the database were not taken into account when creating the Pourbaix plots of the CIGS compositional elements, since the software encountered some problems with the use of these two species.

3.2.1. Acid leaching

Acid leaching at the ambient temperature of 20 °C was extensively used for dissolution of Ag and In. In all these experiments, the selected leaching agent was HNO_3 . The reason behind the selection of this specific mineral acid as the leaching agent was its oxidizing ability (i.e. its ability to oxidize the elements it reacts with) [80]. Because of this oxidizing ability, HNO_3 is able to dissolve even the noble metal Ag, found in its metallic form in the conductive grid of the cell, by forming Ag^+ and NO_3^- in the leachate:



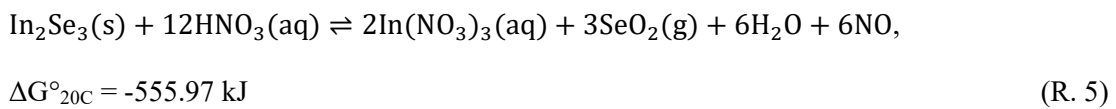
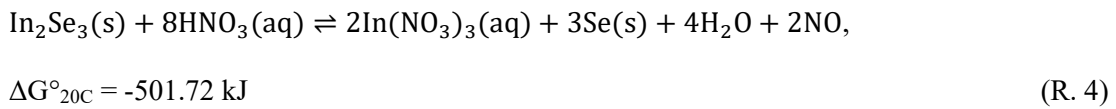
Both reactions have negative ΔG° values, meaning that the formation of products is favored under the standard conditions, based on (Eq. 3). However, the low $\Delta G^\circ_{20\text{C}}$ of (R. 3) shows that this can easily change with a change in the reaction's conditions. Moreover, it is worth noting that at lower concentrations of HNO_3 , (R. 2) is expected to be favored over (R. 3), since (R. 3) requires a higher concentration of HNO_3 per silver atom.

Regarding the leaching of the other target element, In, a considerable amount of this element is expected to be found in the CIGS compound, which has a chalcopyrite crystal structure [21]. It is known from the literature that chalcopyrite (CuFeS_2) has a dense crystal structure and

tends to form leaching product layers, like elemental sulphur etc, around its particles when leached. Because of that, an oxidizing agent, e.g. H₂O₂, is usually added in the leaching solution, in order to oxidize the product layer, dissolve it and, thus, promote the leaching of the unreacted core [83]. As HNO₃ has oxidizing properties itself, its use as leaching agent for CIGS was worth investigating. The effectiveness of this acid for leaching the CIGS compound compared to other acids was also confirmed in practice by Amato et al. [42].

For the thermodynamic simulation of the leaching of the CIGS compound, run in HSC, the simple selenides Cu₂Se, In₂Se₃ and Ga₂Se₃ were used instead of the CIGS compound, as the latter is not available in the software's database. According to the simulations, many reactions are likely to take place between the selenides and the HNO₃. A detailed list of possible reactions is given in the Supporting file of Paper I of this thesis. In summary, the selenides react with the HNO₃ and may form the respective metal cations and NO₃⁻, water, NO_x and Se, SeO₂(g), SeO₂(s) and/or SeO₂(aq). In order to find which reactions were the most likely to take place under the experimental conditions, Pourbaix diagrams for each of the compositional elements of the CIGS compound in the presence of the other CIGS compositional elements were constructed in HSC. In short, a Pourbaix (or E_h-pH) diagram plots the equilibrium potential (E_h) between a metal and its various oxidized species as a function of pH. They show which species is thermodynamically stable at a given E_h and pH [84].

Considering the case of In first, its Pourbaix plot (Fig. 3a) showed that dissolution of In in aqueous solutions is favored by oxidizing and highly acidic (pH<0) conditions, forming mainly In³⁺ and InOH⁺² or, if the oxidizing potential is very high, In₂(SO₄)₃(aq). At the same time, Se may react with the acid towards formation of various products, depending on how oxidizing its environment is (Fig. 3b). More specifically, Se is mainly present in the form of insoluble selenides, if the conditions are not oxidizing enough. As the potential increases, Se tends to form elemental Se. Even further increase of the potential leads to dissolution of Se, either as H₂SeO₃(aq) or, at even higher potentials, as In₂(SO₄)₃(aq). Therefore, some possible reactions describing the leaching of In₂Se₃ from HNO₃ could be:



The highly negative $\Delta G^\circ_{20\text{C}}$ values of all reactions show that these reactions are expected to be spontaneous, as the formation of products is highly favored. However, it is worth noticing that,

based on the coefficients of reactions (R. 4) and (R. 5), these two reactions demand a considerable amount of HNO_3 in order to take place. Their kinetics cannot be predicted from this data, however, the possibility of formation of elemental Se or insoluble selenides suggests that, if a dense leaching product layer is formed around the particles, the leaching rate of In and Se may become slow, or stop before it is completed, if the access of the HNO_3 to the surface of the unreacted CIGS core is hindered. Finally, the more extensive list of possible reactions

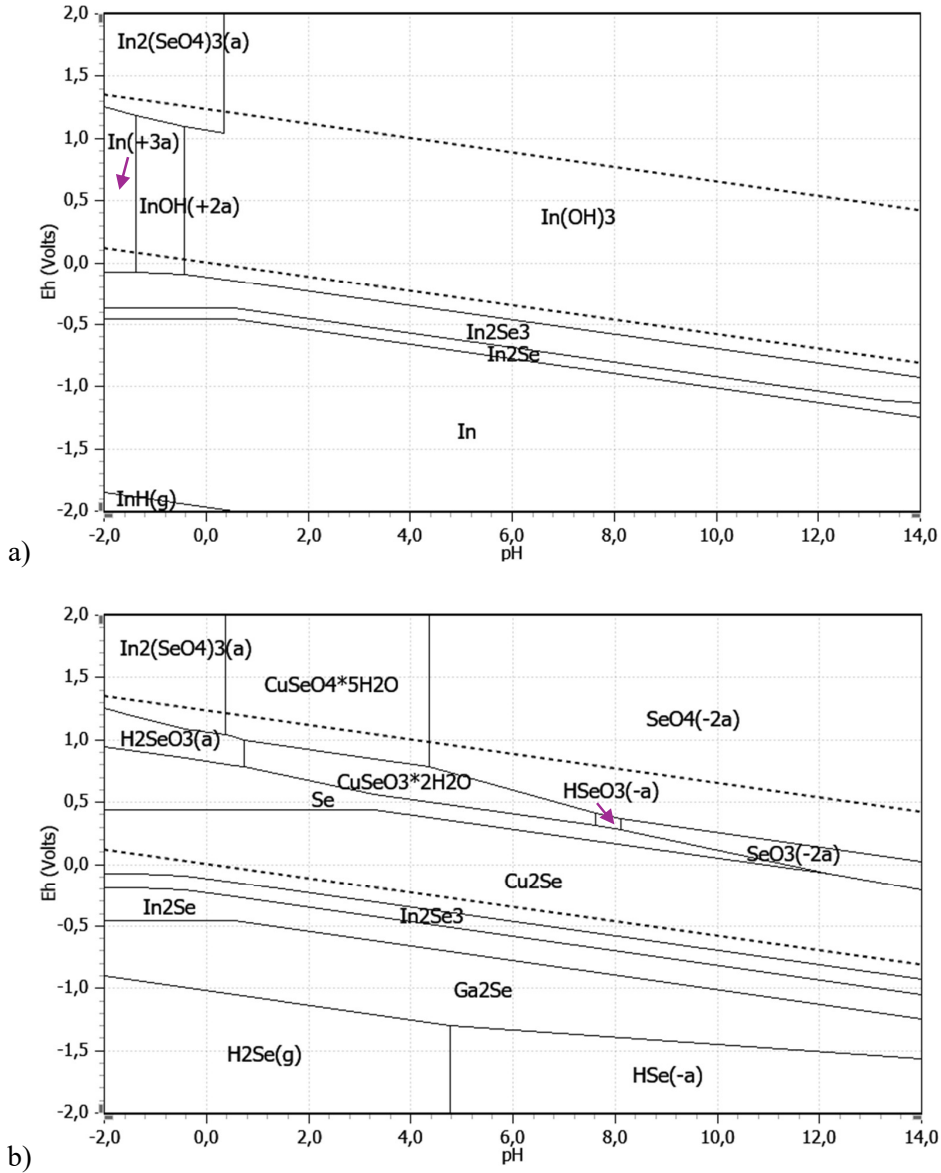


Fig. 3: Pourbaix plots of a) In and b) Se, both in presence of the other CIGS compositional elements (species with an “a” in parenthesis are aqueous species, while the ones without are in the solid state).

between In_2Se_3 and HNO_3 presented in the Supporting file of Paper I of this thesis suggests that lower concentrations of HNO_3 favor the formation of NO , while higher concentration the formation of NO_2 . The reactions of Cu_2Se and Ga_2Se_3 with HNO_3 are similar with that of In_2Se_3 . The Pourbaix plots for Cu and Ga in the presence of the other CIGS elements are presented in Fig. A1a and b of the Appendix, respectively.

Less noble metals may oxidize towards formation of oxides with limited solubility, when they react with HNO_3 [85-87]. In the case of Mo (found in its metallic form in the back contact of the CIGS solar cells), the species $\text{MoO}_2(\text{s})$ and $\text{MoO}_3 \cdot \text{H}_2\text{O}(\text{s})$ are thermodynamically favorable under acidic and oxidizing conditions (Fig. A1c of the Appendix). Other species of Mo discussed in the literature, and which could potentially be present, are $\text{MoO}_3(\text{aq})$ and $\text{MoO}_3 \cdot 2\text{H}_2\text{O}(\text{s})$ [88-89]. The solubility of the molybdenum oxides and hydrates in HNO_3 solutions depends on the temperature and HNO_3 concentration [88-89]. The case is similar for elemental Fe and Cr, both found in the stainless-steel substrate of the CIGS solar cells used for the experiments of this work. It is well-known method in the steel industry that HNO_3 can be used for “pickling” or passivation of stainless-steel through the formation of a chromium oxide layer. During this process, some Fe from the surface of the stainless-steel dissolves, until a layer of chromium oxides is formed, hindering further leaching [90]. Therefore, any contamination of the leachate from the stainless-steel substrate of the cells is expected to be limited.

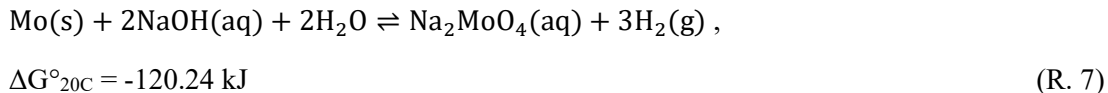
To sum up, the Ag and CIGS present in CIGS solar cells are expected to dissolve when acidic and oxidizing conditions are used for their leaching. The nobility of the metallic Ag and the tendency of Se from the CIGS to form insoluble selenides or elemental Se are the reasons why relatively high oxidizing conditions are needed for the dissolution of the two materials. The predicted behavior of the CIGS compound under acid leaching conditions is in good agreement with the known leaching behavior of chalcopyrite. Under the same conditions, Mo tends to form mainly insoluble oxides and their hydrates. Similar is the case for Cr, leading to the passivation of the stainless-steel substrate, in which it is found. As a result, the contamination of the leachate with soluble species of Fe and Cr coming from the stainless-steel substrate is expected to be limited.

3.2.2. Alkaline leaching

As previously explained, when Mo is leached with HNO_3 , only partly soluble products are formed. Therefore, when Mo was the target element for dissolution, alkaline leaching was investigated instead. In the literature, strongly alkaline solutions are recommended for the dissolution of MoO_3 towards the formation of soluble molybdates, but not for the dissolution of metallic Mo [91], i.e. the form in which Mo is present in CIGS solar cells. Although it is not clear from the literature if the stated ineffectiveness of alkaline leaching for metallic Mo applies even to small concentrations of the element, no literature dealing with such reactions was found. The development of a leaching process for the direct conversion of elemental Mo to MoO_4^{2-} could be beneficial though, since it would require fewer steps compared to the case of first converting Mo to MoO_3 in one step and then MoO_3 to MoO_4^{2-} in a following step. Provided

that this direct conversion does not require harsh leaching conditions, a method with fewer processing steps could i) reduce the total environmental impact of the recycling of the solar cell, ii) reduce the likelihood for the valuable CIGS material, which is also present in the sample, to undergo changes and losses from one step to the other and iii) make the total recycling process simpler, something which can be attractive for an industrialized process.

The Pourbaix diagram of Mo constructed in HSC (Fig. A1c of the Appendix), indicates that the dissolution of Mo is possible if $\text{pH} > 10$, through the formation of MoO_4^{2-} and without the need to form the MoO_3 phase first. More specifically, for $\text{pH} > 10$, the metallic Mo tends to oxidize to $\text{MoO}_2(\text{s})$, for a relatively short range of reducing potential. As the potential increases, MoO_4^{2-} is the dominant species, for a wide range of both reducing and oxidizing conditions. Therefore, the expected total reaction for the dissolution of metallic Mo towards the formation of MoO_4^{2-} is:



The highly negative value of the $\Delta G^\circ_{20\text{C}}$ of the reaction (R. 7) implies that the reaction is expected to be spontaneous, as it is greatly shifted towards the products side. No conclusions on the reaction rate can be drawn from this data though.

Regarding the CIGS compositional elements, the constructed Pourbaix plot of In (Fig. 3a) shows that, under alkaline conditions, In is expected to form mainly $\text{In}(\text{OH})_3(\text{s})$ for a broad range of pH and potential values. Se may dominantly remain as insoluble selenides, if the potential is reducing, or dissolve as SeO_3^{2-} or SeO_4^{2-} , under oxidizing conditions (Fig. 3b). Given that for the alkaline experiments no oxidizing or reducing agents were used, a mix of Se-products can be expected. Cu is expected to be present mainly in the solid form, since under reducing conditions it tends to remain as an insoluble selenide, while in oxidizing environments it tends to form $\text{Cu}(\text{OH})_2(\text{s})$ (Fig. A1a of the Appendix). Similarly with Se, a mix of Cu-containing solids can be expected. The case of Ga is similar to that of In, forming mainly $\text{GaOOH}(\text{s})$ (Fig. 1Ab of the Appendix). It is worth clarifying here that when alkaline leaching was employed, the Ag grid had already been removed and the stainless-steel had already been passivated in a previous process step (see Section 4.3). Therefore, no reactions of Ag, Cr and Fe in alkaline solutions are investigated.

To sum up, from a thermodynamic point of view, the following scenario was considered likely to happen, during alkaline leaching at $\text{pH} > 10$: the Mo layer, positioned between the stainless-steel substrate and the CIGS layer, was expected to dissolve, eventually leaving the CIGS layer unsupported. The CIGS was expected to dissolve partly, as the presence of some insoluble Cu selenides was predicted. In and Ga, as well as some Cu, were expected to mainly form insoluble hydroxides and some Se would also dissolve in the leachate. Given that undissolved selenides of Cu could remain on the cell, there was a chance for the CIGS material to be recovered unaffected in the solid form, if its reactions with the leaching agent had a much lower rate than the dissolution of Mo. Therefore, the rate of the reactions had to be tested experimentally.

Finally, in some experiments of alkaline leaching, tartaric acid was also added in the solution mix. This acid has $pK_{a1}=2.98$ and $pK_{a2}=4.38$ [92] and it is known from the literature that it can react with Mo, towards formation of several different complexes [93-95].

3.3. Considerations regarding the processes developed in this work

The aim for the developed processes in this thesis was to solve the problem of the use of harsh recovery conditions for the recycling of CIGS solar cells, while at the same time achieving high recovery and selectivity. The use of HNO_3 and $NaOH$ (with or without the addition of tartaric acid) as the only chemicals in the studied processes is advantageous, not only for its simplicity, but also due to the already existing broad knowledge and experience on how to work with them, in case of future scale-up of the process. Although HNO_3 is considered to be more expensive than other common acids [42], its oxidizing ability renders it nevertheless to be a cost-effective leaching agent, while, simultaneously, it is expected to passivate the stainless-steel substrate of the solar cell and reduce in this way the leaching of the unwanted Cr and Fe impurities. Finally, since the reactions used in the particular thesis take place in aqueous solutions, any NO_x and SeO_2 gases produced are expected to react with water, towards the formation of soluble HNO_3 and H_2SeO_3 , respectively, reducing potential gaseous emissions and environmental impacts from these. Finally, the fact that this research aims to use relatively low concentrations of the leaching reagents (no more than 2 M) while still achieving high recoveries ensures also to minimize formation of gaseous products as well as potentially lower expenses for purchase of chemicals.

4. Materials and methods

The main leaching agents used for the acid and alkaline leaching experiments performed in this thesis were HNO_3 and NaOH , respectively. In some cases of alkaline leaching experiments, tartaric acid was also added, aiming for the formation of tartrate anion as a potential complexation agent. The same type and product of solar cell, i.e. a CIGS solar cell with a flexible stainless-steel substrate and a Ag conductive grid, was used in all of the experiments. Different experimental set ups were used for the various leaching experiments, depending on the different needs. Elemental characterization of the liquid samples was performed with Inductively Coupled Plasma-Optical Emission Spectroscopy (ICP-OES). Morphological studies of the solid samples were conducted mainly with Scanning Electron Microscopy (SEM) and a few of them with an Optical Microscope. Elemental analysis of the solids samples was performed with Energy Dispersive X-ray Spectroscopy (EDS) and the identification of their crystalline phases with Powder X-ray Diffraction (XRD). The content of organic materials in solid samples was measured using ThermoGravimetric Analysis (TGA) when required.

4.1. CIGS solar cell samples

The solar cell samples used throughout this work were all provided by the Swedish manufacturing company Midsummer A.B. and each of them had a size of $15.6 \times 15.6 \text{ cm}^2$. They were all flexible CIGS solar cells with a stainless-steel substrate, a Ag conductive grid and TCO layer made of ITO. Other important layers present in the cell, as well as information on the elemental composition, morphological characteristics and crystalline structure of various layers were revealed after characterization of the initial samples (called “untreated samples” onwards) took place and this information is presented later in Section 5.1. For the performance of the experiments, the solar cell samples had to be cut into smaller pieces of similar size and composition, so that they fit into the leaching containers. A picture of the untreated sample and the way it was cut for the acid and alkaline leaching experiments is presented in Fig. A2 of the Appendix.

4.2. Chemicals

Concentrated HNO_3 69% (Suprapur, Merck) diluted with Milli-Q (MQ) water with a resistivity of $18.2 \text{ M}\Omega\cdot\text{cm}$ was used for all the acid digestion and leaching experiments, as well as for the dilution and acidification of all the liquid samples whose elemental composition was determined with the ICP-OES. NaOH pellets (purity >98%, Merck) dissolved in MQ water for the alkaline leaching experiments. In some of the alkaline leaching experiments, DL-tartaric acid ($\geq 99\%$, Sigma Aldrich) was also added in the reaction vessel.

4.3. Experimental

Different experimental set ups and equipment were used for the experiments, depending on the specific needs. In short, a characterization of the untreated solar cell took place first, in order to offer a reference for the evaluation of the impact of the various treatment methods that were later tested on the samples. The first recycling method investigated was acid leaching experiments aiming to the dissolution of Ag and In. These experiments explored the idea of recovering Ag and In by first dissolving them. For the conditions which offered the highest recoveries of the two metals, a few additional experiments were performed: one for checking if further leaching of the treated samples was possible and one for checking the leaching capacity of the same solution during multiple leaching cycles. All these experiments were performed at ambient temperature (~ 20 °C).

A different approach tested was the recovery of Ag and the In-rich ITO layer as solids. These experiments were performed using US-leaching, aiming to selective dissolution of layers placed below the targeted ones and liberation of the solid Ag and ITO in particulate form from the cell's surface, due to the action of US. As this approach gave very promising results, the remaining cell, consisting of the stainless-steel substrate and the layers up to the CIGS, was then used for the subsequent alkaline leaching experiments.

The alkaline leaching experiments which followed were primarily aimed at investigating the possibility of leaching metallic Mo with NaOH solutions of concentrations 0.1-0.5 M at ambient temperature. Then a split-plot factorial experiment followed, in order to investigate the effect of several factors on the Mo leaching yield during alkaline leaching. Finally, based on the conclusions drawn from the results of the analysis of the factorial experiment, two final experiments with alkaline leaching were performed, aiming to the selective and efficient recovery of the CIGS layer as a solid fraction, through selectively dissolving the Mo layer.

The solid samples were always washed with Milli-Q water after the completion of the experiments and let air-dry, before any analysis took place. In the case an ICP-OES analysis of leaching solution was required, the samples were collected, prepared and measured the same day, since precipitation of a few elements had been observed with time. All experiments were performed in triplicates.

Finally, regarding the experimental conditions, it should be clarified that the surface to liquid ratio (A:L) was used instead of the S:L. The reason behind that was the very small concentrations of the target elements in the solar cell samples, as all valuable elements were present in thin films. As a result, the total mass of the sample would be almost equal to the mass of the stainless-steel substrate and any differences in the samples' masses would be due to differences between the masses of the substrates, which could be misleading. Therefore, instead of the mass of the sample, the geometrical flat surface area of it was used (for example, a sample with dimensions 4.0×4.0 cm² had a geometrical flat surface area of 16 cm²).

4.3.1. Experimental procedures and setups

The different experimental procedures followed during the performed experiments are presented below. Detailed procedures for sample preparation before analysis are also described in this section.

4.3.1.1. Digestion of the untreated solar cell for characterization purposes

Acid digestion of the samples was performed for characterization purposes, mainly targeting the quantification of the total Ag and In in the cell. The digestion was performed using 8 M HNO_3 at $\sim 20^\circ\text{C}$ and A:L=1:3 cm^2/ml . The experiments were conducted by immersing the sample in the acid solution of proper volume, before the mechanical stirring (RSLab-3 mechanical stirrers) at 200 rpm was started. Translucent plastic vessels were used as reactor containers and these were covered with a lid (with a small hole in its center, so that the mechanical stirrer can go through) in order to reduce evaporation (only ~ 0.7 ml of solution evaporated in 24 h). Alkaline digestion was performed in order to quantify the total amount of Mo in the solar cell. The alkaline digestion conditions were 1 M NaOH at $\sim 20^\circ\text{C}$ and A:L=1:3 cm^2/ml . The sample was immersed in the alkaline solution, the plastic container used as a reaction vessel was closed with a lid and stirring at 200 rpm was applied, using an orbital shaker (PSU-10i by Grant-bio). In all cases, the progress of the digestions was checked by determining the elemental composition of the solution at specific time points. The completion of the dissolution of the target elements was finally checked with SEM-EDS analysis of the solid phase. It should be clarified that only complete digestion of specific elements whose quantification was of vital importance for this research was attempted, not of all the elements present in the cell.

4.3.1.2. Acid leaching targeting the dissolution of Ag and In

Acid leaching experiments for investigating the effect of HNO_3 concentration, A:L and leaching time on the leaching yield and efficiency of Ag and In were performed, using exactly the same experimental set up and procedure as for the case of acid digestion experiments, described in Section 4.3.1.1. Three different HNO_3 concentrations and three different A:L were selected and all the possible combinations between them were tested. More specifically, the selected concentrations were 0.1, 0.5 and 2 M and the A:L values 1:7, 1:5 and 1:3 cm^2/ml . As soon as the conditions offering the highest efficiency in Ag and In leaching were found, the leached samples were subjected to one more leaching cycle, under exactly the same conditions, for investigating the possibility of increasing the total leaching yield by refreshing the leaching solution. This experiment not only had an economic interest, but it could also give information on the leaching mechanism. The leaching yields of all these experiments were checked in predetermined time points by measuring the concentration of the elements present in aliquots taken from the leachate.

Another experiment performed under the conditions offering the highest Ag and In dissolution, was investigating the repeated leaching capacity of the solution. Reuse of the leachate can reduce costs in case of upscaling of the process and the concentrations of dissolved elements play a significant role in the success of subsequent refining/recovery methods [96]. For this purpose, as soon as one leaching cycle was completed, the leached sample was replaced by an untreated one and another leaching cycle started. In other words, the same leaching solution was reused in the new leaching cycle. Ten leaching cycles were performed in total, because, in case of even more cycles, extensive evaporation of the solution with time would give unreliable results. Agitation was performed using an orbital shaker (PSU-10i by Grant-bio) at 200 rpm. The elemental composition of the leachate was measured after each leaching cycle.

4.3.1.3. US-leaching targeting the recovery of Ag and ITO in solid form

US-leaching was tested as an alternative route to the dissolution of Ag and In, as the new approach was aiming for the liberation of Ag and the In-rich ITO from the cell's surface as solids. More specifically, selective leaching of layers placed underneath Ag and ITO was targeted with the use of dilute HNO₃, while the action of the US would assist the liberation of Ag and ITO (which would have remained unsupported after the leaching of the layers underneath them), in solid form. For conducting the US-leaching experiments, the sample was immersed in a 0.1 M HNO₃ leaching solution of proper volume, so that A:L=1:3 cm²/ml, contained in a glass beaker. The beaker was placed in a US bath (model USC-THD/HF by VWR, 230 V version, 132 kHz US frequency and 80 W output power) and US-leaching at the US power of choice was performed. The two US power settings selected for investigation were the minimum and maximum power setting of the bath. These values were indicated by the manufacturer as "power 1" for the 40% and "power 9" for the 100% of the maximum power of the bath (i.e. the minimum power was about 32 W and the maximum of about 80 W). In order to keep the temperature as constant as possible, and be able to make valid comparisons between experiments, the temperature of the water of the US bath was kept in the range of 22-30 °C by refreshing the water when necessary. The effect of the treatment conditions on the liberation of the solid materials with time was checked visually and under the microscope.

The results were used in the development of a US-leaching process for the recovery of the solid Ag and ITO, characterized by high recovery efficiency and selectivity. In order to describe this process, it is necessary to already mention that the US-leaching experiments described previously concluded that the minimum US power was suitable for selective and efficient removal of ITO and the maximum US power was suitable for a complete and selective recovery of the Ag grid. These conclusions, along with the selection of the suitable ultrasonication times, made the development of a 2-step US-leaching process for selective and highly efficient recovery of solid Ag and ITO feasible. The steps of the process are described in Fig. 4: In the first step, the sample was US-leached for 3 min at the minimum US power setting, in order to selectively remove the ITO. The liberated solids and leachate were separated from the remaining cell, which was supplied with fresh leaching solution and then subjected to a second US-leaching step. In this step the maximum US power was applied, aiming to the liberation of

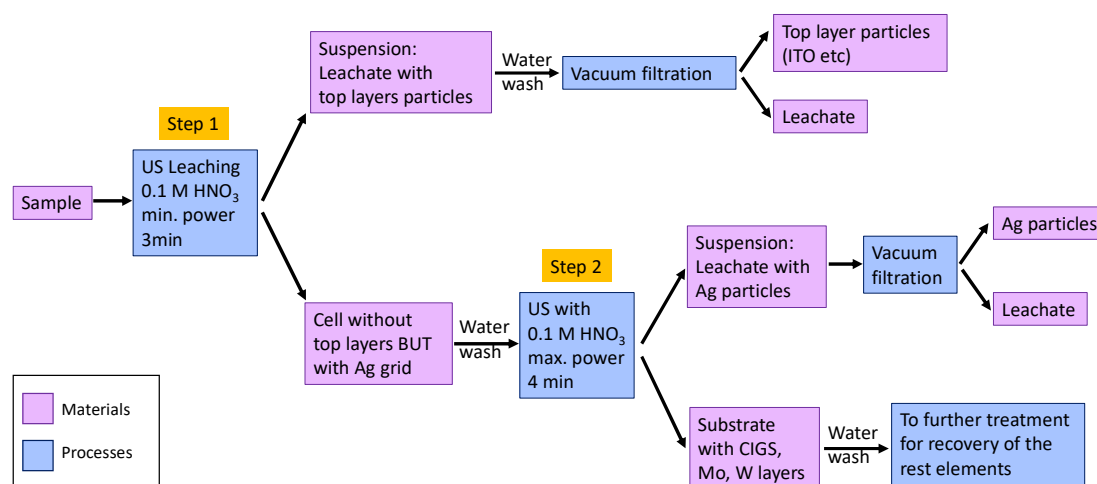


Fig. 4: Graphical representation of the developed 2-step US-leaching process for selective recovery of ITO and Ag particles from CIGS solar cells.

the Ag grid. The resulting fractions were separated again and characterization of all the fractions of the process followed.

The ITO purity was determined by digesting a known amount of the liberated solids coming from the first US-leaching step in a 4 M HNO₃ solution at ~20 °C and checking the progress of the digestion with time by determining the elemental composition of aliquots taken from the digestate. A similar digestion procedure was followed for the particles recovered from the second US-leaching step. However, in the case of Ag, both its purity and recovery efficiency were determined by digesting the recovered particles. It should be clarified here that, in order to avoid any losses of the Ag particles during filtration, when the Ag recovery efficiency had to be determined, the liberated particles were not filtered. Instead, they were left in the beaker with the original leachate and the proper amount of HNO₃ for their digestion was added in situ (the cell had been removed though).

4.3.1.4. Alkaline leaching investigating the possibility of direct Mo dissolution

The possibility of leaching directly the metallic Mo layer (without formation of MoO₃ first in a separate step) from the part of the cell remaining after the 2-step US-leaching process (i.e. the stainless-steel substrate and any layer deposited on top of it up to the CIGS layer) was investigated through testing three different NaOH concentrations, equal to 0.1, 0.3 and 0.5 M, at ~20 °C and A:L= 1:3 cm²/ml. These experiments were performed by immersing the sample in the leaching solution contained in a close plastic container and applying agitation at 200 rpm, using an orbital shaker (PSU-10i by Grant-bio). The progress of the leaching reaction with time was checked by taking aliquots of the leachate at predetermined time points and measuring their elemental composition.

4.3.1.5. Split-plot factorial experiments on factors affecting the alkaline leaching of Mo

As soon as it was confirmed that direct leaching of metallic Mo with alkaline solutions was possible, factorial experiments were performed, in order to identify the factors and their interactions which are significant for the leaching recovery of Mo. Five factors were chosen as design factors: the leaching temperature (A), the presence of a sodium tartrate in the leaching solution (B), the pH of the leaching solution (C), the A:L (D) and the leaching time (E). The min/max levels of the factors were decided to be the ones indicated in Table 1. It is worth noting that factor B is a qualitative factor, in this case meaning that B was either absent (L1) from or present (L2) in the leaching solution. The concentration of the sodium tartrate was the same for all runs in which it was present, at about 0.25 M. Due to limited resources, an unreplicated split-plot design consisting of $2^5=32$ runs was chosen, with factors A, B and C as whole-plot (WP) factors (due to many practical difficulties with changing them) and factors D and E as Sub-plot (SP) factors. A graphical representation of the experimental design is presented in Fig. 5. Details on how the design of split-plot factorials is performed can be found in Section A3 of the Appendix.

Table 1: Factors investigated for Mo alkaline leaching and their levels.

Factor		Level			
Name (units)	Symbol	Min		Max	
		Physical value	Coded value	Physical value	Coded value
Temperature (°C)	A	30	-1	50	1
Presence of salt	B	L1	-1	L2	1
pH	C	10	-1	12	1
A:L (cm ² /ml)	D	1:6	-1	1:3	1
Time (h)	E	8	-1	24	1

The experiment was conducted by pouring the desired amount of leaching solution into a plastic container for each of the runs, immersing the sample in it, closing the container and placing it into a shaking water bath (SW23 by Julabo) at 150 rpm, so that leaching temperatures higher than the ambient could be reached, for the indicated leaching time. The order in which the WP were performed was determined randomly and it is the one shown in Fig. 5. All the SP of a particular WP were run simultaneously in the water bath and the position of each container was selected randomly. Immediately after the completion of a run, the elemental composition of its leachate was determined.

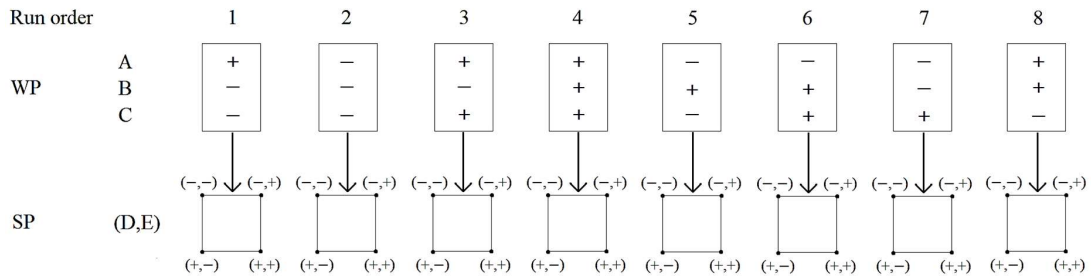


Fig. 5: Graphical representation of the unreplicated split-plot design with 3 WP factors and 2 SP factors, all at 2 levels each, performed for investigating the factors and their interactions affecting the leaching of Mo.

4.3.1.6. Alkaline leaching of Mo targeting the recovery of CIGS in solid form

Two final experiments, investigating the selective and efficient recovery of the CIGS as a solid through the alkaline leaching of Mo, were performed with an alkaline solution of pH=11 and A:L=1:6 cm²/ml at 50 °C. The difference between the two experiments was that in the first one only NaOH was present in the initial leaching solution, while in the second a mix of NaOH and sodium tartrate (coming from the reaction of tartaric acid with NaOH) was used. The specific conditions were selected based on the conclusions drawn from the split-plot factorial experiments described in Section 4.3.1.5.

The experiments were conducted using an automatic titration system (905 Titrand, Metrohm), in order to keep the pH constant. Before leaching started, an initial solution, contained in a borosilicate vessel with a lid with holes, so that the mechanical stirrer, the pH electrode (6.0260.010, Metrohm) and the ORP electrode (6.0451.100, Metrohm) could pass through it, was first let to reach about 50 °C and then titrated to pH=11 using a NaOH solution of 1 M. In the first experiment, the initial solution was just MQ water. In the second experiment, the initial solution was 0.5 M NaOH and 0.25 M tartaric acid. From the reaction of these two, a solution of sodium tartrate with pH close to neutral was formed (i.e. after the titration, only NaOH and sodium tartrate should be present in the aqueous solution). In both experiments, as soon as the leaching solution was heated up and titrated to pH=11, a blank sample was taken, in order to be used for matching the sample matrix of the ICP-OES standard solutions with the sample matrix of the unknowns. Finally, the sample was immersed into the leaching solution and the leaching process started. The titration was automatically controlled and all the data (added volume of NaOH, pH and ORP of the leachate) were recorded using Tiamo 2.5 software. Sampling was performed at predetermined time points and their elemental composition was analyzed, so that the progress of leaching can be followed.

Finally, the experiments were repeated for the leaching time at which high selectivity and efficiency in the CIGS recovery was achieved and two different methods were tested for removing the CIGS layer after the successful leaching of Mo: in the first method the sample

was placed in a beaker along with its original leachate and treated at the maximum US power setting in the US bath. The treatment lasted until all the CIGS material was removed from the substrate or for up to 60 min, if its removal was not complete until that moment. The second method was brushing (a toothbrush of medium softness was used for this purpose) and new replicates were made for it. The recovered solids were centrifuged and washed as soon as each experimental run was completed, to avoid any precipitation of elements with time. Analysis of the leached substrates and recovered solids followed, for a comparison of the two alkaline leaching methods (i.e. with or without sodium tartrate) for Mo leaching and CIGS recovery.

4.3.2. Characterization methods

For the elemental analysis of the liquid samples an ICP-OES (iCAP PRO Duo, ThermoScientific) was used. To ensure that no changes in the samples took place with storage time (e.g. precipitation of some elements), collection, preparation and analysis of the samples were performed the same day. All collected aliquots were filtered with a 0.45 μm syringe filter and then appropriately diluted prior to analysis using HNO_3 of such concentration so that the diluted sample contained 0.5-1 M HNO_3 . Dilution was necessary, in order to ensure that all elemental concentrations were within the linear range of the calibration, while acidification prevented or slowed down possible precipitation reactions. The concentrations of Ag, Cr, Cu, Fe, Ga, In, Mg, Mo, Se, Sn, Ti, W and Zn in digestates and leachates were quantified using elemental standards (prepared from 1000 ppm elemental stock solutions, Inorganic Ventures). In all measurements, 1 ppm Y was added and used as an internal standard. A correction for the interference of Mo with the In peak at 325.609 nm was also applied, according to the instructions given in the instrument's operating manual.

The morphology of the surface of the solid samples was observed mainly with SEM (FEI Quanta 200 FEG SEM). In a few cases, morphological traits of the solid samples were studied with Optical Microscopy (Vert.A1, Zeiss), when lower magnifications were sufficient or required. The elemental analysis was performed with EDS (Oxford Instruments X-Max EDS detector) coupled with the SEM. The SEM-EDS analysis took place under various conditions (e.g. kV, spot size etc), depending on the needs of each sample. However, for the EDS analysis, a voltage of at least 20 kV was always used, in order to ensure reliable results. Especially for distinguishing between Mo and S, 30 kV was required, due to the overlap of the peaks of the two elements at low keV values. The crystalline phases of the solid samples were identified with Powder XRD (D8 Discover, Bruker), using $\text{Cu K}\alpha$ radiation. All samples were analyzed in the form of powders (i.e. if they were solids deposited on the substrate, they were first removed from the substrate mechanically). The instrument software EVA and JCPDS database were used for phase identification. Finally, in the case where the quantification of the organics content was necessary, a Thermogravimetric Analysis (TGA) with instrument Q500, TA Instruments, using air atmosphere, was performed. It should be clarified that, when solid particles were characterized, the sample had resulted by mixing the powders from the triplicates, i.e. one analysis was performed, not three, due to the very small amount of material.

5. Results and Discussion

In this section, the results of the characterization of the untreated sample and all the leaching experiments are presented. The formulas used for calculations of purities, leaching yields and efficiencies are given in Section A4 of the Appendix. Uncertainties are presented as one standard deviation for the average of the respective triplicates.

5.1. Characterization of the untreated solar cells

The surface of the CIGS solar cell samples used was completely covered with a dark-colored material, on top of which a white grid consisting of parallel lines was deposited (Fig. 6a). SEM analysis showed that the white lines had a width of about $130\ \mu\text{m}$ (Fig. 6b) and consisted of small particles (Fig. 6c). Most of these particles had a size of about $1\ \mu\text{m}$, although a few of them could reach $10\ \mu\text{m}$ or larger sizes (Fig. 6c). EDS analysis showed that these lines were the lines of the Ag conductive grid, since the particles consisted of Ag and some small amount of carbon (the residual of organic compounds used in the Ag paste).

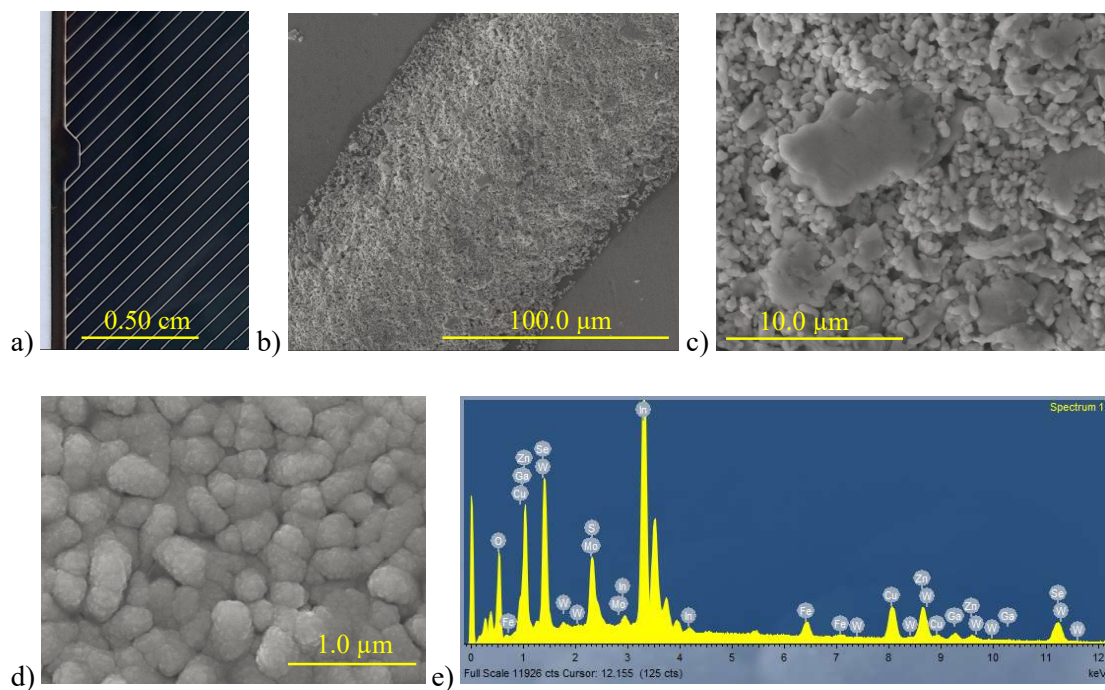


Fig. 6: Characterization of the CIGS solar cell with the Ag conductive used in this thesis. a) picture of the top surface of the solar cell with the white Ag grid lines, b) magnification of a Ag line, c) Ag particles of the Ag grid, d) top functional layer (ITO) from the area between the grid lines and e) elemental analysis of (d) (contributions from underlying layers are also present).

SEM analysis of the surface of the dark-colored area covering the cell, revealed a homogeneous nodular structure, with the nodules having a size of about 0.4 μm (Fig. 6d). Since ITO was used in the samples as the TCO layer (the top functional layer of the cell according to Section 2.2.), the observed morphology of this surface can be assigned to the ITO layer. EDS analysis revealed the presence of multiple elements in the area: Cu, Fe, Ga, In, Mo, S, Se, W and Zn (Fig. 6e). Since Fe is normally not an element used in the functional layers of a CIGS solar cell, it can be said with certainty that this signal came from the stainless-steel substrate, since the thickness of the complete stack of the functional layers of the PV cell is comparable to the size of the interaction volume of the electron beam which can exceed the 1 μm in depth and width, depending on the acceleration voltage and the density of the material [97]). In other words, the electron beam penetrated the whole stack of the functional layers and interacted with all of them. The presence of the rest of the detected elements was in good agreement with the theory, as discussed later. The absence of any Sn from the EDS spectrum, despite the presence of the ITO layer on the top of the analyzed surface, can be expected, due to the very low Sn concentration in the interacted total volume. The initial morphology of the untreated CIGS layer (or any other layer deposited below ITO) though could not be studied, due to the fact that the specific layer was sandwiched between other layers.

Table 2: Total or maximum leachable mass/cell of the elements present in the untreated solar cell sample, based on the performed acid and alkaline digestions.

Element	Concentration in untreated cell (mg/cell)	Comment
Ag	64.1 \pm 4.7	Total (acid dig.)
Cu	16.5 \pm 0.8	Max. leachable (alk. dig.)
Ga	6.8 \pm 0.4	Total (alkal. dig.)
In	43.4 \pm 5.5	Total (acid dig.)
Mg	\leq 1	Max. leachable (acid dig.), too low to say if total
Mo	70.3 \pm 5.7	Total (alkal. dig.)
Se	64.2 \pm 1.6	Max. leachable (alkal. dig.)
Sn	\leq 1	Max. leachable (acid dig.), too low to say if total
Ti	2.8 \pm 1.1	Max. leachable (alkal. dig.)
W	55.8 \pm 4.4	Total (alkal. dig.)
Zn	11.3 \pm 2.6	Total (acid dig.)

Quantification of the total concentrations of all the elements present in the untreated samples was not relevant to the scope of the particular thesis, which focused mainly on the recovery of Ag and In. Therefore, the performed digestions targeted the complete dissolution of Ag and In, but also of Mo since the alkaline leaching experiments targeted the dissolution of the latter, so

that their recovery rate can be calculated. The maximum leachable amounts of other elements achieved at the same time were also recorded, however, they were not necessarily equal to the total amounts present in the cell, as some of these elements had not dissolved completely. Depending on the element, the maximum yields were achieved between 8-24 h. The results showed that 64.1 ± 4.7 mg Ag, 43.4 ± 5.5 mg In and 70.3 ± 5.7 mg Mo were present in each solar cell. Table 2 summarizes the total or maximum leachable amount of each element per cell, for all the elements measured. Fe and Cr were omitted from the table though, since they both come from the stainless-steel substrate.

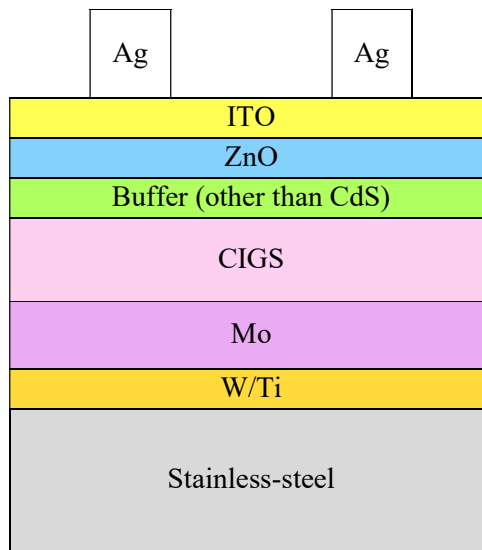


Fig. 7: Graphical representation of the untreated solar cell used in this thesis (not to scale). The known layers and materials are presented.

After detecting the elements present in the sample, determination of the composition and relative position of the functional layers was considered necessary, as this knowledge can be useful for their separation. Unfortunately, XRD could not be used to detect the unknown layers, which had very low thickness. As a result, assumptions on the layers present and their composition had to be based on the SEM-EDS and ICP-OES results, in combination with the information found in the literature. Following this approach, it was concluded that the layers illustrated in Fig. 7 were present. More specifically, between the stainless-steel substrate and the Mo back contact, at least one layer containing the detected W and Ti should have been deposited. According to literature, these two elements can be used as an alloy barrier for stainless-steel substrates, in order to hinder the diffusion of Fe into the CIGS layer and prevent in this way the reduction in cell's efficiency [98]. The Mo layer should then follow and, on top of it, the CIGS. The composition of the buffer layer was not clear, however, since no Cd was

detected and the manufacturer is known for their Cd-free solar cells, it should consist of one of the alternative materials (see Section 2.2.). It cannot be said though which one it was, since all of the alternatives discussed contain elements which were detected by the characterization techniques and all of them could also belong to other functional layers too (e.g. In is an element which can be found in the CIGS, ITO and In₂S₃ buffer layers). The presence of Zn indicated the use of ZnO as window layer, which was a reasonable assumption, due to its common use for this purpose. The small amounts of Mg detected suggested the possible presence of a Mg-doped ZnO layer. Finally, the detection of Sn with ICP-OES confirmed the presence of ITO as the TCO layer. It is important to stress that other layers might also be present, however, the ones mentioned are the most important ones in terms of both mass and function.

5.2. Results and discussion of leaching experiments

The results of the acid leaching, US-leaching and alkaline leaching experiments are presented in this section, in the mentioned order. After the presentation of each group of results, discussion follows.

5.2.1. Results of acid leaching targeting the dissolution of Ag and In

In this section, the experiments investigating the effect of HNO₃ concentration and A:L on the leaching efficiency of Ag and In are presented first. Thereafter, the results of the 2-cycle leaching process, aiming at investigating the possibility of increasing the total leaching yield of cells leached under the conditions achieving the highest Ag and In recovery in the experiments of the first section, follow. The last section consists of the results of the experiments investigating the leaching capacity of the same leachate solution under multiple leaching cycles, using untreated samples in each leaching cycle.

5.2.1.1. Results of the investigation of different HNO₃ concentrations and A:L

The results of the leaching experiments performed using 0.1 M HNO₃ and different A:L are presented in Fig. 8. These conditions were not effective for the leaching of the majority of the elements. Especially in the case of Ag, such results can be expected, since Ag is a noble metal and requires strong oxidizing conditions in order to react during the limited time (32 h) for leaching. The behavior of In was somewhat different to that of Ag, as 8-9 mg/cell of In (about 20 wt% of the total In) leached even after only 1 h of leaching and this value remained relatively constant during the 32 h, for all the A:L tested. The leaching efficiencies of Ag and In are summarized in Table 3. Although for the majority of the rest of the elements no more than trace amounts leached, Zn was an exception, since it achieved complete leaching already at 1 h under all A:L tested. Another element present in the leachates at 1 h, at relatively low concentrations (close to 5 mg/cell) under all leaching conditions, was Fe, which should have come from a passivation reaction of the stainless-steel substrate. Finally, some Mo also leached, however, the high error observed in its leaching for A:L=1:5 cm²/ml (Fig. 8b) does not allow any conclusions to be drawn for the effect of A:L on its dissolution rate.

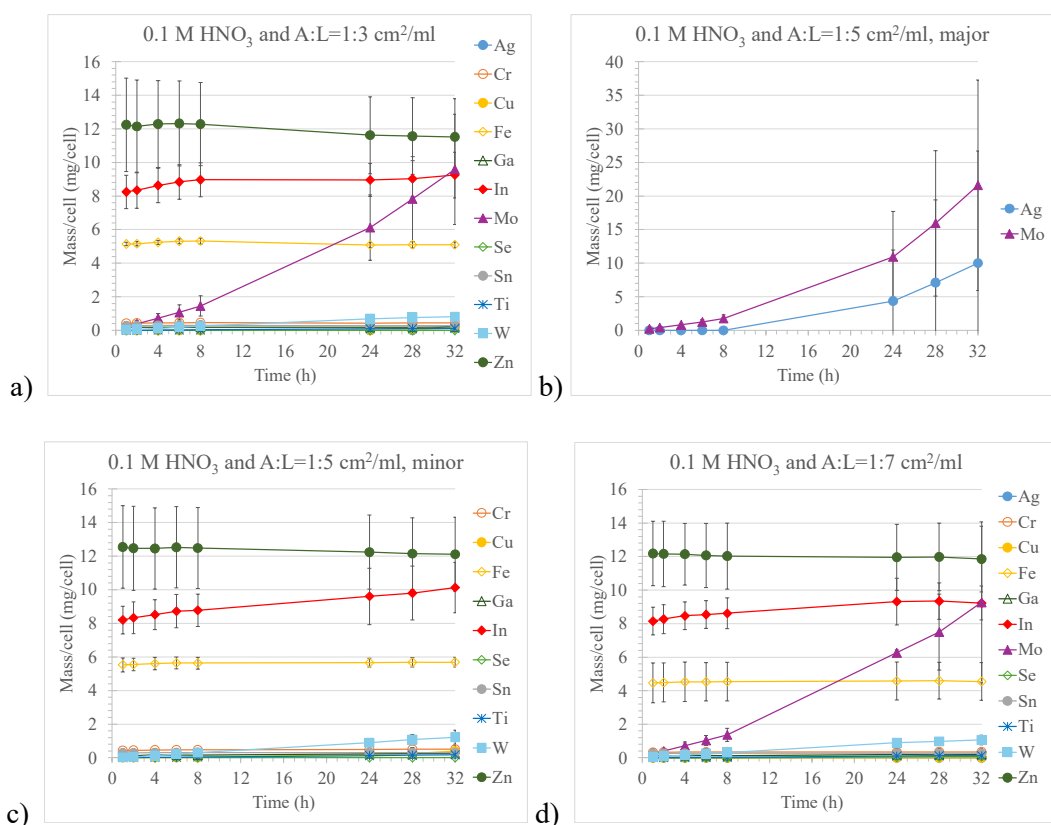


Fig. 8: Leaching yield/cell with time for leaching with 0.1 M HNO₃ and A:L equal to a) 1:3, b-c) 1:5 (b for the major and c for the minor elements in the leachate) and d) 1:7 cm²/ml.

Table 3: % Leaching efficiency of Ag and In for leaching with 0.1 M HNO₃ and A:L equal to 1:3, 1:5 and 1:7 cm²/ml.

Time (h)	A:L=1:3 cm ² /ml		A:L=1:5 cm ² /ml		A:L=1:7 cm ² /ml	
	Ag (%)	In (%)	Ag (%)	In (%)	Ag (%)	In (%)
1	n.d.	19±5	n.d.	19±4	n.d.	19±4
2	n.d.	19±5	n.d.	19±5	n.d.	19±4
4	n.d.	20±5	n.d.	20±5	n.d.	20±4
6	n.d.	20±5	n.d.	20±5	n.d.	20±4
8	n.d.	21±5	n.d.	20±5	n.d.	20±5
24	n.d.	21±5	7 -7 +12	22±7	n.d.	21±6
28	n.d.	21±5	11 -11 +20	23±7	n.d.	22±5
32	n.d.	21±6	16 -16 +27	23±6	n.d.	21±5

n.d.: not detected

At the concentration of 0.5 M HNO₃, more elements started dissolving and higher efficiencies were achieved for many of them (Fig. 9). Although this concentration still proved ineffective for leaching any Ag within the first 8 h, its dissolution efficiency exceeded 60 wt% at 24 h of leaching for all the A:L tested. More specifically, for A:L=1:3 cm²/ml, the average leaching efficiency between 24-32 h of leaching was about 87 wt% (corresponding to about 56 mg/cell), for A:L=1:5 cm²/ml it was close to 79 wt%, while for A:L=1:7 cm²/ml close to 70 wt%. The

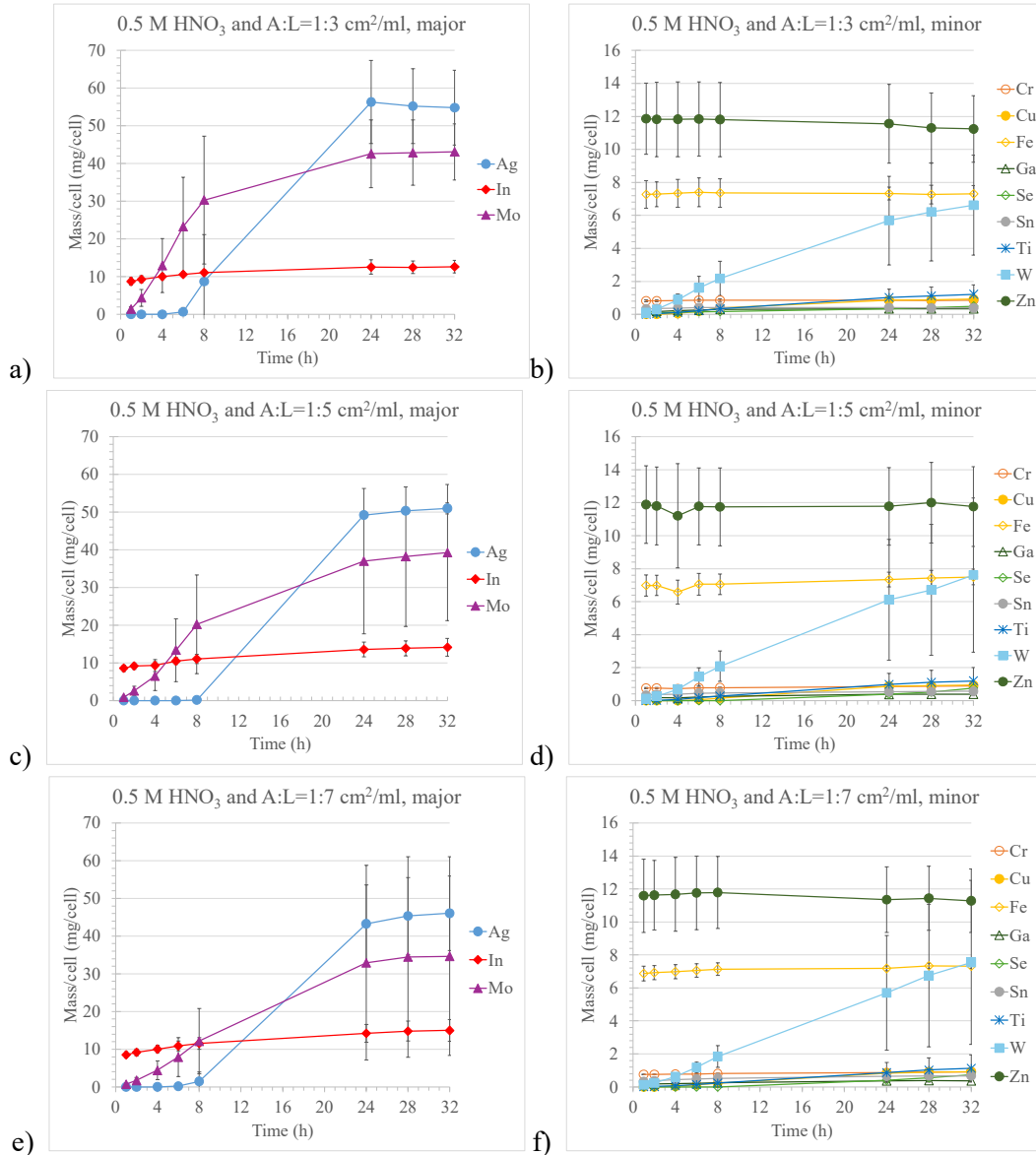


Fig. 9: Leaching yield with time for leaching with 0.5 M HNO₃ and A:L equal to a-b) 1:3, c-d) 1:5 and e-f) 1:7 cm²/ml. In the plots a, c and e the major elements in the leachate under the respective conditions are presented, while in plots b, d, and f the minor ones.

calculated efficiencies of Ag at different leaching times are presented in Table 4. It is noticeable that high standard deviations were observed and, consequently, any effect of the A:L on the leaching of Ag could not be drawn. For the same reason, it cannot be said with absolute certainty if a plateau in efficiency was achieved after 24 h or if the reaction rate was just very slow. The leaching efficiency of In also increased with an increase in the HNO₃ concentration, starting from about 20 wt% after 1 h and slowly reaching approximately 30-35 wt% (corresponding to about 13 mg/cell) after 32 h of leaching, for all A:L tested, as indicated in Table 4. An element leached in final amounts comparable to that of Ag was Mo. In contrast to Ag though, its leaching started as soon as the process started. Any effect of the A:L on its leaching rate was inconclusive though. Some W also leached; its dissolution increased linearly with time and reached about 7 mg/cell after 32 h of leaching, for all A:L tested. The behavior of Zn and Fe was the same as for lower HNO₃ concentration, with the only difference being that slightly more Fe leached for the case of 0.5 M HNO₃, reaching about 7 mg/cell. The concentrations of any other element in the leachate remained at very low levels, of no more than 1-2 mg/cell for the entire time range investigated and regardless of the A:L.

Table 4: % Leaching efficiency of Ag and In for the leaching experiments with 0.5 M HNO₃ and A:L equal to 1:3, 1:5 and 1:7 cm²/ml.

Time (h)	A:L=1:3 cm ² /ml		A:L=1:5 cm ² /ml		A:L=1:7 cm ² /ml	
	Ag (%)	In (%)	Ag (%)	In (%)	Ag (%)	In (%)
1	n.d.	20±5	n.d.	20±4	n.d.	20±4
2	n.d.	21±5	n.d.	21±5	n.d.	21±5
4	n.d.	23±5	n.d.	21±6	n.d.	23±5
6	1+2 -1	24±5	n.d.	24±5	n.d.	25±6
8	14+20 -14	26±5	n.d.	25±6	2±4	27±7
24	88+12 -24	29±8	77±7	31±9	68±21	33±10
28	86+14 -22	29±8	79±6	32±9	71±21	34±10
32	86+14 -22	29±8	80±8	33±10	72±21	35±11

n.d.: not detected

The final concentration tested, 2 M HNO₃, significantly increased the leaching efficiency of most of the elements (Fig. 10). This HNO₃ concentration was high enough to cause dissolution of the metallic Ag even from the first hour of leaching and leach more than 60 wt% of it even after 8 h (Table 5), regardless of the A:L tested. A complete leaching of Ag (i.e. about 64 mg/cell) was achieved at 24 h for A:L=1:3 cm²/ml, while for the other two A:L values the highest efficiencies were achieved at 28 h and were about 75 wt% and 80 wt%, respectively.

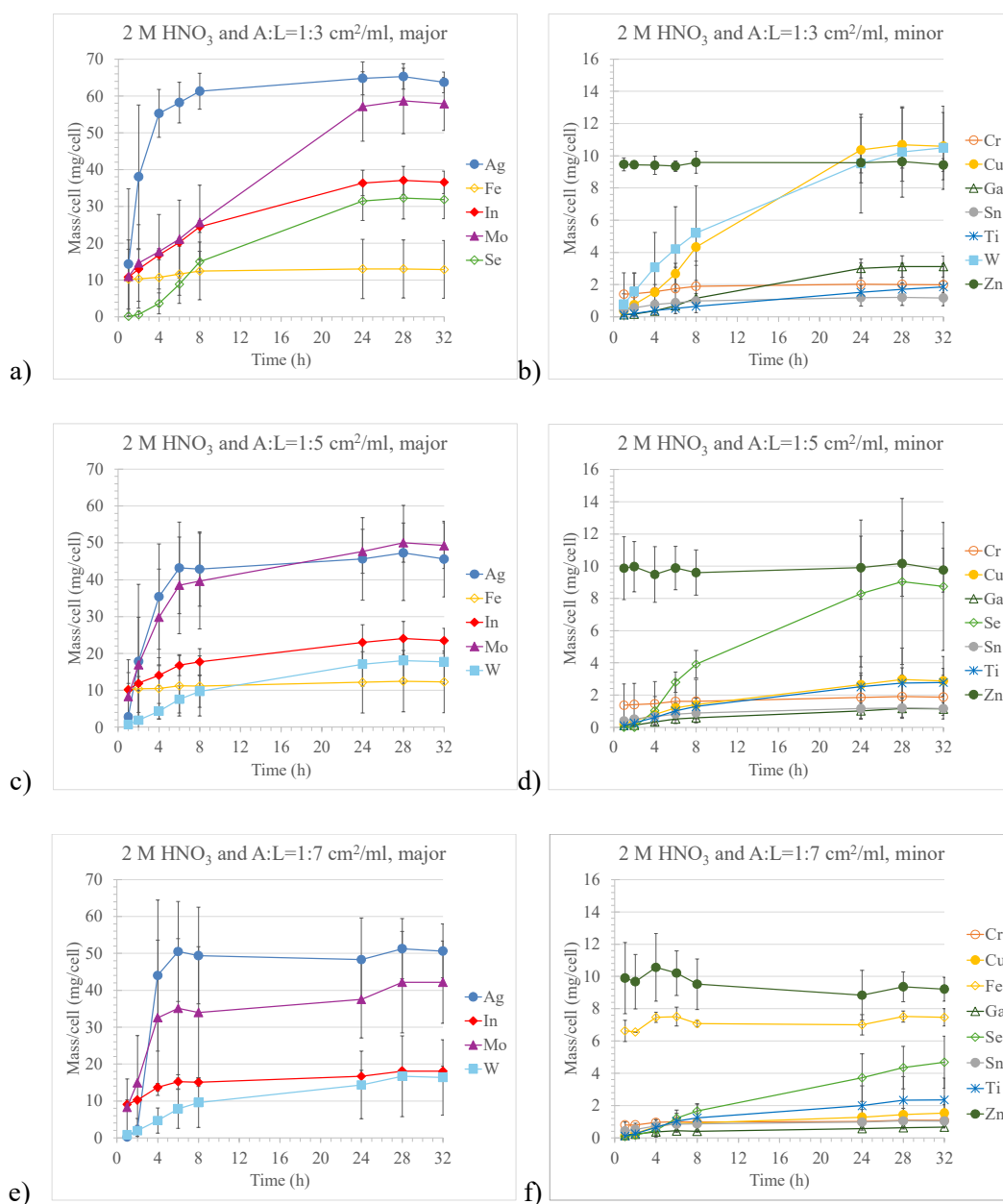


Fig. 10: Leaching yield with time for leaching with 2 M HNO₃ and A:L equal to a-b) 1:3, c-d) 1:5 and e-f) 1:7 cm²/ml. In the plots a, c and e the major elements in the leachate under the respective conditions are presented, while in plots b, d, and f the minor ones.

Even if this indicates that there was a trend of increase in the leaching efficiency of Ag with the A:L, the standard deviations were again large. Regarding the leaching of In, it started again from leaching efficiencies close to 20 wt% in the first hour and slowly increased to 85 wt%, 55 wt% and 42 wt% for A:L equal to 1:3, 1:5 and 1:7 cm²/ml, respectively, after 24 h of

leaching. The maximum In yield achieved was about 37 mg/cell. Here one can safely draw the conclusion that higher leaching efficiencies and rates were achieved with higher A:L (Table 5). Mo was again the contaminant element with final concentration in the leachate similar to that of Ag, for all A:L tested, and high uncertainties were observed. Se was one of the elements whose both leaching yield and dissolution rate increased considerably when 2 M HNO₃ was used. Its highest yield, achieved for A:L=1:3 cm²/ml, was equal to about 33 mg/cell, after a plateau was achieved at 24 h. Cu exhibited the same behavior as Se, with its highest value reaching about 13 mg/cell. The last element exhibiting an increase in its leaching yield with time was Ga, reaching a maximum yield of about 3 mg/cell after 24 h. An opposite trend in the dissolution yield and rate with A:L seemed to be the case for W leaching, although its standard deviation was considerable. The maximum yield achieved for W was close to 18 mg/cell for both A:L equal to 1:5 and 1:7 cm²/ml. Zn leaching was complete again for all A:L tested and the concentration of Fe remained constant, at values similar to the ones for 0.5 M HNO₃ (taking into account the considerable standard deviation). The rest of the elements remained at low yields again, however, the fact that their maximum yields were closer to 2 mg/cell this time indicated some increase in their leaching yield too with increase in HNO₃ concentration.

Table 5: % Leaching efficiency of Ag and In for the leaching experiments with 2 M HNO₃ and A:L equal to 1:3, 1:5 and 1:7 cm²/ml.

Time (h)	A:L=1:3 cm ² /ml		A:L=1:5 cm ² /ml		A:L=1:7 cm ² /ml	
	Ag (%)	In (%)	Ag (%)	In (%)	Ag (%)	In (%)
1	22 ⁻²² ₊₃₃	25±4	4 ⁻⁴ ₊₁₀	23±7	n.d.	21±6
2	59±35	30±5	28 ⁻²⁸ ₊₃₅	27±8	3±5	24±4
4	86 ⁻¹⁶ ₊₁₄	39±8	55±26	32±11	69±37	32±7
6	91 ⁻¹⁵ ₊₉	47±8	67±24	39±11	79 ⁻²⁷ ₊₂₁	35±9
8	96 ⁻¹⁵ ₊₁₄	56±11	67±21	41±14	77 ⁻²⁶ ₊₂₃	35±7
24	≥ 99	84 ⁻¹⁹ ₊₁₆	71±23	53±18	75±23	38±9
28	≥ 99	85 ⁻²⁰ ₊₁₅	74±25	55±18	80±19	42±7
32	≥ 99	84 ⁻¹⁸ ₊₁₆	71±21	54±15	79±17	42±8

n.d.: not detected

5.2.1.2. Results of the experiment using a fresh leaching solution for a second leaching cycle

The results of the experiments described in section 5.2.1.1. revealed that the highest Ag and In recoveries (>99 wt% and about 85 wt%, respectively) were achieved when the solar cells were leached with 2 M HNO₃ and A:L=1:3 cm²/ml for about 24 h. It can be observed (Fig. 10a and b) that, under these conditions, the leaching yields of all the compositional elements of the CIGS compound have reached a plateau. However, none of these elements leached completely, according to the maximum leachable amounts given in Table 2. The observed plateau could indicate either that the leaching reactions had reached an equilibrium or that they had stopped for some reason, e.g. due to the formation of an insoluble product layer around the particles, which hindered further leaching.

In order to investigate which of the two scenarios was true and the possibility to increase the total leaching yields of the CIGS compositional elements, the samples which had already been leached under the conditions giving the highest Ag and In yields were subjected to a second leaching cycle with same conditions, but a fresh leaching solution. If the reason for the plateau formation was that equilibrium had been reached in the first cycle, then the second cycle could cause further leaching, as there were no leaching products present in the fresh leaching solution and the leaching agent was present again at its initial concentration. In other words, under this scenario, the reaction was expected to take place again in the second cycle, according to Le Chatelier's principle. On the other hand, if the observed leaching yields during the second cycle were considerably small, that would be an indication of insoluble product layer formation.

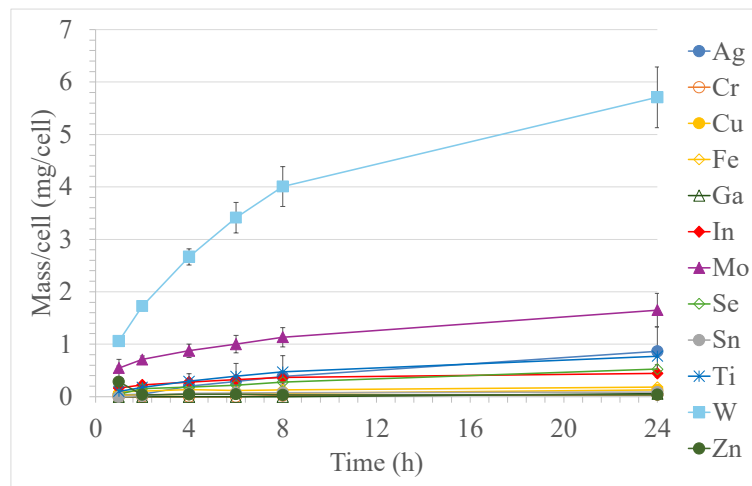


Fig. 11: Leaching yield with time for leaching with 2 M HNO₃ and A:L equal to 1:3 cm²/ml of the second leaching cycle, using fresh leaching solution.

The results of the second leaching cycle are presented in Fig. 11 and prove that a refreshed leaching solution was ineffective for dissolving the CIGS compositional elements further, as none of their yields exceeded 0.5 mg/cell at 24 h of leaching. Therefore, the plot suggests that further leaching of the CIGS layer was not possible, due to the formation of an insoluble product layer around the CIGS particles, in agreement with the predicted leaching behavior of the CIGS compound (Section 3.2.1.).

5.2.1.3. Results of multiple leaching cycle experiments using the same solution

The results of the experiments aiming at the concentration of the leachate and investigation of its leaching ability by reusing the same solution, of initial concentration 2 M HNO₃ and A:L=1:3 cm²/ml, in multiple leaching cycles with untreated samples in each cycle, are presented in Fig. 12. It can be easily observed that the concentration of the majority of elements increased with the number of the leaching cycle. The figure shows that after 10 leaching cycles the leachate contained about 850 ppm Ag and 400 ppm In. Except for these two elements, many others were present in the solution, with the major contaminants being Mo, Se and Zn, at concentrations of about 540 ppm, 270 ppm and 150 ppm, respectively. After the 10 cycles, the experiment was stopped, only due to evaporation of the solution with time (about 10 v/v % after the 10 cycles).

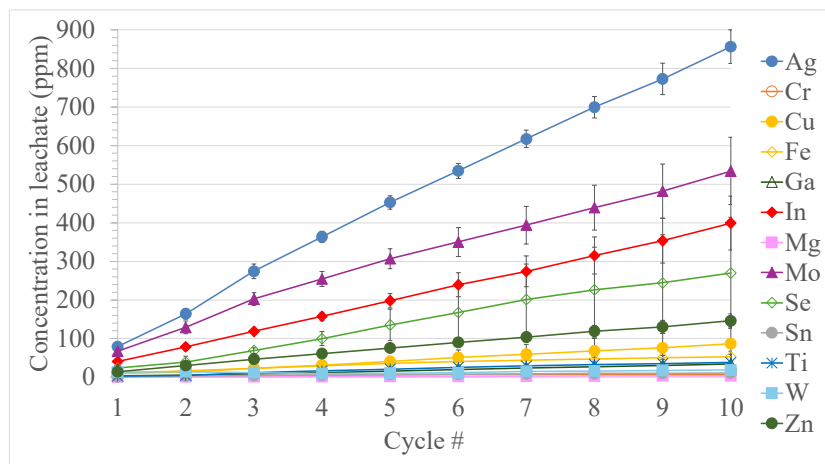


Fig. 12: Concentration of the elements present in the leachate vs cycle number for the multiple leaching cycles experiment using the same leachate.

What is not entirely clear from Fig. 12 is if the leaching yield per cycle for each of these elements had remained constant. Instead, this is shown in Fig. 13, which compares the observed concentration of each element in the leachate for each cycle with a straight line that shows the

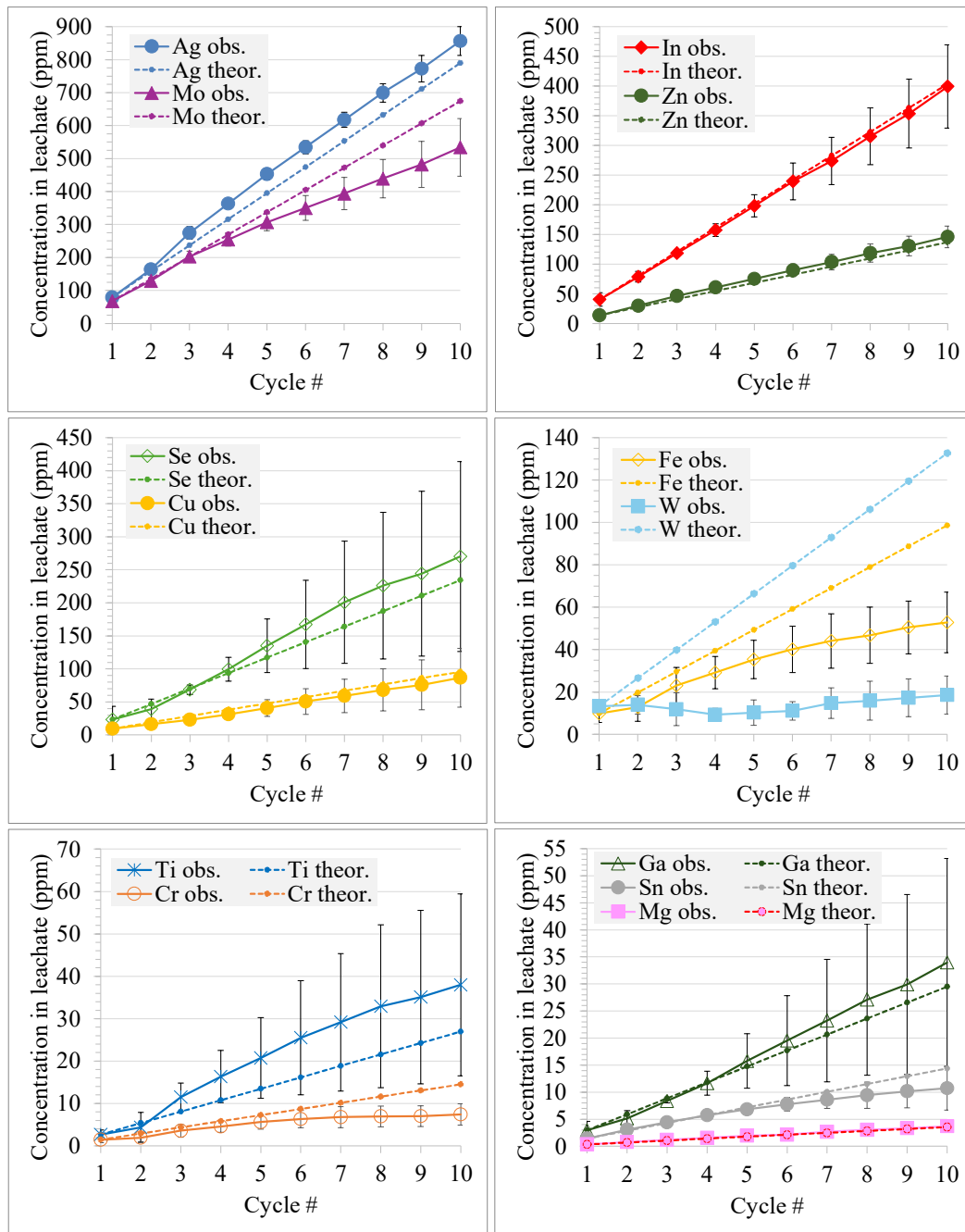


Fig. 13: Theoretical and observed concentrations of leached elements vs cycle number for the multiple leaching cycles experiment using the same leachate.

extrapolated yield from first leaching cycle. We will refer to the latter values as “theoretical” ones from now on. More specifically, the leaching solution was able to leach completely the Ag of all 10 solar cells. The fact that the observed values were a bit higher than the theoretical

might be due to sample-to-sample differences in the Ag content or some measurement error for the first cycle. Regarding the compositional elements of the CIGS material, their concentrations increased linearly, according to the predictions from the first cycle. Similar was also the case for Mg, Ti and Zn. The concentration of Mo, however, gradually fell below the theoretical line and that might be because of i) lower Mo leaching efficiency, due to the increased concentration of soluble Mo-leaching-products in the leachate (Le Chatelier's principle), probably in combination with the decrease in HNO_3 concentration with the leaching cycle, and/or ii) decreased Mo leaching rate as HNO_3 concentrations become lower and/or iii) decreased solubility of the formed oxides/acids at lower HNO_3 concentrations. Similar trends were observed for Fe, Cr and Sn, whose concentrations in the leachate increased in the first few leaching cycles and then started forming a plateau. However, a decrease in the Fe leaching efficiency was not expected. This is because in Section 5.2.1.1. it was shown that acid concentrations as low as 0.1 M HNO_3 can leach Fe within 1 h without leaching any Ag even hours later, so, given that here the Ag was able to leach completely even at the tenth leaching cycle, the concentration of HNO_3 should still be considerably high. Therefore, the plateau in the leaching of Fe might have to do with saturation of the solution in the formed soluble Fe-species. Finally, the case of W was clearly a case of saturation, immediately after the first leaching cycle, since the W concentration in the leachate remained constant afterwards.

5.2.2. Discussion on the results of acid leaching targeting the dissolution of Ag and In

The acid leaching experiments targeting the dissolution of Ag and In showed that their leaching efficiency increased with an increase in HNO_3 concentration and, in many cases, the leaching reactions proceeded faster as well. The same trends were observed for the majority of the elements present in the CIGS solar cell. This behavior was expected, as, according to Le Chatelier's principle, higher reactant concentrations shift a reaction towards the side of products. Increased reactant concentration also increases the reaction rate according to the kinetic rate laws. In the case of Zn and Fe, their concentration in the leachate remained constant after only 1 h of leaching. For Zn, this indicated a high reactivity, since complete dissolution was achieved, but for Fe the reason was most probably that a passivation layer had formed on the stainless-steel surface.

Regarding the factor A:L, for HNO_3 concentration up to 0.5 M, it did not affect significantly the leaching yields of any element. However, at the highest HNO_3 concentration tested, 2 M, In and most elements showed a tendency towards higher efficiencies and leaching rates with increase in A:L (i.e. with lower solution volumes). For the case of Ag though, it cannot be said with certainty that this factor had an effect on the Ag leaching, due to the large standard deviations. The observed trend was not expected, as normally the opposite is true, i.e. the reaction rate increases when the A:L decreases (i.e. with higher solution volumes). A reason behind the observed behavior might be a less efficient stirring of the larger solution volumes, which may have compromised the mixing and refreshing of the species at the surface of the particles. The observed trend could also be the result of better in-mixing of oxygen into the solution of low volume during stirring, as oxygen can act as an oxidizing agent, and, thus, assist

the leaching reactions. Further investigation of the matter would be required though, in order to give a more certain explanation.

Based on the results and observations made during these acid leaching experiments, it would be useful to create a scenario on how the leaching of different materials seems to take place for the range of the tested conditions: In the beginning of leaching, Zn always reacts fast with the HNO_3 and gets completely dissolved within 1 h. Within the same time, passivation of the stainless-steel takes place and gets completed. An amount of In, close to 20 wt% of the total In in the sample, also always dissolves very fast along with Zn and Fe. This In most likely does not come from the CIGS material, since no other compositional elements of it leached so fast. Therefore, it should come from another In-containing layer(s). Except for purely chemistry-related reasons, the faster leaching kinetics of these layers compared to others, could also be a result of the small thickness and relative position of them. For example, in the case of leached Fe, the fact that the bottom side of the stainless-steel substrate is completely exposed to HNO_3 enables its passivation to take place fast. In the case of Zn, this element is normally present in the CIGS solar cell in the form of oxides. ZnO reacts with HNO_3 through neutralization reactions, which are usually very fast. Thus, although the ZnO layers are sandwiched between others, they can come into contact with the acid from the sides of the sample and dissolve quickly. Similar might be the case of the quickly leachable In, if that comes from an easily soluble In-containing layer. Moreover, as the window and buffer layers are the thinnest of all main layers present in the cell (≤ 100 nm [21]), their small thickness might have also played an important role in the fast dissolution rate of Zn and the 20 wt% In, if these elements were contained in these layers.

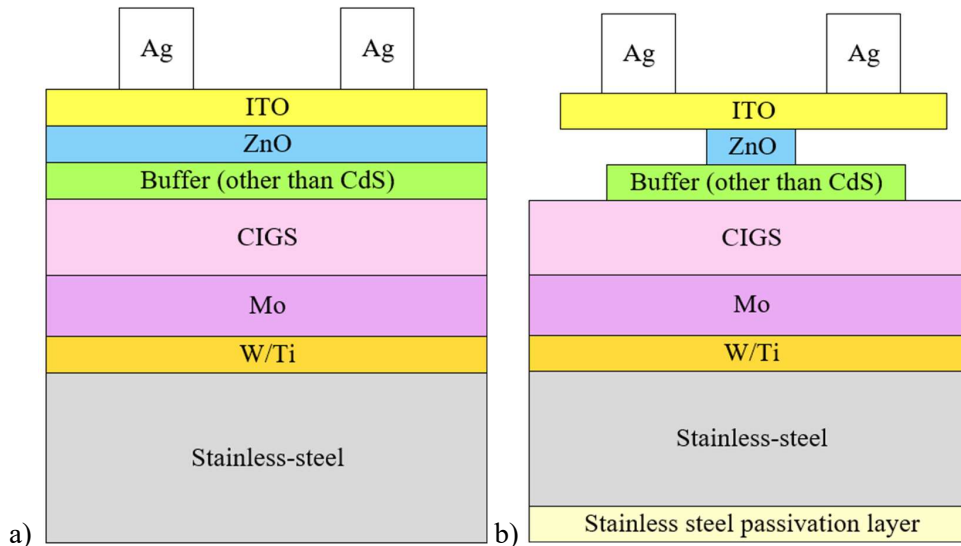


Fig. 14: Graphical representation of the state of the solar cell a) before and b) after the first few minutes of leaching with HNO_3 (not to scale).

As soon as the ZnO layer starts dissolving, a gap is left in its place and, therefore, space for the acid to start attacking the layers deposited above and beneath the ZnO layer is created (Fig. 14). For higher acid strengths, the dissolution of Ag, Mo and W then follows. Regarding the leaching of Ag, kinetics-related reasons seem to affect its dissolution, as in the experiments performed with 0.5 M HNO₃ there was almost no Ag leached until the first 6 h (despite the fact that the surface of at least some of the Ag particles was exposed to HNO₃), however, a few hours later (24 h), not only more than 60% of the total Ag leached, but a plateau in its leaching yield had already been reached. Of course, as Ag is a noble metal, a relatively slow reaction rate could be a reason behind its observed leaching behavior. Another reason for the slow dissolution rate might be that not all of the Ag particles are directly exposed to the acid, if the porosity between them is not high enough to allow unhindered access of the leaching agent. However, in that case, the particles on the top surface of the grid should have dissolved relatively fast, which was not the case. Residual organic material from the Ag paste may also cover partly the surface of some of the particles, hindering the access of the acid. Finally, a likely scenario is that a very thin layer of other products (e.g. sulphides) may form on the surface of the Ag particles, either before or during leaching, but dissolve after a few hours, allowing then the Ag to start dissolving. Regarding Mo and W, their leaching starts early in the process, although for the first 2 h of leaching their concentrations are still low. Given that these elements are present in the solar cell in their metallic form and in similar concentrations with Ag, the fact that the dissolution of these layers (which are sandwiched between other materials) always starts before the dissolution of Ag (which is placed on the top of the cell) supports the assumption that some species form on the surface of the Ag particles and make its leaching slower, except the noble nature of the metal.

The dissolution of the CIGS layer takes place last. As this functional layer is the thickest of all functional layers present in a CIGS solar cell, this might be a reason behind its slower leaching rate. Another reason is the compact chalcopyrite crystal structure of the CIGS compound and the fact that it tends to leach through product layer formation (Section 3.2.1.). A strong indication of product layer formation in the experiments of this work is that the leaching yields of all CIGS compositional elements reached a plateau after some time and complete leaching was not achieved, under any condition tested. That was the case even when a fresh leaching solution was used for continuing the leaching, after the plateau had been reached, using 2 M HNO₃ (proving that the reason behind the incomplete first leaching was not the consumption of the leaching agent). Another confirmation of the formation of insoluble products on the surface of the CIGS particles which cause the observed slow and incomplete dissolution of the CIGS is that, when the same solution of initial concentration equal to 2 M HNO₃ was used for 10 leaching cycles, the ability of the solution to leach the CIGS compositional elements did not decrease with the leaching cycle (confirming again that consumption of the leaching agent was not the cause of the incomplete leaching of the CIGS). Therefore, the results from CIGS leaching are in good agreement with the predictions discussed in Section 3.2.1. and the leaching mechanism of the CIGS compound with HNO₃ under the investigated conditions seems to take place through formation of a shrinking core of the unreacted material.

In short, the chemistry, thickness, relative position and formation of product layers on the surface of the unreacted particles seem to play an important role in the kinetics and efficiency of the leaching of Ag, In and other elements found in CIGS solar cells with HNO₃, for the range of the conditions tested. This implies that both reaction and mass transfer may control the leaching process, depending on the leached material. The leaching process begins with the fast, and soon complete, leaching of Zn and passivation of the stainless-steel substrate and some leaching of In (probably coming from a layer(s) other than the CIGS), regardless of the process conditions. Mo and W leaching follow and a bit later Ag. The nobility of the latter and possible existence of some other materials deposited/formed on its surface might be the reasons for its slower leaching rate. Complete leaching of Mo and W is not possible. The CIGS layer reacts with the leaching agent the last and its leaching seems to take place through formation of insoluble product layer on the surface of the unreacted CIGS particles, which behave as shrinking cores as leaching progresses. In total, the leaching of all materials present in the cell seems to proceed according to the reactions predicted in Section 3.2.1.

When reusing the leachate of initial HNO₃ concentration equal to 2 M and A:L=1:3 cm²/ml, the concentrations of Ag, In and most of the elements in the solar cell increase linearly with the number of the leaching cycle, for at least the first 10 cycles. About 850 ppm Ag and 400 ppm In were contained in the leachate after 10 cycles and the achievement of constant leaching efficiencies per cycle (≥ 99 wt% for Ag and 85 wt% for In) indicated that even more cycles can take place. Therefore, enrichment of this leachate as well as savings in the consumption of chemicals is possible. At the same time, the concentration of some contaminant elements like Cr, Fe, Mo, Sn and W tends to form a plateau after a number of cycles, resulting in lower contamination per Ag or In atom in the final leachate. Although there are many reasons which could potentially explain the observed trend, the high complexity of the system, when the concentrations of the plethora of elements present in it increase, makes further investigation necessary, in order to draw safer conclusions.

Finally, an observation worth discussing is the very large uncertainties in the yields of many leached elements, under all experimental conditions. There are many reasons which could cause that, like a wide distribution of particle sizes, different defects in the samples and slightly different chemical and physical properties of the cells (since the samples used in this work were real manufacturing solar cell waste, thus, some defects and cell-to-cell differences should be expected). Differences in the Ag particle size have already been discussed during the characterization of the untreated cell (Fig. 6c). An example of different amounts of Ag in two grid lines is shown in Fig. 15a-b. Fig. 15c also shows an area of the Ag grid which looks very sintered, meaning that its surface area is greatly reduced and, therefore, its leaching is expected to take place at a much slower pace compared to that of smaller particles.

From a practical point of view, the experiments showed that a complete dissolution of Ag and a considerable dissolution of In can be achieved even at room temperature, within 24 h, without the need for HNO₃ concentrations as high as the ones used in the literature, since 2 M HNO₃ proved efficient. This HNO₃ concentration, however, causes an increase in the leaching yield

of many other elements present in the cell too, introducing a considerable amount of impurities in the leachate. An example on how the increase in the HNO_3 concentration affected the leaching yields of all elements, when using A:L equal to $1:3 \text{ cm}^2/\text{ml}$, can be found in Table A1 of the Appendix. The leachate can be reused in multiple leaching cycles though and be enriched in Ag and In, as it maintains its ability to dissolve these metals efficiently for at least the first 10 cycles.

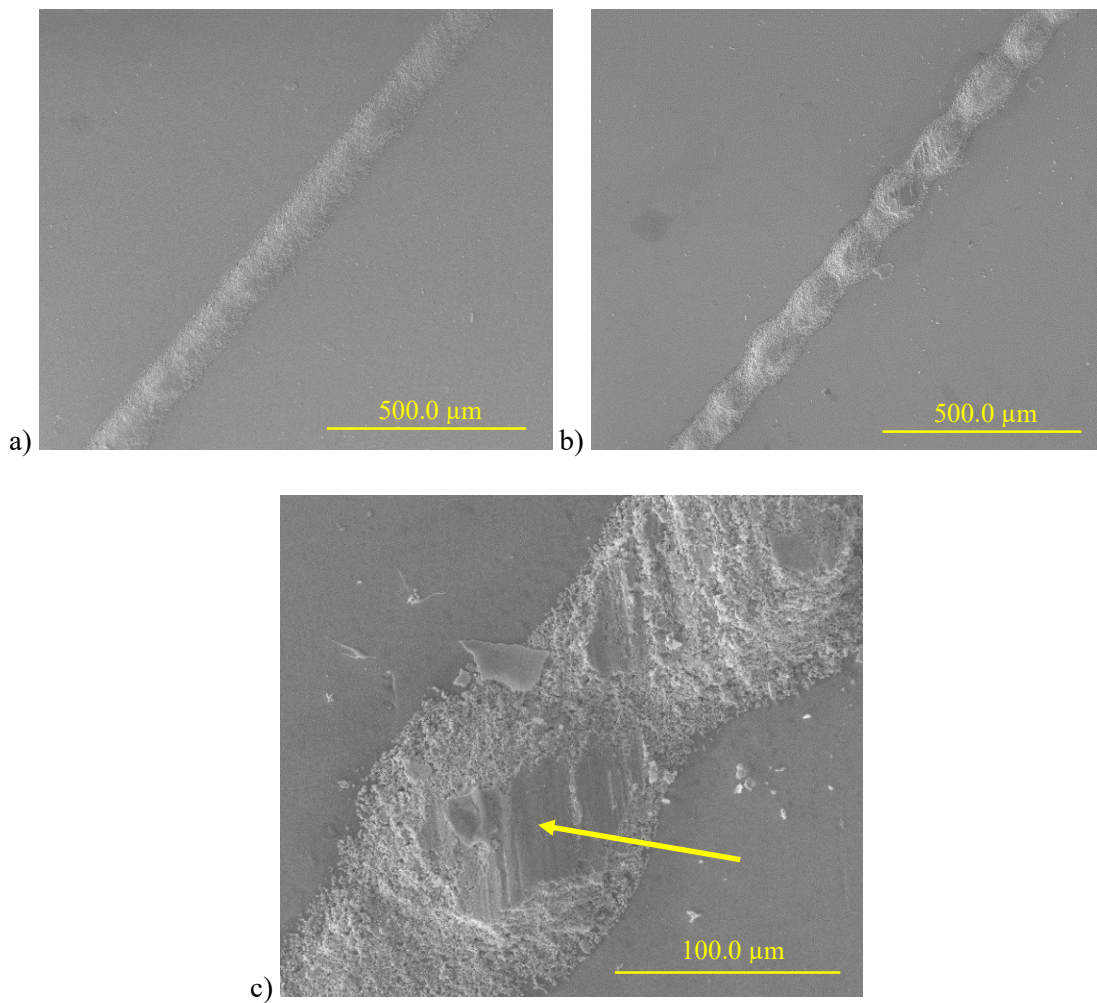


Fig. 15: a) and b) Ag grid lines of an untreated solar cell having different morphology and Ag amounts and c) a magnification of (b) showing an area with considerable loss of surface area.

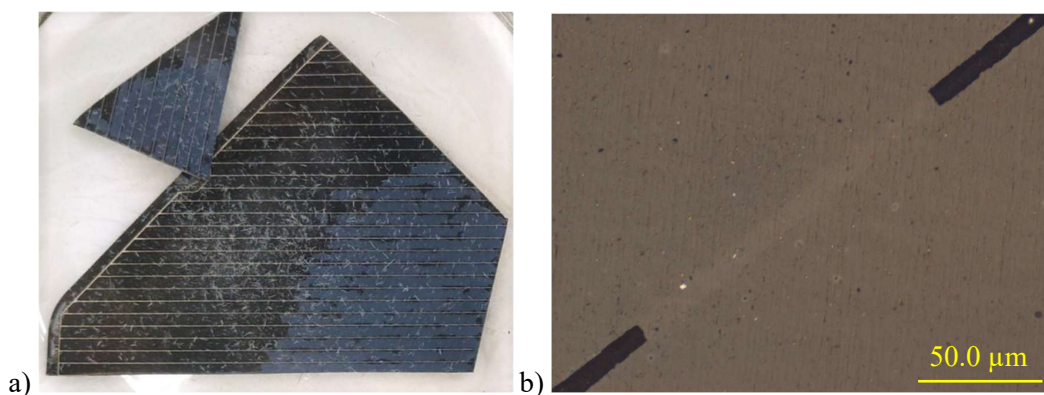
5.2.3. Results of US-leaching targeting the recovery of Ag and ITO in solid form

Since the results in previous section with acid leaching experiments showed that high leaching efficiencies of Ag and In were always accompanied by a considerable amount of contamination from other elements, a different approach was explored in order to improve the separation selectivity. Two conclusions drawn from the acid leaching experiments with 0.1 M HNO₃, i.e. that this acid concentration does not leach Ag for at least the first few hours, but it does dissolve completely all the Zn in less than 1 h, gave the idea of selectively leaching the ZnO layer. That would leave the valuable ITO and Ag on top unsupported and, thus, they could easily liberate as solid particles by applying US. The effects of US power and residence time on the selectivity and efficiency of Ag and ITO recovery were explored. Finally, a process for selectively and efficiently removing both materials was developed.

5.2.3.1. Results for the selection of the optimum US-leaching times

At the minimum US power setting, a selective removal of the top layers (i.e. those containing mainly ITO), but without a removal of the Ag grid for the first few minutes of the treatment was observed (Fig. 16a). The Ag grid remained unaffected until 4 min of leaching, when small pieces started to liberate (Fig. 16b). The amount of remaining top layer material seemed to remain unaffected for treatment times longer than 4 min (Fig. 16c). Therefore, it was concluded that 3 min treatment at the minimum US power setting was optimal for the recovery of ITO layer without losses of Ag into the recovered ITO-containing solid fraction. At the maximum US power setting, 15 min proved enough for a complete removal of the Ag grid (Fig. 17b), as the white Ag grid lines observed in the untreated cell (Fig. 17a) disappeared completely.

From those results, an optimal 2-step US-leaching process for selective and high efficiency recovery of ITO and Ag was developed. This optimum process consisted of a first step at the minimum US power setting for 3 min in order to selectively remove the top layers and then a second step at the maximum US power setting for 15 min in order to completely remove the Ag grid.



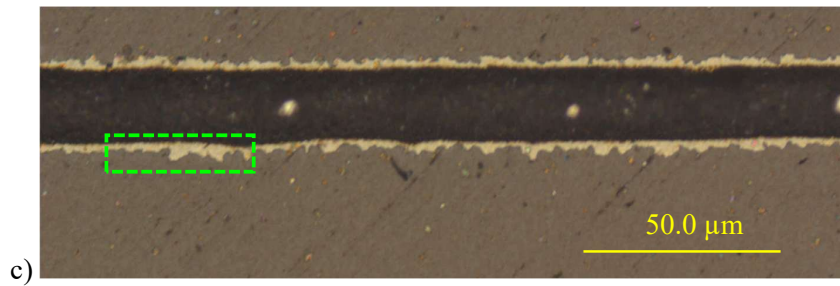


Fig. 16: Observations on the US-leaching experiments using the minimum US power setting: a) solar cell sample after 1 s (blue areas: unaffected; black areas: free of top layers; scattered particles: liberated top layers particles), b) liberation of small pieces from the Ag grid after 6 min, c) magnification of a Ag grid line from (b) with remaining top layers materials (yellowish material in the green rectangle) attached to the grid line (black line).

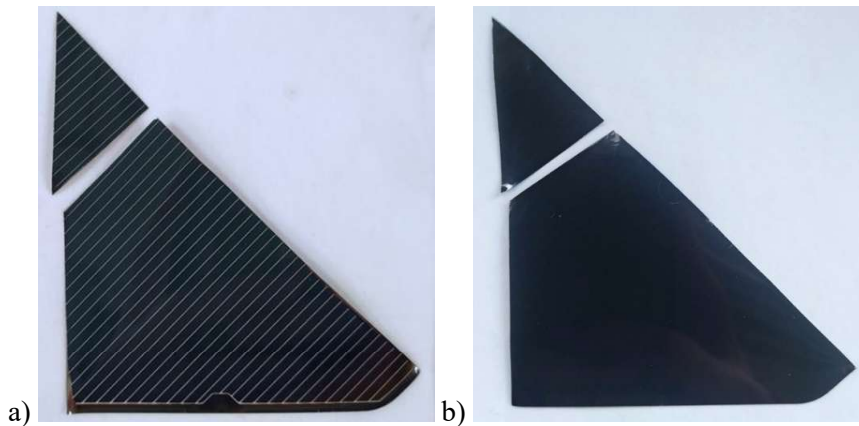


Fig. 17: Solar cell sample a) before and b) after 15 min of US-leaching at maximum US power.

5.2.3.2. Results of the highly efficient and selective 2-step US-leaching process

The results of the characterization of the leachates and recovered solid particles from the two steps of the optimal US-leaching process are presented here. Regarding the first step of the process, the elemental analysis of the leachate confirmed that no Ag dissolved during this step, since its concentration in the leachate was no more than 0.1 mg/cell (Fig. 18). It also confirmed that the major elements leached were Zn and In, along with a smaller amount of Fe, in agreement with the results of Fig. 8a. The amount of In leached was less than 10 wt% of the total In present in the cell, while for Zn it was about 75 wt%.

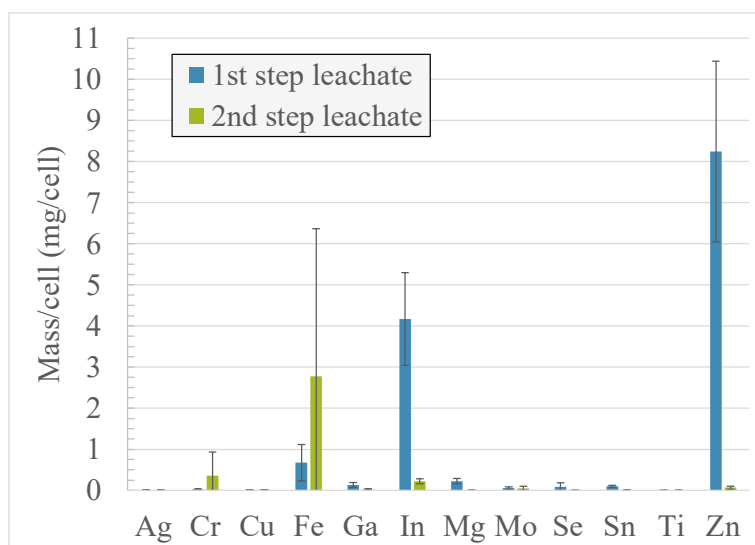
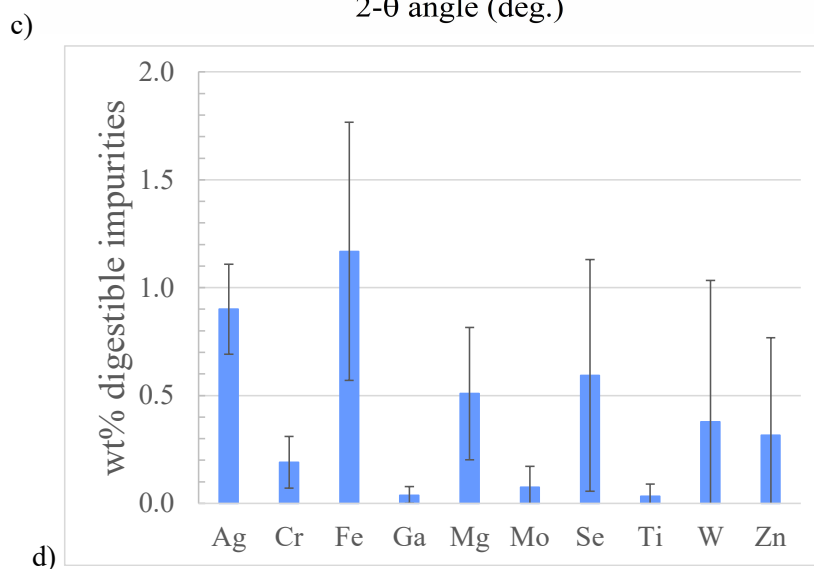
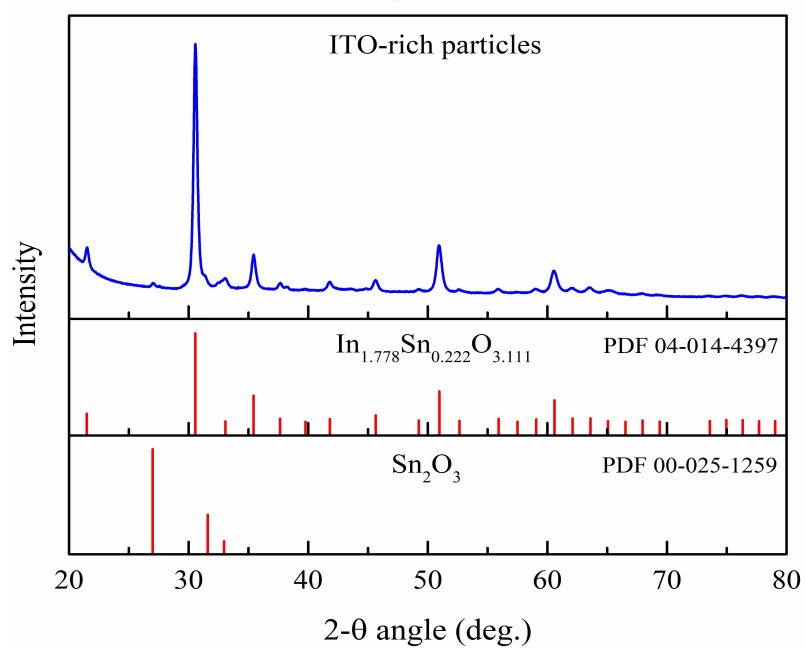
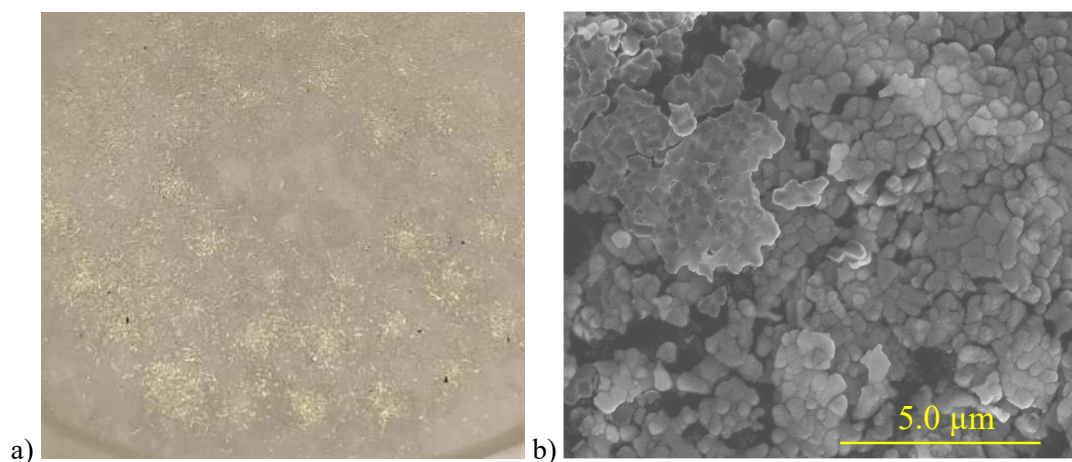


Fig. 18: Elemental analysis of the 1st and 2nd step leachates of the developed 2-step US-leaching process.

The solid particles recovered after the first step (Fig. 19a) were liberated in clusters of flake shape and had a morphology (Fig. 19b) very similar to that of the surface of the untreated sample (Fig. 6d). This similarity indicated that the particles mainly came from the ITO layer and there was no observable effect of the treatment on their morphology. The presence of ITO as the main crystalline phase of the recovered solids was confirmed by XRD analysis (Fig. 19c). A minor phase of Sn₂O₃ was also detected, which may be the result of a reaction of some Sn from ITO with HNO₃. The total ITO content of the particles, based on analysis after digestion, and assigning all the In and Sn to ITO, was concluded to be 70.36±6.08 wt%, with the main impurities being Cr, Fe, Se and traces of Ag. More specifically, the amount of Ag in the digestate was equal to 0.9 wt% (Fig. 19d) and most likely came from some scratching of the cell when tweezers were used. This amount corresponds to only 0.15 wt% of the total Ag in the cell, therefore, it is negligible. The biggest part of impurities consisted of some hard-to-digest Fe- and Se-containing particles, with some Cr present in them too (Fig. 19e). These particles were most likely residues of the selenization process, used for the manufacturing of the cell [99], which had deposited on the stainless-steel substrate. The solubility of these particles was very low and the amount which dissolved is presented in Fig. 19d, which shows only the digestible concentrations of impurities in the total mass of the recovered particles. The estimated total composition of the recovered ITO-rich particles, including both the digestible and non-digestible fraction, is summarized in Table 6. Since the exact amount of the non-digestible Cr, Fe and Se could not be quantified through the digestion, the given numbers for these elements are their minimum amounts present in the total ITO fraction (i.e. equal to their digestible amounts).



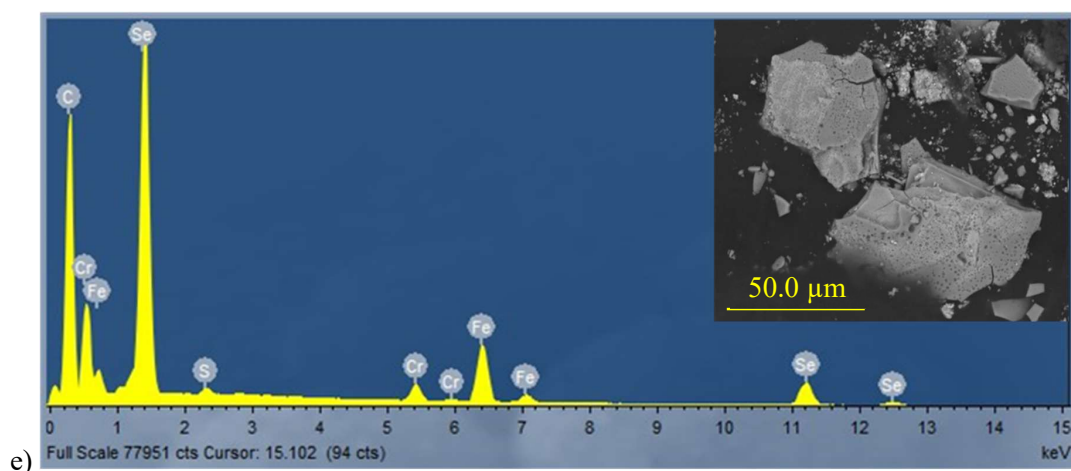


Fig. 19: Analysis of the solid particles recovered from the first US-leaching step: a) recovered particles after filtration, b) their morphology, c) identification of their crystalline phases, d) levels of the digestible impurities in the total recovered fraction, e) EDS spectrum of the non-digestible particles shown in the inset.

Table 6: Average wt% elemental composition of the two types of recovered particles after the two-step US-leaching.

	Ag	Cr	Cu	Fe	Ga	In	Mg	Mo	Se	Sn	Ti	W	Zn	Organ.	Rest (mainly O, S)
ITO-rich	0.90	>0.19	-	>1.17	0.04	52.64	0.51	0.07	>>0.59	5.29	0.03	0.38	0.32	-	<<37.87
Ag-rich	94.96	>0.01	0.02	>0.03	-	0.12	0.06	-	>0.07	0.02	-	-	0.02	3.12	<1.58

Quantification of the % recovery of ITO was not possible in a reliable way, since the total amount of ITO in the cell was unknown and the amount of Sn present in the compound (which could potentially be used for calculation purposes) was so low that it made the determination of the total Sn concentration unreliable. Therefore, the assessment of ITO recovery was based on visual and microscopic observations of the amount of the top layers material which had remained attached on the surface of the sample after the treatment. This amount was concluded to be very small, since it was located only in the area below and around the Ag grid lines, as it becomes apparent from Fig. 20a (area II). The presence of oxides, i.e. top layers, was also confirmed by the detection of an oxygen peak in the EDS spectrum of the same area (Fig. 20b). The bulk area between the grid lines was free of such leftovers (area III), as the absence of the O peak in its EDS spectrum indicated (Fig. 20c), proving that the treatment removed all layers placed above the CIGS layer. These observations suggested that the recovery of ITO could be considered as ≥ 99 wt%.

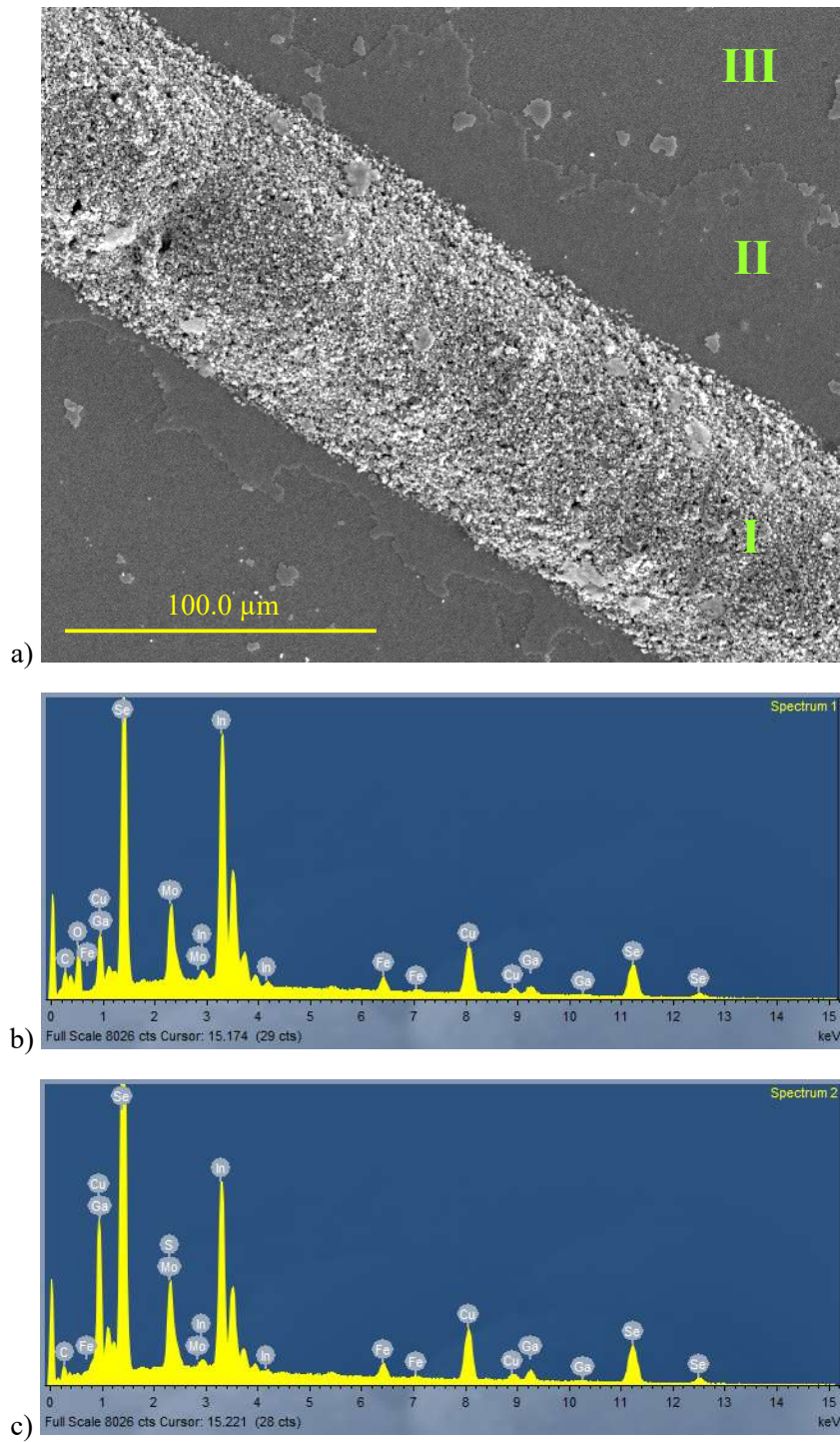


Fig. 20: a) SEM image of the area around an Ag grid line after the first step of the 2-step US-leaching process and b, c) EDS spectra of the regions II and III of (a), respectively. The areas I, II and III correspond to the Ag grid, top layers leftovers and CIGS layer, respectively.

Continuing with the second step of the process, the Ag grid again remained unleached, as confirmed by the elemental analysis of the leachate (Fig. 18). No losses of In were observed in the leachate either. It was mainly the stainless-steel elements which leached during this step, yet at low concentrations.

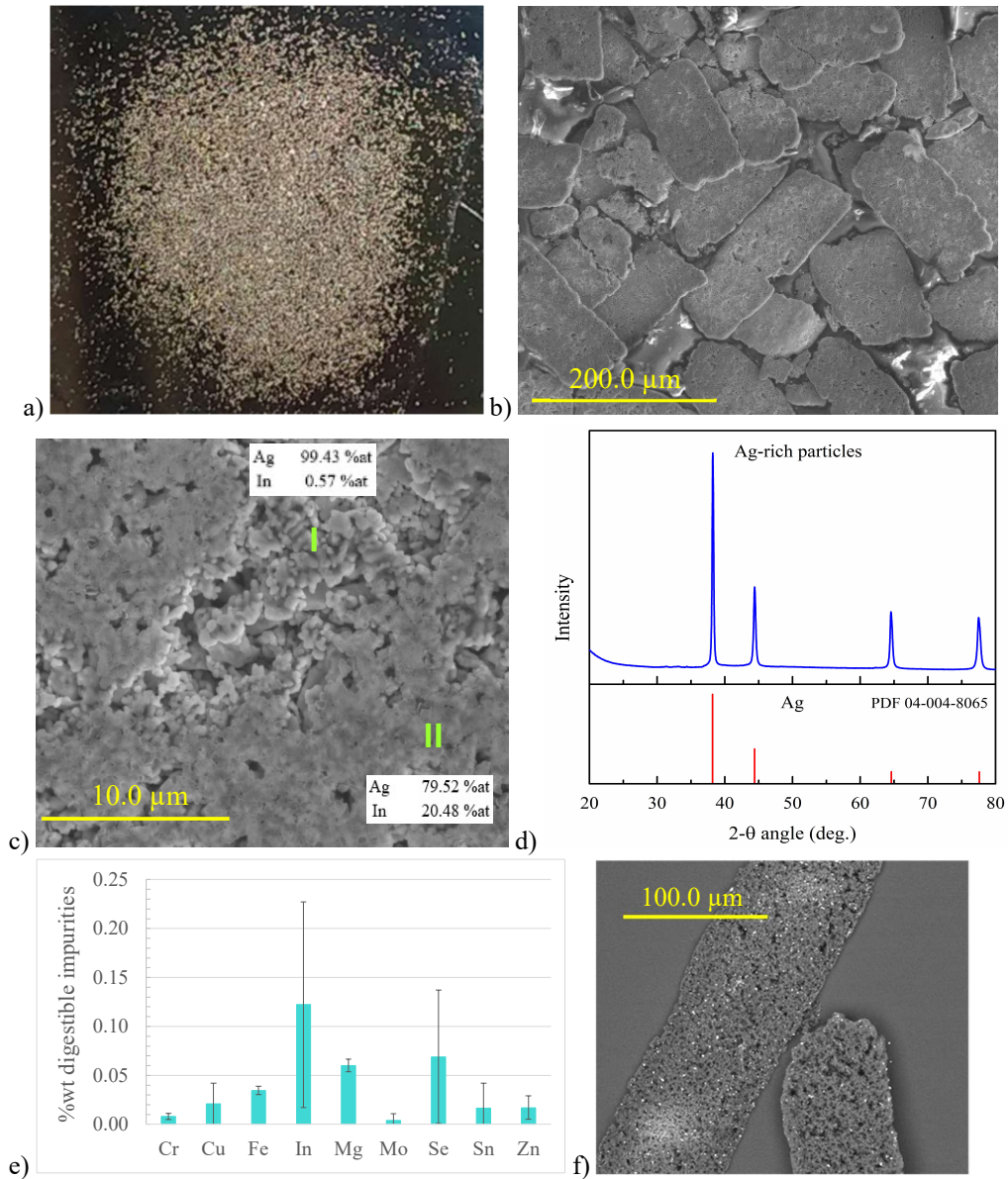


Fig. 21: Analysis of the solid particles recovered from the second US-leaching step: a) recovered particles, b, c) their morphology at higher and lower magnification, respectively, showing also some ITO residues in (c), d) identification of their crystalline phases, e) levels of the digestible impurities in the total recovered fraction and f) SEM image of the non-digestible organics.

The solids recovered after the second step (Fig. 21a) were in the form of rectangular pieces of width close to 100 μm and length of a few hundreds of μm (Fig. 21b). Each of these pieces was an aggregate of much smaller particles of submicron sizes. The XRD analysis detected metallic Ag as the only crystalline phase present in the recovered solid fraction. Therefore, it was concluded that the treatment resulted in detachment of the Ag grid from the underlying surface and the breakage of the grid lines into shorter pieces of the original grid. This scenario was also supported by the fact that the width of the pieces was similar to that of the Ag grid lines of the untreated cell (Fig. 6b). The SEM-EDS analysis of the recovered Ag also showed that some pieces of the ITO layer could still be found undissolved underneath the liberated Ag grid (area II of Fig. 21c). The total Ag content of the pieces, based on their digestion, was 94.96 ± 1.29 wt%. Both digestible and non-digestible impurities were found in the recovered fraction. The digestible impurities were only a very small part of the total impurities and the main digestible impurity was In, coming from the pieces of ITO layer that remained attached to the Ag grid lines (Fig. 21e). More than half the mass of non-digestible impurities originated from the organic leftovers of the Ag paste used for creating the Ag grid (Fig. 21f). This fraction showed up by performing a TGA, which measured about 3 wt% organic content of the Ag pieces. The remaining content of the non-digestible impurities was the particles containing Fe, Se and some Cr. The estimated total composition of the recovered Ag-rich particles is summarized in Table 6. Again, since the exact amount of the non-digestible Cr, Fe and Se could not be quantified through the digestion, the given numbers are minimum values, based on the digestible amounts.

Quantification of the % recovery of Ag was based on digestion experiments of the recovered solid fraction and gave a yield of 72.7 ± 2.2 mg Ag/cell. This amount is somewhat larger than the total amount of Ag measured in the elemental characterization of the untreated solar cells of 64.1 ± 4.7 mg/cell (Table 2), but when considering the errors in these average values, the recovery of Ag can be considered to be ≥ 99 wt%.

5.2.4. Discussion on the results of US-leaching

Based on the results of the 2-step US-leaching experiments, described in previous section, a scenario on the various phenomena which take place can be formulated. During the first step at the minimum US power setting, the highly soluble ZnO reacts immediately with 0.1 M HNO_3 . This very fast reaction (about 75 wt% of the Zn dissolves in only 3 min) leaves a gap between the ITO and the CIGS layers (Fig. 14b). Since a large part of the ITO layer becomes unsupported, the cavitation effect created by the action of the US can easily break the crystalline ITO layer and, thus, liberate it from the cell's surface. A very small amount of ITO remains trapped around and below the Ag grid lines and its liberation does not improve with the treatment time. The Ag grid lines probably protect the remaining ITO from the action of the powerful jets, which the imploded bubbles create. During the 3 min of US-leaching, a small amount of In (about 10 wt% of the total In in the cell) also dissolves. This may originate from partial dissolution of ITO or other easily soluble In-containing layers, as discussed in Section 5.2.2. The recovered ITO-rich particle fraction consists of about 70.5 wt% ITO. The impurities come from other liberated particles, rich in Se and Fe with some Cr, which are probably

residues remaining on the surface of the stainless-steel substrate after the selenization process applied during manufacturing. A pretreatment step using US and only pure water may potentially remove these particles and increase the purity of the ITO-rich fraction, without causing any dissolution of materials.

In the second US-leaching step, still with 0.1 M HNO₃ but at the maximum US power setting, some passivation of the stainless-steel substrate takes place, but no other elements dissolve. The high US power of this step liberates the Ag grid within 15 min. In this step, the US power is high enough to allow the created jets to reach the ITO, which had remained around and below the Ag lines, effectively, break it and liberate it together with the Ag grid. The grid is liberated as short fragments of the initial grid, so, most of the Ag is recovered in the form of elongated aggregates (not as individual particles). The recovered grid fragments contain about 95.0 wt% Ag and more than half of the remaining impurities consists of the organic residues from the original Ag paste. A further separation of the organics at a later stage should be easily achievable (e.g. through a thermal removal method or a selective dissolution).

Finally, it is interesting to note that although 75 wt% of the total Zn leached in the first US-leaching step, almost no Zn was detected in any other fraction later. The most likely explanation for that is that, since ZnO is so highly reactive, most of the remaining 25 wt% continued reacting while the filtration after the first US-leaching step was taking place.

5.2.5. Results of alkaline leaching investigating the possibility of direct Mo dissolution

The progress of 24 h alkaline leaching of the solar cell samples (after their 2-step US-leaching treatment) when using 0.1, 0.3 and 0.5 M NaOH are presented in Fig. 22. The results show that a complete leaching of Mo was possible within this time, for all the NaOH concentrations tested. It was also interesting to observe that W leached completely, too. The main difference between these plots was the dissolution rate: the higher the NaOH concentration, the faster the reactions reached an equilibrium of complete dissolution. More specifically, when leaching with 0.1 M NaOH, a complete dissolution of Mo and W was accomplished after 24 h, while when using 0.3 and 0.5 M NaOH only 8 h were required. The leaching rate of other metals present in the cell was also affected by the NaOH concentration: for the same treatment time, higher amounts of Se, In, Ga and Cu leached into the solutions of higher NaOH concentration. The concentration of Ti in the leachate was negligible in all cases. Finally, Fe and Cr were close or below the detection limit of the ICP-OES and, therefore, not presented in the plots.

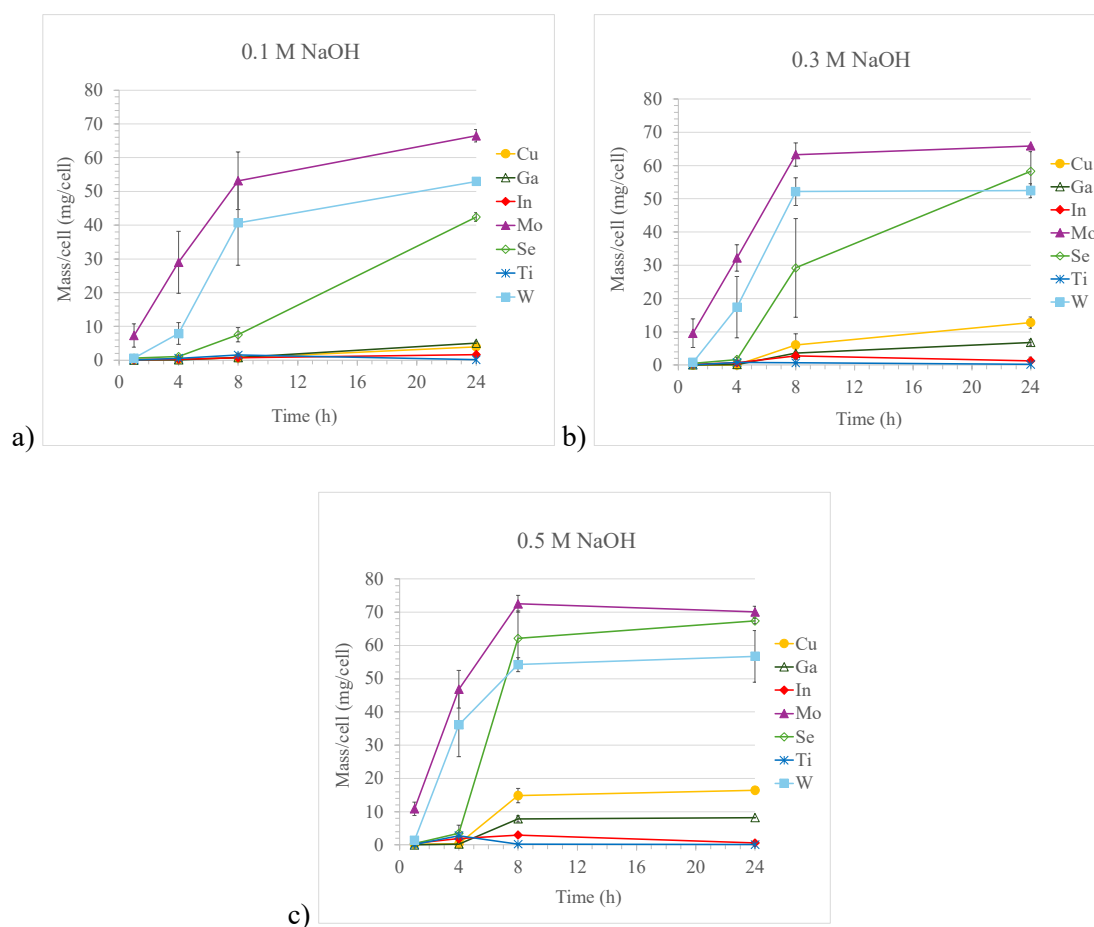


Fig. 22: Leaching yields per cell with time for leaching of CIGS solar cells with a NaOH solution of a) 0.1 M, b) 0.3 M and c) 0.5 M at 20 °C.

5.2.6. Discussion on the results of alkaline leaching investigating the possibility of direct Mo dissolution

The results of the alkaline leaching experiments performed with 0.1-0.5 M NaOH at 20 °C proved that direct dissolution of the metallic Mo present in the CIGS solar cells is possible under these conditions, as predicted by thermodynamics (Section 3.2.2.). Its dissolution can be completed within no more than 24 h. The actual leaching time required depends on the NaOH concentration used, with higher NaOH concentrations associated with higher leaching rates. A complete leaching of Mo is always accompanied by a complete leaching of W and a considerable dissolution of Se too. On the other hand, the leaching rate of Cu, In and Ga is very low for NaOH concentrations as low as 0.1 M, but the rates increase as the NaOH concentration increases, making the process less selective in the latter case. However, the three times longer leaching times required when leaching with 0.1 M NaOH (i.e. 24 h), compared to leaching with

at least 0.3 M NaOH (i.e. 8 h), could play an important role in case of industrial scale-up of the process. Therefore, an investigation on the impact of various factors on the leaching yield of Mo was deemed necessary and the results are described in next section.

5.2.7. Results of split-plot factorial experiment on factors affecting the leaching of Mo

The design matrix of the split-plot factorial experiment, performed in order to investigate the significance of several factors and their interactions on Mo yield during alkaline leaching, is presented in Table 7, along with the resulting responses. The log of the responses was found to give better results compared to the original values; therefore, it was decided to be used for the analysis. Details on how the analysis of split-plot factorials is performed can be found in Section A3 of the Appendix.

The contrasts, Sum of Squares (SS), effects and parameters for Mo leaching for all runs were first calculated. Then, the two normal probability plots of the effects were constructed (Fig. 23), in order to detect the significant main effects and interactions. As the main effects A, B, C, D and E fell away from the respective straight lines of Fig. 23, they were decided to be significant. The four-factor interaction ABDE could be significant as well, however, interactions higher than second order are usually non-significant [100]. This interaction was decided in the end to be included in the model, since later analysis (e.g. evaluation of plots of residuals) showed more satisfactory results when included.

Based on the selected significant main effects and interactions, the fitted regression model was constructed:

$$\widehat{\log(y_{Mo})} = 0.827 + 0.152 \cdot x_1 + 0.185 \cdot x_2 + 0.364 \cdot x_3 - 0.111 \cdot x_4 + 0.203 \cdot x_5 - 0.084 \cdot x_1 \cdot x_2 \cdot x_4 \cdot x_5 \quad (\text{Eq. 25})$$

The residuals were then checked. The normal probability plots for the WP and SP residuals were constructed first (Fig. 24a and b, respectively). Since all the residuals fell approximately on the respective straight line, no serious violations of the normality assumption were observed. Next, the WP and SP residuals were plotted against the run order (Fig. 25a and b, respectively), in order to check for violations of the constant variance assumption. As both plots looked structureless, with the residuals distributed around zero and no big differences in the variances were observed, the plots were considered satisfactory. Next type of residuals plots checked for constant variance were those plotted against the respective fitted values. The WP residuals were plotted against the average of the fitted value per WP and the SP residuals were plotted against the fitted values, as shown in Fig. 25c and d, respectively. Both plots looked reasonably good. Finally, it is also recommended to plot the WP residuals against the SP residuals. As can be seen in Fig. 25e, their plot looked satisfactory, since it was structureless and with a relatively constant variance.

Table 7: Design matrix of the split-plot factorial experiment and observed values of the response variable, i.e. leaching yield of Mo [mg/cell].

WP (or run order)	Run name	A	B	C	D	E	y _{Mo}	logy _{Mo}
2	(1)	-	-	-	-	-	0.67	-0.174
1	a	+	-	-	-	-	2.40	0.380
5	b	-	+	-	-	-	2.31	0.364
8	ab	+	+	-	-	-	4.17	0.620
7	c	-	-	+	-	-	11.00	1.041
3	ac	+	-	+	-	-	22.73	1.357
6	bc	-	+	+	-	-	6.66	0.823
4	abc	+	+	+	-	-	19.48	1.290
2	d	-	-	-	+	-	0.38	-0.420
1	ad	+	-	-	+	-	0.74	-0.131
5	bd	-	+	-	+	-	2.38	0.377
8	abd	+	+	-	+	-	3.75	0.574
7	cd	-	-	+	+	-	7.84	0.894
3	acd	+	-	+	+	-	7.90	0.898
6	bcd	-	+	+	+	-	7.06	0.849
4	abcd	+	+	+	+	-	17.32	1.239
2	e	-	-	-	-	+	7.97	0.901
1	ae	+	-	-	-	+	1.41	0.149
5	be	-	+	-	-	+	5.00	0.699
8	abe	+	+	-	-	+	54.35	1.735
7	ce	-	-	+	-	+	10.59	1.025
3	ace	+	-	+	-	+	43.63	1.640
6	bce	-	+	+	-	+	27.30	1.436
4	abce	+	+	+	-	+	53.66	1.730
2	de	-	-	-	+	+	1.55	0.190
1	ade	+	-	-	+	+	10.38	1.016
5	bde	-	+	-	+	+	4.06	0.609
8	abde	+	+	-	+	+	3.36	0.526
7	cde	-	-	+	+	+	4.73	0.675
3	acde	+	-	+	+	+	6.91	0.839
6	bcde	-	+	+	+	+	32.95	1.518
4	abcde	+	+	+	+	+	63.09	1.800
	Average						13.99	0.827

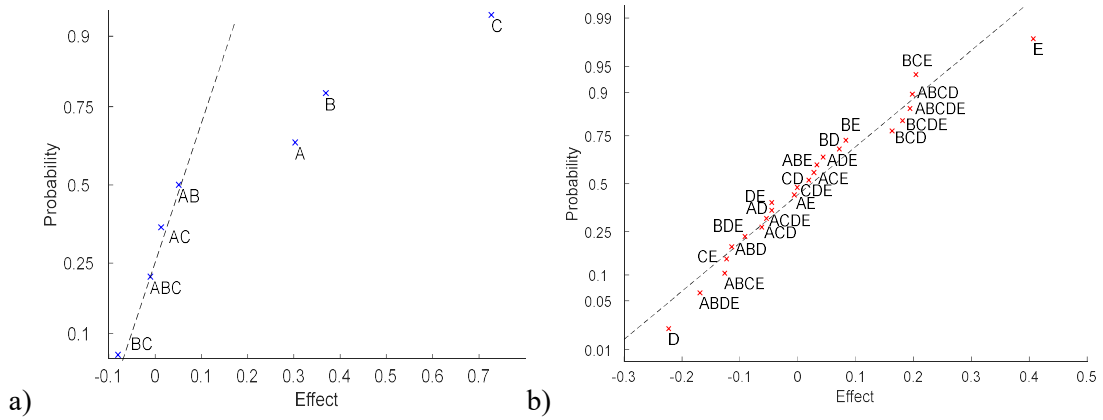


Fig. 23: Normal probability plots for the (a) WP and (b) SP effects. The straight lines were drawn manually for the WP effects and automatically by MATLAB [101] for the SP effects.

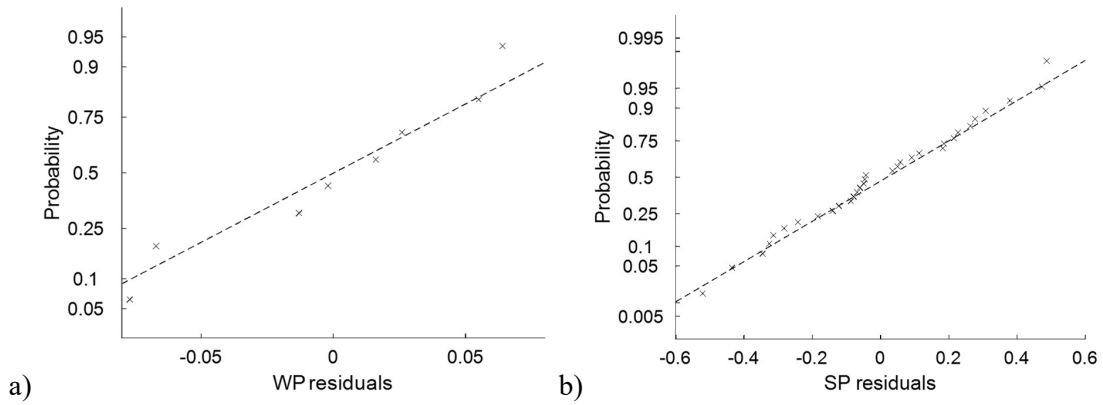
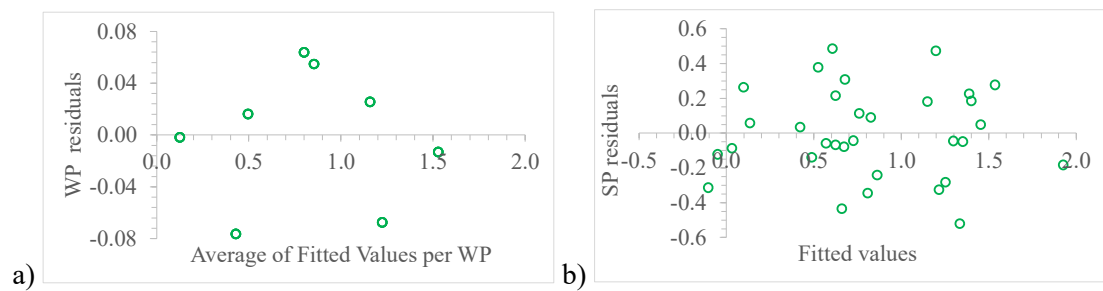


Fig. 24: Normal probability plots for the a) WP and b) SP residuals.



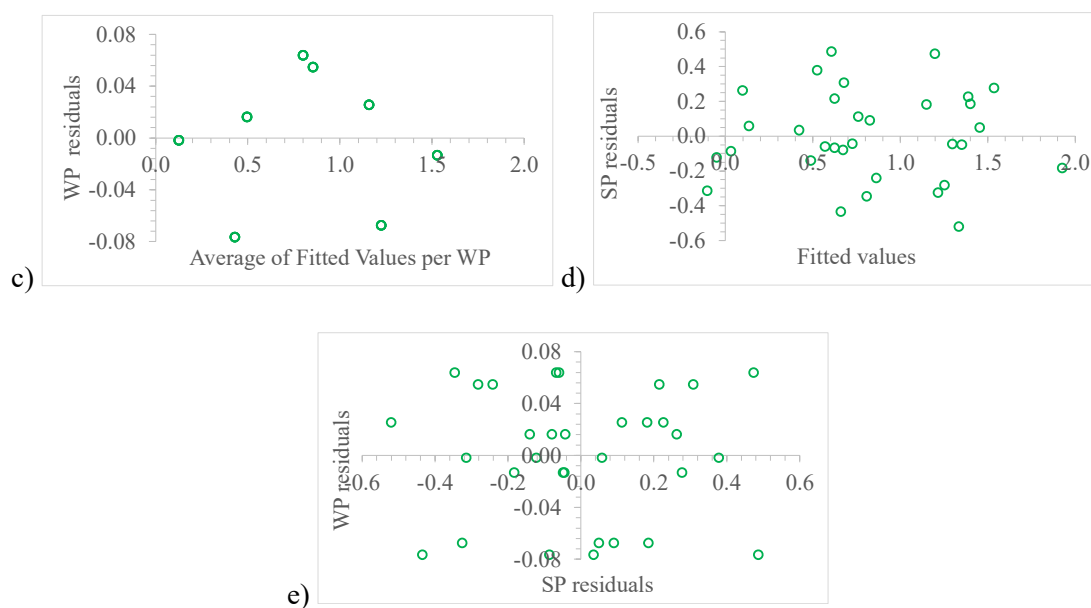


Fig. 25: Plots of residuals for Mo leaching: a) WP and b) SP residuals vs run order, c) WP residuals vs average fitted value per WP, d) SP residuals vs fitted value and e) WP vs SP residuals.

The assessment of the adequacy of fit of the proposed model was based on the calculation of the measures of adequacy of fit of the model R^2 , R^2 -Adjusted (R^2_{Adj}), Prediction Error Sums of Squares (PRESS) and R^2 -Prediction (R^2_{Pred}) statistics; one of each for the WP sub-model and one of each for the SP sub-model. Instructions on how these values are calculated for the type of split-plot factorial used in these experiments are given in Section A3 of the Appendix.

The obtained values were $R^2_{WP}=0.9879$, $R^2_{WP_Adj}=0.9788$, $R^2_{SP}=0.4603$ and $R^2_{SP_Adj}=0.3832$. The large values of R^2_{WP} and $R^2_{WP_Adj}$ indicate that a large proportion of the variability in the data was explained by the selected WP effects A, B and C. On the other hand, the small values of R^2_{SP} and $R^2_{SP_Adj}$ indicate that only a small proportion of the variability in the data was explained by the selected SP factors D and E, as well as the interaction ABDE.

The assessment of the model adequacy continued with the calculation of $PRESS_{WP}$ and $PRESS_{SP}$. $PRESS_{WP}$ was found equal to 0.097. This low value indicated that the WP sub-model had a good performance in predicting the responses of future experiments. On the other hand, $PRESS_{SP}$ was found equal to 2.508. This relatively high value indicated that the performance of the SP sub-model in predicting the responses of future experiments was relatively poor.

The last measures of adequacy left to calculate were $R^2_{WP_Prediction}$ and $R^2_{SP_Prediction}$. Their calculation concluded $R^2_{WP_Pred.}=0.984$ and $R^2_{SP_Pred.}=0.407$. The high value of $R^2_{WP_Pred}$ confirms the good predictive performance of the WP sub-model. On the contrary, the low value of $R^2_{SP_Pred}$ confirmed the poor predictive performance of the SP sub-model.

5.2.8. Discussion on the results of the split-plot factorial on factors affecting the alkaline leaching of Mo

The results of the split-plot factorial experiments on alkaline leaching of Mo indicated that all investigated factors (i.e. leaching temperature, pH, presence of sodium tartrate in the leachate, A:L and leaching time) were significant. An increase in the factors' levels was also associated with an increase in the leaching yield of Mo. The only exception was A:L, for which the opposite trend was observed. These results are in good agreement with the fundamental principles of chemistry and leaching theory (Section 3.1).

The suggested model seemed to be satisfactory, based on the analysis of residuals. However, the calculation of common measures of adequacy of fit of model showed that, although the suggested WP sub-model explained a high proportion of the variability of the data and had a good predictive capability, the opposite was true for the suggested SP sub-model. In other words, the predictability of the suggested model was excellent at WP level, but compromised at SP level. One of the reasons for the poor performance of the SP sub-model could be the inclusion of non-significant terms in it. However, it should be mentioned that when the removal of some of the terms was tested, significant distortions in the residuals' normal probability plots were caused. Therefore, it was decided to keep the initially proposed model unchanged. Another reason behind the poor performance of the SP sub-model could be that a linear model was not suitable, e.g. in case of significant curvature, which would require a different design for the inclusion of quadratic terms too. Significant cell-to-cell differences can also be suspected as a source of the poor SP predictability, while errors during the performance of the experiments or the analysis of the samples are always a likely scenario. Thus, in case of future optimization of the process, it would be advisable for all these factors which possibly led to the poor prediction performance at SP level to be checked first.

Nevertheless, the obtained results are seen as satisfactory enough to show the direction which future alkaline leaching experiments targeting the Mo dissolution should take. More specifically, if high Mo leaching efficiency is targeted, the leaching process should be performed at temperatures higher than the ambient and pH values higher than 10. Longer leaching times, as well as lower A:L values, should also be expected to increase the efficiency. Finally, the presence of sodium tartrate clearly contributes to higher Mo leaching yields, however, as it is an extra chemical used and it can also react with elements like In and Cu [102-103], its suitability for the specific application has to be investigated further if selectivity of the leaching process is also desirable.

5.2.9. Results of alkaline leaching targeting the recovery of CIGS in solid form

The results of the alkaline leaching experiment targeting the recovery of the CIGS material in solid form through a selective dissolution of the Mo layer underneath, are presented in this section. The elemental composition of the CIGS material before the sample enters the alkaline leaching process is first presented, so that it can be used as a reference for the impact of alkaline

leaching on the composition of the recovered CIGS material. Then the results of alkaline leaching experiments performed at a constant pH=11 and 50 °C follow; divided in those which used only NaOH and those which also used sodium tartrate.

5.2.9.1. Composition of unleached CIGS

In order to assess the selectivity of the tested alkaline leaching conditions, the composition of the CIGS material just before the alkaline leaching step (i.e. immediately after exiting the 2-step US-leaching process) had to be determined. From now on, this material will be described by the term “unleached CIGS”. The results of its elemental analysis using EDS are presented in Table 8. Except for the CIGS compositional elements, a peak assigned to S was also detected. It is known from the literature that some S is usually added to the CIGS layer during manufacturing [104]. However, a small amount of S was also contained in the carbon sticky pad used for the SEM-EDS analysis and, therefore, it cannot be said with certainty how much of this S came from the actual sample and how much it came from the carbon pad. Therefore, the composition of the unleached CIGS was calculated for two extreme scenarios: one based on the assumption of complete absence of S from the CIGS compound and one based on the scenario that the whole amount of S came from the CIGS compound. The two calculated compositions were similar though, as the amount of S was small, only 1.9 wt%.

Table 8: Elemental composition of the unleached CIGS material, based on EDS analysis.

	With S				Without S			
	Wt%		Atomic%		Wt%		Atomic%	
	Average	σ	Average	σ	Average	σ	Average	σ
Cu	15.8	0.2	20.1	0.4	16.1	0.2	21.1	0.3
Ga	5.6	0.2	6.5	0.3	5.7	0.2	6.8	0.2
In	29.8	0.5	20.9	0.3	30.3	0.7	21.9	0.5
Se	46.8	0.8	47.8	1.1	47.8	0.5	50.2	0.5
S	1.9	0.6	4.7	1.4	-	-	-	-

5.2.9.2. Alkaline leaching at pH=11 at 50 °C using only NaOH

The results of leaching at constant pH=11, utilizing continuous NaOH addition at T=50 °C for the purpose of dissolving Mo, are presented in Fig. 26. The plot shows that the leaching yield of Mo has already reached a plateau at 16 h, achieving a maximum efficiency of about 88 wt%. The leaching reaction of W was much slower, with about 55 wt% of it dissolving at that time. It only reached a maximum at 24 h, achieving a maximum efficiency of about 84 wt%. The leaching efficiencies of Mo and W with time are summarized in Table A2 of the Appendix.

Regarding the rest of the elements, only some small amounts of Se, Ga and Ti were detected in the leachate, even at 24 h of leaching (Fig. 26b). More specifically, the leaching yield of Se increased with the leaching time, but it remained well below 3.5 mg/cell for up to 24 h of leaching, corresponding to less than 5 wt% of the leachable Se in the cell. On the other hand, the leaching of Ga and Ti reached a plateau after 6 and 18 h, respectively, reaching about 0.6 mg/cell for Ga and 1.0 mg/cell for Ti. It is worth noting that neither In nor Cu were detected in the leachate.

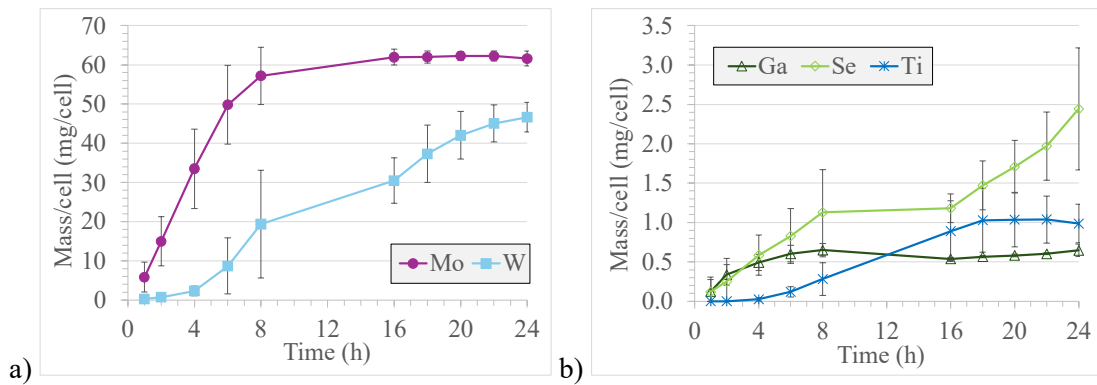


Fig. 26: Leaching yields of the a) major and b) minor elements of the leachate when using a NaOH solution of pH=11 at 50 °C.

In total, the treatment time which seems most promising for a selective recovery of the CIGS material was that of 8 h, as 84 %wt of Mo dissolution (almost reaching its plateau) was achieved, in combination with a very low loss of Se into the leachate and a minor amount of leached Ti as additional contamination. Therefore, the experiments were repeated for 8 h of leaching and, then, the cell pieces were subjected to US, aiming to the liberation of the CIGS layer as particles. However, the ultrasonication proved unsuccessful for this purpose, since, even after 60 min at the maximum US power setting, most of the CIGS material was still attached to the cell. On a different set of triplicates, brushing was tested as an alternative method for the removal of the CIGS layer from the substrate after the 8 h of leaching and this successfully removed the CIGS layer from all the triplicates, with brushing times ranging from a few seconds up to a few minutes. Therefore, this treatment combination was selected as the most promising and a detailed analysis of its solid fractions was made.

More specifically, SEM-EDS analysis of the substrate after the leaching and brushing of the solar cell (Fig. 27) concluded that the CIGS layer had been removed from the bulk surface of the substrate, with only a few traces remaining trapped in the areas where the Ag lines used to be. A very small peak which could be assigned either to Mo or S was detected in the same area.

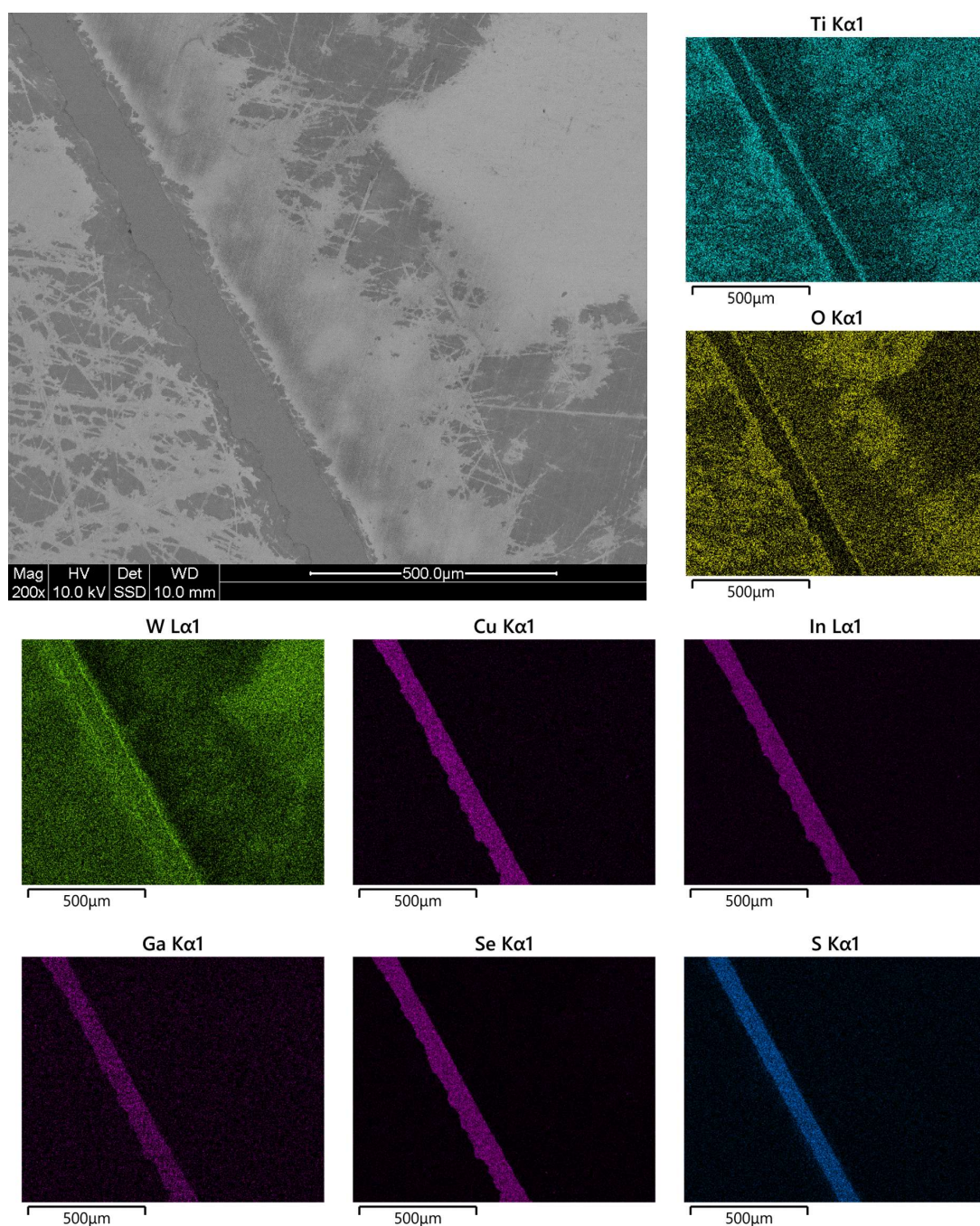


Fig. 27: SEM-EDS mapping of an area of the substrate of an alkaline-leached (NaOH solution pH=11, 50 °C, 8h) and brushed cell. The peak of S could also be attributed to Mo, since they overlap.

The peak might have been due to the presence of some S in the CIGS structure or even traces of Mo remaining trapped along with the CIGS material (only the S map is shown in Fig. 27,

since it was exactly the same as for Mo). However, Mo was confirmed to be absent from the bulk substrate surface. The only elements detected on the substrate were W, Ti and O. Notably, Ti and O were detected at the same areas, implying that most likely TiO_2 had formed, according to the Pourbaix diagram of Ti (Fig. A1d). This phase will be considered as TiO_2 from now on.

Analysis of the liberated solids showed that the crystalline structure of the recovered CIGS material was the same as the one of the untreated CIGS (Fig. 28) and the CIGS was the only crystalline phase detected. SEM-EDS mapping of the liberated particles confirmed that the main compound present was the CIGS (Fig. 29). Its elemental composition is presented Table 9. By comparing this composition with the one of the unleached CIGS (Table 8), it is concluded that the composition of the CIGS also remained unchanged under these treatment conditions. Small amounts of Mo and TiO_2 were also detected by SEM-EDS (Fig. 29) in this fraction. Mo was found in the same particles as the CIGS, due to the incomplete leaching of the former. Some S might have been present too, since the strongest peaks of Mo and S coincide. As for the TiO_2 , it probably came from some scratching of the TiO_2 layer during brushing, as Fig. 27 suggests. The total elemental composition of the particles' fraction is presented in Table 9. Table 9 also shows that the concentration of Ti was at the level of detection limit. Moreover, it

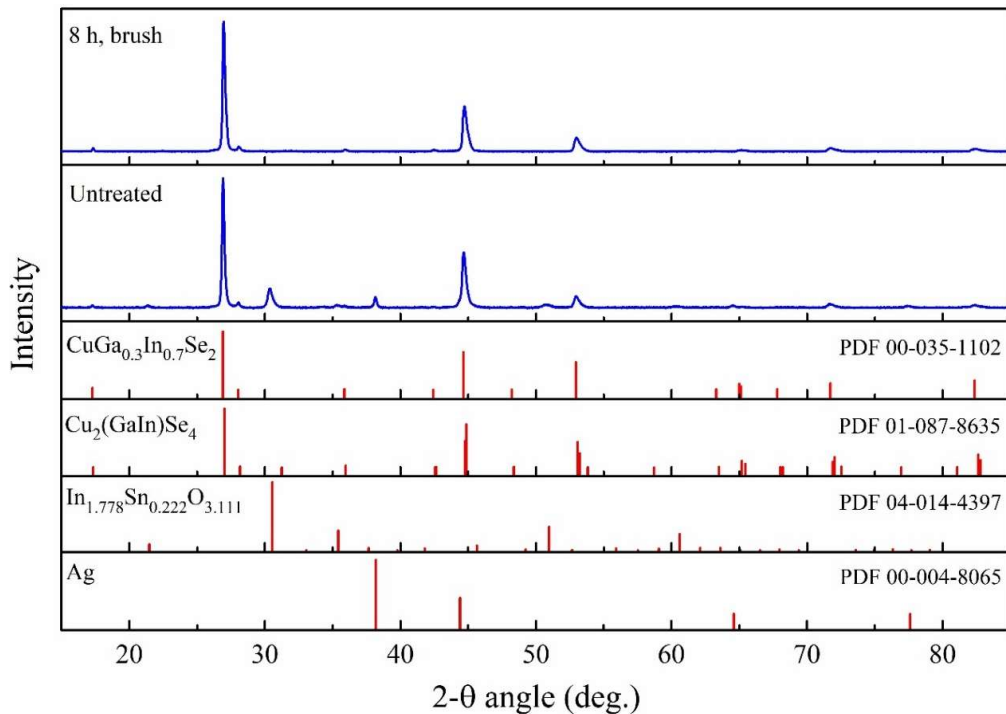


Fig. 28: XRD analysis of the solids recovered after the alkaline leaching (NaOH solution pH=11, 50 °C, 8 h) and brushing of the solar cells, in comparison with the untreated CIGS material. The phases which were present in the untreated cell, but removed before the alkaline leaching, are not identified in detail, except for the strongest peaks, belonging to Ag and ITO.

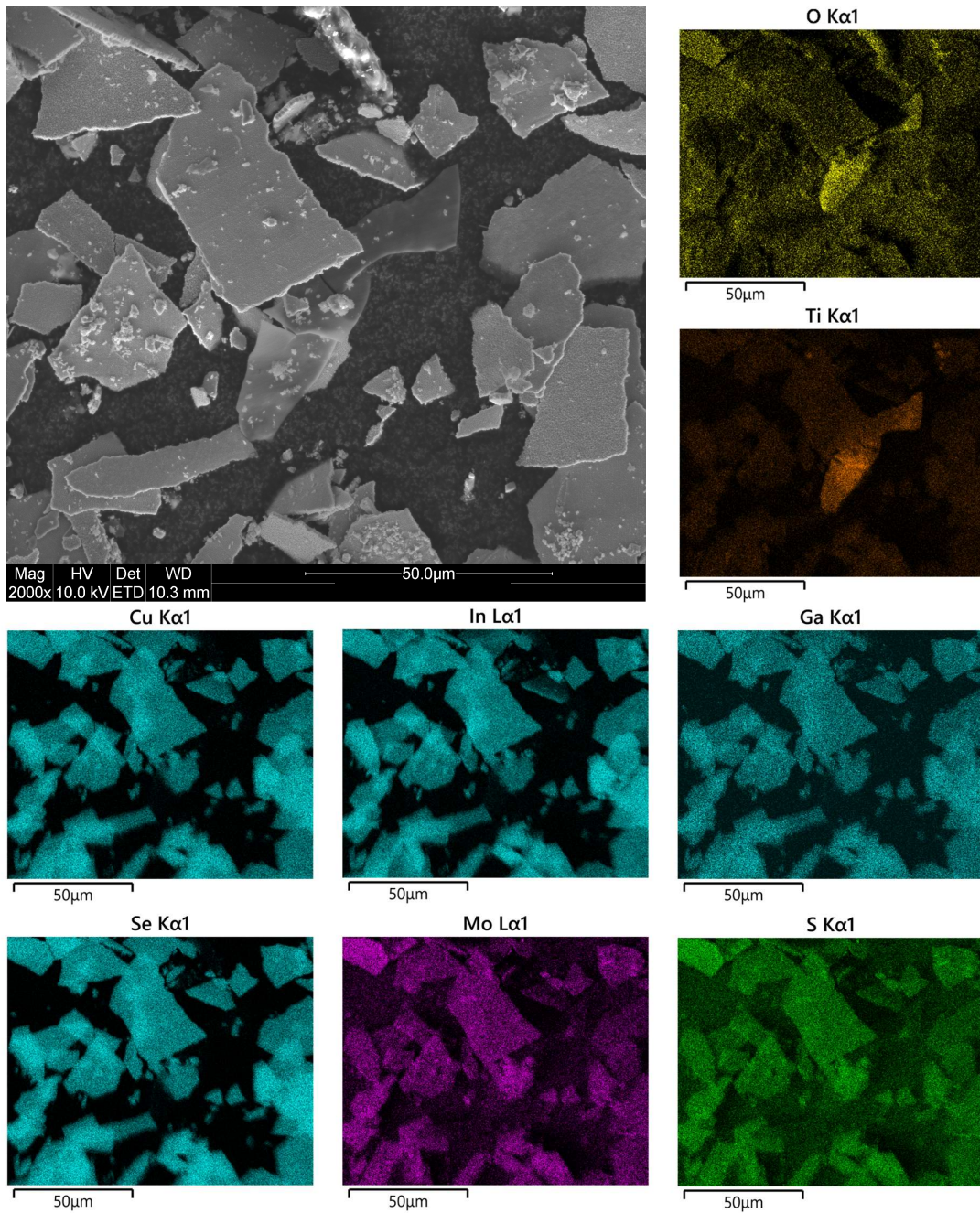


Fig. 29: SEM-EDS mapping of the solids liberated after brushing the solar cells leached with a NaOH solution of pH=11 at 50 °C for 8 h.

is noted that W was absent, meaning that any undissolved W had remained attached on the substrate. Based on the results of Table 9, the purity of the recovered CIGS was about 95 wt%.

Table 9: Elemental composition, based on EDS analysis, of the solids liberated after brushing the solar cells leached with a NaOH solution of pH=11 at 50 °C for 8 h.

CIGS only								
With S					Without S			
	Aver. wt%	σ	Aver. atomic%	σ	Aver. wt%	σ	Aver. atomic%	σ
Cu	15.6	0.2	19.5	0.3	16.0	0.2	20.7	0.1
Ga	5.3	0.1	6.0	0.1	5.4	0.1	6.4	0.1
In	26.4	0.6	18.2	0.4	26.9	0.7	19.2	0.6
Se	50.4	0.6	50.6	0.7	51.7	0.5	53.7	0.4
S	2.3	0.2	5.7	0.6	-	-	-	-
Total solids								
With S					Without S			
	Aver. wt%	σ	Aver. atomic%	σ	Aver. wt%	σ	Aver. atomic%	σ
Cu	15.2	0.2	19.3	0.3	14.9	0.2	19.4	0.2
Ga	5.2	0.1	6.0	0.1	5.0	0.1	6.0	0.1
In	26.0	0.6	18.3	0.4	25.8	0.6	18.6	0.5
Mo	3.2	0.1	2.7	0.1	6.5	0.5	5.7	0.5
S	1.3	0.2	3.4	0.6	-	-	-	-
Se	48.8	0.6	49.9	0.6	47.5	0.8	49.9	0.6
Ti	0.3	0.0	0.5	0.0	0.3	0.0	0.5	0.0

5.2.9.3. Alkaline leaching at pH=11 at 50 °C using NaOH and sodium tartrate

The results of leaching at constant pH=11, utilizing continuous NaOH addition at T=50 °C, with sodium-tartrate added as additional reagent, for the purpose of dissolving Mo, are presented in Fig. 30. By adding sodium tartrate in the leaching solution, the leaching rates and efficiencies were increased for most of the elements (Fig. 30), compared to the case without the sodium tartrate (Fig. 26). More specifically, both Mo and W dissolved almost completely, at 96 wt% and 99 wt%, respectively, at 8 h. However, the CIGS material also leached to a greater extent under these conditions, with 1.9 mg Cu/cell, 5.2 mg In/cell, 2.0 mg Ga/cell and 13.9 mg Se/cell present in the leachate at 8 h of leaching and their dissolution increased considerably for longer treatment times. Also dissolved Ti increased to about 5.0 mg/cell (plateaued after 8 h), compared to leaching using only NaOH, which was almost double the maximum amount dissolved under the digestion conditions (Table 2). As the leaching of Mo was almost complete at the 8 h, while the CIGS material had only started showing some considerable dissolution, this treatment time was considered as worth investigating further.

The experiments were repeated for 8 h and, then, ultrasonication of the leached cells followed, in order to remove the remaining CIGS material. Contrary to the case of leaching using only NaOH, the CIGS material was removed easily from the surface of the solar cell this time, in a

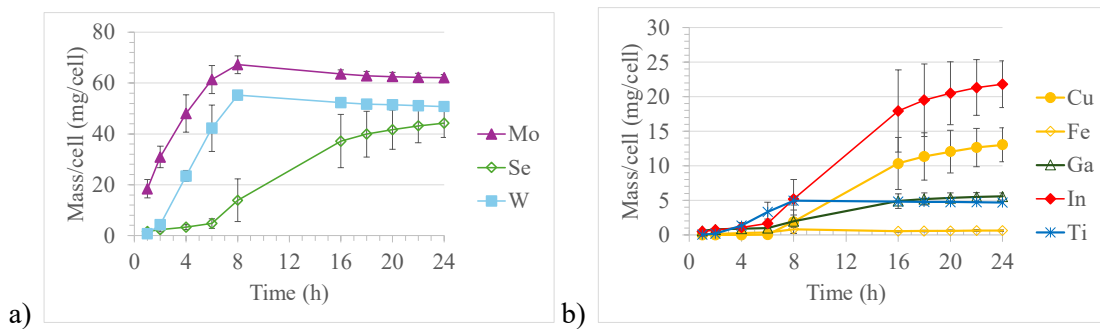


Fig. 30: Leaching yields of the a) major and b) minor elements of the leachate when using a NaOH and sodium tartrate solution of pH=11 at 50 °C.

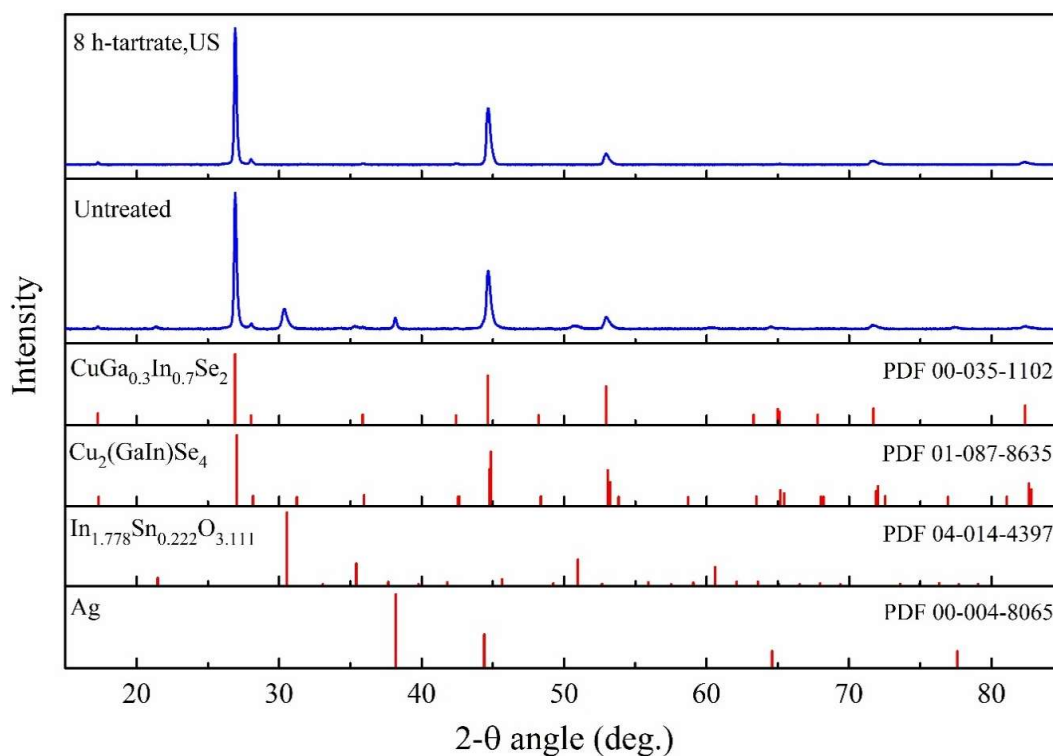


Fig. 31: XRD analysis of the solids recovered after the alkaline leaching (NaOH and sodium tartrate solution pH=11, 50 °C, 8 h) and ultrasonication of the solar cells, in comparison with the untreated CIGS material. The phases which were present in the untreated cell, but removed before the alkaline leaching, are not identified in detail, except for the strongest peaks, belonging to Ag and ITO.

few seconds or minutes. The easy removal of the CIGS material with US, when using sodium tartrate as an extra reagent in the alkaline leaching, was the result of a more extensive

dissolution of all the layers underneath the CIGS. As the US treatment proved successful, no brushing was tested. Brushing though was expected to decrease the treatment time even further, due to the applied mechanical friction.

The analysis of the surface with SEM-EDS (not shown here) of the remaining substrates confirmed the absence of any functional layer, as only peaks coming from the stainless-steel and a very small peak of Si were detected. The XRD analysis of the collected solids showed that for 8 h of leaching, the only crystalline phase was the CIGS, with crystalline structure same as the one of the untreated cell (Fig. 31). SEM-EDS of the liberated particles (not shown here) did not reveal any extra phases. The total elemental composition of the recovered fraction, as well as that of the CIGS only, are presented in Table 10. The measured values confirm that the recovered CIGS particles are similar to that of the untreated sample (Table 8). It should be mentioned that a peak of oxygen was also detected in the EDS spectrum, however, it could not be concluded if it was contamination or if some oxides had formed. Based on the results of Table 10, the purity of the recovered CIGS was about 95 wt%.

Table 10: Elemental composition, based on EDS analysis, of the solids liberated after ultrasonicing the solar cells leached with a NaOH and sodium tartrate solution of pH=11 at 50 °C for 8 h.

CIGS only								
With S					Without S			
	Aver. wt%	σ	Aver. atomic%	σ	Aver. wt%	σ	Aver. atomic%	σ
Cu	15.7	0.5	19.9	0.8	16.1	0.4	21.2	0.5
Ga	4.6	0.2	5.3	0.2	4.7	0.2	5.6	0.2
In	31.7	0.7	22.3	0.5	32.4	0.9	23.6	0.7
Se	45.7	0.6	46.6	0.9	46.8	0.5	49.6	0.2
S	2.3	0.6	5.9	1.5	-	-	-	-
Total solids								
With S					Without S			
	Aver. wt%	σ	Aver. atomic%	σ	Aver. wt%	σ	Aver. atomic%	σ
Cu	15.3	0.5	19.7	0.8	14.9	0.6	19.8	0.7
Ga	4.5	0.2	5.2	0.2	4.4	0.2	5.3	0.2
In	31.3	0.7	22.4	0.5	31.0	0.6	22.8	0.6
Mo	3.2	0.3	2.7	0.3	6.5	1.3	5.7	1.2
S	1.5	0.6	3.7	1.5	-	-	-	-
Se	44.2	0.6	45.9	0.9	43.0	1.0	46.0	0.8
Ti	0.2	0.0	0.3	0.1	0.2	0.0	0.3	0.1

5.2.10. Discussion on the results of alkaline leaching targeting the recovery of CIGS in solid form

The alkaline leaching experiments performed on the solar cells (after their treatment with the 2-step US-leaching process), with the aim of recovering CIGS as solid particles through the selective dissolution of the Mo layer underneath, can be considered successful. It was demonstrated that the metallic Mo can dissolve with high efficiency (88 wt% of total), even for the relatively mild leaching conditions of pH=11 and 50 °C, and in no longer than 16 h, when only NaOH is used as the leaching agent. If also 0.25 M sodium tartrate is present in solution, even higher Mo dissolution rate and efficiency, 96 wt% of total after 8 h, are achieved. The results are in good agreement with the conclusion of factorial experiments that the presence of sodium tartrate increases the leaching efficiency of Mo.

A considerable amount of W also dissolves at the same time, reaching its maximum dissolution efficiency of 84 wt% at 24 h of leaching with NaOH and 99 wt% at 8 h of leaching with a mixture of NaOH and sodium tartrate. In general, similar conclusions can be drawn for all the other elements present in the sample, namely the CIGS compositional elements and the Ti. The dissolution of CIGS when leaching with only NaOH is very slow, with only small amounts of Ga and Se found while In and Cu in the leachate are below their detection limits of the ICP-OES. However, when sodium tartrate is also present in the leaching solution, all the CIGS elements dissolve to some extent and their concentrations increase with time.

However, regardless of whether tartrate ions are present in the solution or not, the dissolution rate of the CIGS layer under the tested conditions is considerably slower than that of Mo and W. This trait enables the recovery of the CIGS material as solid particles in both cases, as soon as most of the layers underneath it dissolve. The slow kinetics of the reactions between the CIGS and the NaOH and tartrates (when present) allow the CIGS material to remain practically unaffected, both in terms of crystalline structure, as well as composition. The similarities in composition between unleached and alkaline-leached CIGS samples become evident from Fig. 32 (based on the results of Tables 8-10; any presence of S is ignored). It can be concluded from Fig. 32 that, although there is some dissolution of the CIGS material, detected with ICP-OES, after 8 h leaching in presence of tartrate ions, the losses are so small that the elemental composition of the CIGS material is practically unchanged when analyzed with EDS.

The observed increase in the dissolution rate and efficiency of metal elements in the presence of tartrate ions is likely due to metal-complexation reactions, thereby increasing their solubility. Since Se-tartrate complexes are not likely to form, Se is released as counterion when the metal selenides dissolve. In the cases of Mo and W, which usually tend to form molybdate and tungstate anions at pH of the region investigated, and, therefore, may not react with the tartrate ions, their higher dissolution efficiencies and rates in the presence of sodium tartrate might (also) be the result of the increased ionic strength of the solution.

Further investigation of the interactions between the various elements present in the cell and the sodium tartrate would be interesting, as the specific leaching conditions seem promising for efficient leaching of Mo, W and Ti, while keeping the CIGS relatively unaffected for a couple of hours. On the other hand, leaching with only NaOH will reduce costs for chemicals used, the likely contamination from additional chemicals (i.e. sodium tartrate salt) and any additional losses of the CIGS material in the leachate. However, at the current stage of development, the disadvantage of this process is that, since Mo, W and Ti dissolve at lower efficiencies and brushing is used afterwards for the removal of the CIGS layer, contamination from these layers can easily enter the recovered solids fraction. Therefore, further optimization would also be worth investigating.

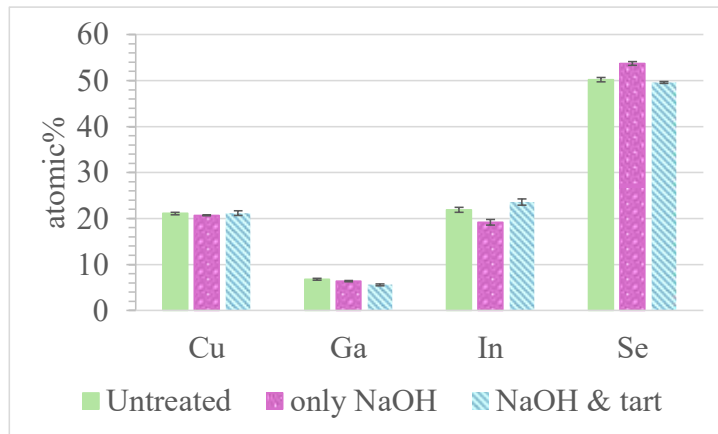


Fig. 32: Comparison of the CIGS composition of the untreated CIGS material and the CIGS material recovered after alkaline leaching with NaOH, in presence and absence of sodium tartrate, for 8 h.

6. Conclusions

The particular thesis demonstrated that an efficient separation of Ag and In coming from CIGS solar cells is possible, even by using mild recovery conditions, of low chemical and energy use. More specifically, it is concluded that when HNO₃ is used as the leaching agent, the efficiency of both Ag and In increases as the acid concentration increases. However, the same is true for most of the contaminant elements as well. The passivation of the stainless-steel though keeps the contamination from Cr and Fe low. Although the effect of the A:L is not clear for the tested conditions, for the highest concentration of HNO₃ tested, 2 M, the dissolution efficiency and rate tend to increase with increase in the A:L, for most of the elements, probably due to ineffective stirring of the higher solution volumes or better in-mixing of oxygen into the low-volume solution. The maximum leaching efficiencies which can be achieved for Ag and In under the range of conditions tested is ≥ 99 wt% and 85 wt%, respectively, using 2 M HNO₃ and A:L=1:3 cm²/ml for 24 h. Enrichment in Ag and In of a leachate of these initial properties proved possible and can reach 850 ppm Ag and 400 ppm In after 10 leaching cycles of 24 h each, without any reduction in the leaching efficiencies of the two metals per cycle. As this is not the case for Cr, Fe, Mo, Sn and W, whose concentrations in the leachate reach a plateau after a few cycles, the leachate can be enriched in valuable metals, while keeping the amount of some of the impurities relatively low. Finally, it is concluded that the total leaching yield of CIGS cannot increase further by refreshing the leaching solution after a plateau in the leaching yield of CIGS is reached, apparently due to formation of insoluble products on the surface of the unreacted CIGS particle. In total, the great disadvantage of this leaching approach is its low selectivity.

Achieving high purities of the recovered Ag and In, while keeping their recovery efficiency high, is possible by combining selective leaching of the easily soluble layers with liberation of the ones on top of them, which remain unsupported. It is concluded that three leaching steps are required in order to achieve complete and selective removal of Ag and the In-rich ITO and CIGS, all in the solid form. More specifically, the following treatment conditions proved successful: a first US-leaching step at low US power for dissolution of ZnO and recovery of ITO, a second US-leaching step at high US power for recovery of the Ag grid and a third step of alkaline leaching for dissolution of the Mo layer and recovery of the CIGS. Only 0.1 M HNO₃ and a few minutes of treatment time are enough for the two US-leaching steps, while the third one uses a NaOH solution of pH=11 at 50 °C and 8 h leaching time. Addition of sodium tartrate can increase the leaching efficiencies and rates of most of the elements, although upto 8 h the dissolution of CIGS is still low. The developed process achieved purities of about 95 wt% for Ag and CIGS and 71 wt% for ITO. The recovered materials have similar composition and crystalline structure with the untreated ones.

To sum up, the particular thesis concluded that valuable materials can be recovered from CIGS solar cells using mild recovery conditions, without compromising the efficiency of the recovery or the purity of the recovered materials. It achieved the recovery of Ag (s), ITO (s), CIGS (s), dissolved Mo (alone or together with W and Ti), dissolved Zn and the stainless-steel substrate

in separate fractions. As soon as the functional layers are recovered, the remaining stainless-steel substrate can also be recycled, using the existing recycling system. The recovery of the valuable Ag, ITO and CIGS in the form of solid particles or fragments of the original materials is also advantageous, as their small size (compared to the case of using whole solar cells) allows higher concentrations of these materials to be used as feed in further processes. This could accelerate significantly the processing time required per mass unit of recycled material and achieve good purification, using established purification technologies. The good recovery selectivities achieved are also expected to increase the value of the recovered materials and render their purification easier, due to the lower impurity levels. Finally, mild leaching conditions seem to have potential to dissolve the recovered solids, if hydrometallurgical treatments are used for the recovery of their valuable metals. The developed methods are simple and can be attractive for the recycling industry, which is still lacking such solutions.

7. Future work

Since an entire separation process was successfully developed for the recovery of valuable materials from CIGS solar cells, the next steps should be its optimization and/or the purification of the recovered fractions. For example, it would be useful to test the effect of the addition of a pretreatment step, in which the solar cells would be ultrasonicated in pure water first, in order to liberate any loose contaminant particles, on the purity of the recovered ITO. Other purification methods for the recovered ITO can also be tested. The study of alkaline leaching was certainly not exhaustive and the effect of parameters, like the concentration of the tartrate ions, on the selectivity of Mo leaching can also be explored. Investigating ways to purify the recovered CIGS and/or extract its compositional elements, using environmentally friendly conditions, is also important. In case of recovering an alkaline leachate containing Mo, W and Ti, methods for their separation should also be tested.

The acid leaching method, using HNO_3 for dissolution of Ag and In, could also be explored further, as the effect of factors like the temperature or the effect of US on the efficiency and kinetics of the leaching reactions were not tested. Methods to separate the leached materials later should also be explored.

Especially for the case of recycling the CIGS compound, a better understanding of its leaching mechanism and assignment of a leaching model would be significant, in order to enable the development of both efficient and environmentally friendly processes. Similarly, more environmentally friendly ways for recycling of Ag should be explored.

Finally, understanding of the mechanism of alkaline leaching in the presence of tartrate can improve the selectivity of Mo leaching and allow the selection of proper separation methods for the dissolved compounds. In future work, it should be investigated if the high efficiencies and dissolution rates achieved were the result of reactions with the tartrate ions or the result of higher ionic strength of the solution containing sodium tartrate. Answers to these questions can show the different paths that research should follow, e.g. a deeper exploration of the reaction mechanisms or substitution of the sodium tartrate with other ionic compounds.

Acknowledgements

This work would not have been possible without the funding from the Swedish Energy Agency (grants number 49349-1 and P2019-90193) and the ÅForsk Foundation (grant number 24-597), the supply of solar cell samples and information about them by Midsummer AB and the assistance of the Chalmers Materials Analysis Laboratory (CMAL) with the operation of the SEM-EDS and XRD instruments.

I would also like to express my gratitude to my supervisor, Burçak Ebin, for offering this PhD position to me, making this way my dream of doing a PhD on recycling of PV come true. I would also like to thank him for his excitement, his patience, the time he spent showing me how to use some of the lab equipment and instruments, his support in good and hard times, the moments of cheerful chatting and the freedom he gave me in many decisions, during all these years. I am also very grateful to my co-supervisor, Stellan Holgersson, for all the hours he spent teaching me how to properly use and take care of the ICP-OES and ICP-MS, all the help I received from him, even before he became my co-supervisor, and all the detailed and insightful comments he always provided on my written work. Thank you so much, Stellan, for everything you taught me, as well as all the funny moments of joking. I also appreciate a lot the feedback from my examiner Christian Ekberg, which always worked as “food for thought” for me.

Of course, I could not miss to acknowledge all my colleagues (juniors and seniors, older and newer) and the great working environment they always create. A special thanks to Léa, Nils and Thomas for the great ideas, support and discussions, both on our projects and on our environmental concerns. Also to Léa, as well as Nathália, Natalie, Esraa and Aarushi, for being wonderful office-mates. I am also very grateful to my colleagues and good friends Dogac, Fredrik, Georgios, Natalie, Pawan and Yigit, for always being there for me and for the great time we have always had, both inside and outside Chalmers.

As the job of a PhD student is not always easy, friends outside Chalmers and family played a special role in motivating and supporting me during all these years. Therefore, I couldn't feel more grateful for having Leatitia & William, Sneha & Nitesh, Petra & Toni, Niloofar & Navid, May-Marie & Hélder & Kai, Sayali & Diraj & Ira, Chiara & Thomas and Shubhankar in my life. Thank you so much guys for all the crazy times, the laughter, the adventures, the love and support you always give. You make me feel like I have a second, huge, family in Sweden. A big thanks also to my good friend, now, and previously MSc student, Co, for all the great work she did as my student and, later, all the mushroom-picking and food-tasting adventures we had together. Looking forward to having even more fun with you! This chapter in my life could not have closed in a more perfect way, without my sweet and adorable Marcus. Thank you so much for making my life so complete and happy! Last but not least, I would like to express my endless gratitude and love to my family, for their unconditional love and support, their patience, their efforts to keep me motivating in hard times and their understanding. Finally, an extra, and big, “thank you” to my beloved sister, Katerina, who has always been here for me, and she has a special place in my heart. I cannot be more grateful for everything you have done for me, my dear sister.

Reference

- [1] International Energy Agency (IEA), Solar PV, 2023, IEA, <https://www.iea.org/reports/solar-pv> (Accessed 20 November 2024)
- [2] Fraunhofer Institute for Solar Energy Systems, PHOTOVOLTAICS REPORT, Germany: Fraunhofer Institute for Solar Energy Systems, 2024
- [3] IRENA and IEA, End-of-Life Management: Solar Photovoltaic Panels, IEA-PVPS Report Number: T12-06:2016, 2016, IRENA, https://www.irena.org/-/media/Files/IRENA/Agency/Publication/2016/IRENA_IEAPVPS_End-of-Life_Solar_PV_Panels_2016.pdf (Accessed 9 March 2025)
- [4] M. Marwede, W. Berger, M. Schlummer, A. Mäurer and A. Reller, Recycling paths for thin-film chalcogenide photovoltaic waste – Current feasible processes, *Renewable Energy* 55 (2013) 220-229, <https://doi.org/10.1016/j.renene.2012.12.038>
- [5] THE EUROPEAN PARLIAMENT AND THE COUNCIL OF THE EUROPEAN UNION, DIRECTIVE 2012/19/EU OF THE EUROPEAN PARLIAMENT AND OF THE COUNCIL of 4 July 2012 on waste electrical and electronic equipment (WEEE), *Official Journal of the European Union* (2012)
- [6] International Energy Agency (IEA), End-of-Life Management of Photovoltaic Panels: Trends in PV Module Recycling Technologies, Report IEA-PVPS T12-10:2018, 2018, IEA-PVPS, https://iea-pvps.org/wp-content/uploads/2020/01/End_of_Life_Management_of_Photovoltaic_Panels_Trends_in_PV_Module_Recycling_Technologies_by_task_12.pdf (Accessed 9 March 2025)
- [7] International Energy Agency (IEA), Fact sheet: Circular Economy in Photovoltaics, 2024, IEA-PVPS, <https://iea-pvps.org/wp-content/uploads/2024/03/IEA-PVPS-Task-12-Circular-Economy-Fact-Sheet.pdf> (Accessed 9 March 2025)
- [8] H. Mirlitz, H. Hieslmair, S. Ovaitt, T. L. Curtis and T. M. Barnes, Unfounded concerns about photovoltaic module toxicity and waste are slowing decarbonization, *nature physics* 19 (2023) 1376–1378, <https://doi.org/10.1038/s41567-023-02230-0>
- [9] International Energy Agency (IEA), Final List of Critical Minerals 2022, 2022 (last update February 2023), <https://www.iea.org/policies/15271-final-list-of-critical-minerals-2022> (Accessed 9 November 2024)
- [10] European Commission: Directorate-General for Internal Market, Industry, Entrepreneurship and SMEs, M. Grohol, and C. Veeh, Study on the critical raw materials for the EU 2023 – Final report, Belgium: European Commission, 2023
- [11] K. L. Nuttall, Evaluating Selenium Poisoning, *Annals of Clinical & Laboratory Science* 36 (4) (2006) 409-420
- [12] M. Jošt, E. Köhnen, A. Al-Ashouri, T. Bertram, Š. Tomšič, A. Magomedov, E. Kasparavicius, T. Kodalle, B. Lipovšek, V. Getautis, R. Schlatmann, C. A. Kaufmann, S. Albrecht and M. Topič,

Perovskite/CIGS Tandem Solar Cells: From Certified 24.2% toward 30% and Beyond, *ACS Energy Letters* 7 (4) (2022) 1298–1307, <https://doi.org/10.1021/acsenergylett.2c00274>

[13] U.S. Geological Survey, Mineral commodity summaries 2024, USA: U.S. Geological Survey, 2024, <https://doi.org/10.3133/mcs2024>

[14] The Silver Institute, World Silver survey 2023, 2023, The Silver Institute, <https://silverinstitute.org/wp-content/uploads/2023/04/World-Silver-Survey-2023.pdf> (Accessed 9 March 2025)

[15] J. Schuster and B. Ebin, Investigation of indium and other valuable metals leaching from unground waste LCD screens by organic and inorganic acid leaching, *Separation and Purification Technology* 279 (2021) 119659, <https://doi.org/10.1016/j.seppur.2021.119659>

[16] International Energy Agency (IEA), Advances in Photovoltaic Module Recycling Literature Review and Update to Empirical Life Cycle Inventory Data and Patent Review, Report IEA-PVPS T12-28:2024, 2024, IEA-PVPS, https://iea-pvps.org/wp-content/uploads/2024/06/IEA-PVPS-T12-28-2024-Report-PV-Recycling-LCI_EPRI.pdf (Accessed 9 March 2025)

[17] A.M.K. Gustafsson, M.R. StJ. Foreman and C. Ekberg, Recycling of high purity selenium from CIGS solar cell waste materials, *Waste Management* 34(10) (2014) 1775–1782, <https://doi.org/10.1016/j.wasman.2013.12.021>

[18] G. Du, Y. Bai, J. Huang, J. Zhang, J. Wang, Y. Lin, L. Lu, L. Yang, S. Bao, Z. Huang, X. Chen, M. Yin and D. Li, Surface Passivation of ITO on Heterojunction Solar Cells with Enhanced Cell Performance and Module Reliability, *ECS Journal of Solid State Science and Technology* 10 (2021) 035008, <https://doi.org/10.1149/2162-8777/abeece>

[19] M. Taguchi, Review—Development History of High Efficiency Silicon Heterojunction Solar Cell: From Discovery to Practical Use, *ECS Journal of Solid State Science and Technology* 10 (2021) 025002, <https://doi.org/10.1149/2162-8777/abdfb6>

[20] Florida's Premier Energy Research Center at the University of Central Florida, Cells, Modules, Panels and Arrays, no date available, Florida's Premier Energy Research Center at the University of Central Florida, <https://energyresearch.ucf.edu/consumer/solar-technologies/solar-electricity-basics/cells-modules-panels-and-arrays/> (Accessed 22 November 2024)

[21] J. Ramanujam and U.P. Singh, Copper indium gallium selenide based solar cells – a review, *Energy & Environmental Science* 10 (6) (2017) 1306–1319, <https://doi.org/10.1039/C7EE00826K>

[22] N. Alhammadi, E. Rodriguez-Ubinas, S. Alzarouni and M. Alantali, Building-integrated photovoltaics in hot climates: Experimental study of CIGS and c-Si modules in BIPV ventilated facades, *Energy Conversion and Management* 274 (2022) 116408, <https://doi.org/10.1016/j.enconman.2022.116408>

[23] D. Zhou, H. Zhu, X. Liang, C. Zhang, Z. Li, Y. Xu, J. Chen, L. Zhang and Y. Mai, Sputtered molybdenum thin films and the application in CIGS solar cells, *Applied Surface Science* 362 (2016) 202–209, <http://dx.doi.org/10.1016/j.apsusc.2015.11.235>

- [24] M. Moradi, R. Teimouri, M. Saadat and M. Zahedifar, Buffer layer replacement: A method for increasing the conversion efficiency of CIGS thin film solar cells, *Optik* 136 (2017) 222-227, <https://doi.org/10.1016/j.ijleo.2017.02.037>
- [25] H. Li, J. Wang, Y. Wang, A. Zhao, B. Li and W. Li, Controllable and innovative preparation of Zn(O,S) buffer layers for CIGS thin film solar cells, *Optical Materials* 138 (2023) 113711, <https://doi.org/10.1016/j.optmat.2023.113711>
- [26] E. Kyriakides, C. Nicolaou, P.S. Ioannou, P. Papagiorgis, G. Itskos and J. Giapintzakis, Single-stage fabrication of buffer and window layers of CIGS thin-film solar cells using pulsed laser deposition, *Solar Energy* 283 (2024) 112993, <https://doi.org/10.1016/j.solener.2024.112993>
- [27] H. Tong, Z. Kou, M. Zhao, D. Zhuang, C. Wang and Y. Li, Influences of Mg concentration in ZnMgO film on energy band alignment at CIGSSe/Zn_{1-x}Mg_xO interface and performances of CIGSSe solar cells, *Solar Energy* 246 (2022) 216-223, <https://doi.org/10.1016/j.solener.2022.09.039>
- [28] X. Shen, M. Yang, C. Zhang, Z. Qiao, H. Wang and C. Tang, Utilizing magnetron sputtered AZO-ITO bilayer structure as transparent conducting oxide for improving the performance of flexible CIGS solar cell, *Superlattices and Microstructures* 123 (2018) 251-256, <https://doi.org/10.1016/j.spmi.2018.09.001>
- [29] J. K. Larsen, H. Simchi, P. Xin, K. Kim and W. N. Shafarman, Backwall superstrate configuration for ultrathin Cu(In,Ga)Se₂ solar cells, *Applied Physics Letters* 104 (2014) 033901, <https://doi.org/10.1063/1.4862651>
- [30] C. Honsberg and S. Bowden, Silicon Solar Cell Parameters, no date available, PVEducation, <https://www.pveducation.org/pvcdrom/design-of-silicon-cells/silicon-solar-cell-parameters#:~:text=An%20optimum%20silicon%20solar%20cell%20with%20light%20trapping,tin%20wafers%2C%20and%20partly%20for%20surface%20passivation%20reasons> (Accessed 26 February 2025)
- [31] J. Park and N. Park, Wet etching processes for recycling crystalline silicon solar cells from end-of-life photovoltaic modules, *RSC Advances* 4 (2014) 34823-34829, <https://doi.org/10.1039/C4RA03895A>
- [32] W. F. Drinkard Jr, M.O. Long and R.E. Goozner, Recycling of CIS photovoltaic waste, US005779877A, filed 12 May 1997 and issued 14 July 1998, <https://patents.google.com/patent/US5779877A/en>
- [33] W. Palitzsch, Method for recycling a thin layer solar module during simultaneous recovering of recyclable material, by loading photovoltaic cells to be processed so that the plastic portion is separated from remaining components of the module, DE102008058530A1, filed 21 November 2008 and issued 27 May 2010, <https://patents.google.com/patent/DE102008058530A1/en?q=DE102008058530A1>
- [34] C.-H. Lai, W.-S. Chen, Y.-L. Chueh, F.-W. Liu and T.-M. Cheng, Method for recovering resource from CIGS thin-film solar cell, US011374144B2, filed 23 October 2020 and issued 28 June 2022, <https://patents.google.com/patent/US11374144B2/en?q=US+11374144B2>

- [35] K. Kushiya and M. Tanaka, CIS based thin film solar cell module, method for producing the same, and method for separating solar cell module, EP1830411A1, filed 22 December 2005 and issued 5 September 2007, <https://patents.google.com/patent/EP1830411A1/en>
- [36] U. Wagner and F. Schmieder, Method for Recycling Thin-Film Solar Cell Modules, US20090308535A1, filed 8 June 2009 and issued 17 December 2009, <https://patents.google.com/patent/US20090308535A1/en?q=US+20090308535A1>
- [37] 周麒麟, 何宇虹, 吴述园 and 朱红生, Method for continuously separating copper, indium and gallium from waste thin-film solar cells, CN113737221A, filed 15 September 2021 and issued 3 December 2021, <https://patents.google.com/patent/CN113737221A/en?q=CN113737221A>
- [38] 廖贻鹏, 刘景文, 伏东才, 刘宁, 刘一宁, 刘敏 and 戴慧敏, A method for recycling copper indium gallium selenide, CN104018186B, filed 24 June 2014 and issued 31 August 2016, <https://patents.google.com/patent/CN104018186B/en?q=CN104018186B>
- [39] C. G. Ferron, Treatment of indium gallium alloys and recovery of indium and gallium, US8834818B2, filed 22 November 2011 and issued 16 September 2014, <https://patents.google.com/patent/US8834818B2/en?q=US8834818B2>
- [40] K. Kushiya, M. Ohshita and M. Tanaka, Development of recycling and reuse technologies for large area Cu(InGa)Se₂-based thin-film modules, 3rd World Conference on Photovoltaic Energy Conversion, 11-18 May 2003, Osaka, Japan, 1892-1895
- [41] F.-W. Liu, T.-M. Cheng, Y.-J. Chen, K.-C. Yueh, S.-Y. Tang, K. Wang, C.-L. Wu, H.-S. Tsai, Y.-J. Yu, C.-H. Lai, W.-S. Chen, Y.-L. Chueh, High-yield recycling and recovery of copper, indium, and gallium from waste copper indium gallium selenide thin-film solar panels, *Solar Energy Materials and Solar Cells* 241 (2022) 111691, <https://doi.org/10.1016/j.solmat.2022.111691>
- [42] A. Amato and F. Beolchini, End-of-life CIGS photovoltaic panel: A source of secondary indium and gallium, *Progress in Photovoltaics* 27 (2019) 229–236, <https://doi.org/10.1002/ppp.3082>
- [43] A.M.K. Gustafsson, B.-M. Steenari, C. Ekberg, Evaluation of high-temperature chlorination as a process for separation of copper, indium and gallium from CIGS solar cell waste materials, *Separation Science and Technology* 50 (1) (2015) 1–9, <https://doi.org/10.1080/01496395.2014.949350>
- [44] A.M.K. Gustafsson, B.-M. Steenari, C. Ekberg, Recycling of CIGS solar cell waste materials: separation of copper, indium, and gallium by high-temperature chlorination reaction with ammonium chloride, *Separation Science and Technology* 50 (15) (2015) 2415–2425, <https://doi.org/10.1080/01496395.2015.1053569>
- [45] Y. Lv, P. Xing, B. Ma, B. Liu, C. Wang, Y. Zhang, W. Zhang, Separation and recovery of valuable elements from spent CIGS materials, *ACS Sustainable Chemistry and Engineering* 7 (24) (2019) 19816–19823, <https://doi.org/10.1021/acssuschemeng.9b05121>

- [46] X. Li, B. Ma, D. Hu, Q. Zhao, Y. Chen and C. Wang, Efficient separation and purification of indium and gallium in spent Copper indium gallium diselenide (CIGS), *Journal of Cleaner Production* 339 (2022) 130658, <https://doi.org/10.1016/j.jclepro.2022.130658>
- [47] B. Ma, X. Li, B. Liu, P. Xing, W. Zhang, C. Wang and Y. Chen, Effective separation and recovery of valuable components from CIGS chamber waste via controlled phase transformation and selective leaching, *ACS Sustainable Chemistry and Engineering* 8 (7) (2020) 3026–3037, <https://pubs.acs.org/doi/10.1021/acssuschemeng.0c00138>
- [48] D. Hu, B. Ma, X. Li, Y. Lv, Y. Chen, C. Wang, Innovative and sustainable separation and recovery of valuable metals in spent CIGS materials, *Journal of Cleaner Production* 350 (2022), 131426, <https://doi.org/10.1016/j.jclepro.2022.131426>
- [49] H.-I. Hsiang, C.-Y. Chiang, W.-H. Hsu, W.-S. Chen, J.-E. Chang, Leaching and resynthesis of CIGS nanocrystallites from spent CIGS targets, *Advanced Powder Technology* 27 (3) (2016) 914–920, <https://doi.org/10.1016/j.apt.2016.02.012>
- [50] S. Gu, B. Fu, G. Dodbiba, T. Fujita, B. Fang, Promising approach for recycling of spent CIGS targets by combining electrochemical techniques with dehydration and distillation, *ACS Sustainable Chemistry and Engineering* 6 (5) (2018) 6950–6956, <https://pubs.acs.org/doi/10.1021/acssuschemeng.8b00787>
- [51] J. E. Hoffmann, Silver processing, 1999, Britannica, <https://www.britannica.com/technology/silver-processing> (Accessed 28 February 2025)
- [52] Environmental Literacy Council, Can You Recycle Silverware?, 2024, Enviroliteracy, https://enviroliteracy.org/can-you-recycle-silverware/#The_Recycling_Process_From_Fork_to_Furnace (Accessed 28 February 2025)
- [53] L. Beck, J. Koppe, W. Krebs and H. Stecher, Method for recovering pure silver from used silver carrier catalysts, 1983, DD268979A1, filed 1 November 1983 and issued 14 June 1989, <https://patents.google.com/patent/DD268979A1/en>
- [54] SIMS LIFECYCLE SERVICES, How we do it, no date available, SIMS LIFECYCLE SERVICES, <https://www.simslifecycle.com/business/e-waste-recycling/how-we-do-it/> (Accessed 28 February 2025)
- [55] 杨建广, 唐朝波, 何静, 杨声海 and 唐谟堂, Method for extracting valuable metals from electronic waste, CN101575715A, filed 22 June 2009 and issued 11 November 2009, <https://patents.google.com/patent/CN101575715A/en?q=CN101575715A>
- [56] 刘维, 焦芬, 覃文庆, 蔡练兵 and 梁超, Method for comprehensively recycling valuable metals of waste circuit board, CN105755289B, filed 28 April 2016 and issued 15 December 2017, <https://patents.google.com/patent/CN105755289B/en?q=CN105755289B>
- [57] 张晓飞 and 苏冠贤, Method of extracting silver from crystalline silicon solar panel, CN106629738A, filed 12 January 2017 and issued 10 May 2017, <https://patents.google.com/patent/CN106629738A/en?q=CN106629738A>

- [58] W. Palitzsch, Method for Concentrating Metals from Scrap Containing Metal, WO2014166484A1, filed 10 April 2014 and issued 16 October 2014, <https://patents.google.com/patent/WO2014166484A1/en?q=WO2014166484A1>
- [59] X. Wang, X. Tian, X. Chen, L. Ren and C. Geng, A review of end-of-life crystalline silicon solar photovoltaic panel recycling technology, *Solar Energy Materials and Solar Cells* 248 (2022) 111976, <https://doi.org/10.1016/j.solmat.2022.111976>
- [60] A. Kuczynska-Łazewska, E. Klugmann-Radziemska, Z. Sobczak, T. Klimczuk, Recovery of silver metallization from damaged silicon cells, *Solar Energy Materials and Solar Cells* 176 (2018) 190–195, <https://doi.org/10.1016/j.solmat.2017.12.004>
- [61] J.-P. Wang, D.-H. Lee, M.-S. Go and E.-K. So, A Study on the Wet Process Conditions That Affect the Selective Recovery of Si from Photovoltaic Cells by Using the Cavitation Effect, *Metals* 12 (2) (2022) 222, <https://doi.org/10.3390/met12020222>
- [62] S. Kang, S. Yoo, J. Lee, B. Boo, H. Ryu, Experimental investigations for recycling of silicon and glass from waste photovoltaic modules, *Renewable Energy* 47 (2012) 152–159, <https://doi.org/10.1016/j.renene.2012.04.030>
- [63] T.-Y. Wang, J.-C. Hsiao, C.-H. Du, Recycling of Materials from Silicon Base Solar Cell Module, 38th IEEE Photovoltaic Specialists Conference, 03-08 June 2012, Austin, TX, USA, 002355-002358, <https://doi.org/10.1109/PVSC.2012.6318071>
- [64] W. Palitzsch, U. Loser, A New and Intelligent De-metalization Step of Broken Silicon Cells and Silicon Cell Production Waste in the Recycling Procedure of Crystalline SI Modules, 2011 37th IEEE Photovoltaic Specialists Conference, 19-24 June 2011, Seattle, WA, USA, 003269–003270, <https://doi.org/10.1109/PVSC.2011.6186635>
- [65] L. Punathil, K. Mohanasundaram, K. S. Tamilselavan, R. Sathyamurthy and Ali J. Chamkha, Recovery of Pure Silicon and Other Materials from Disposed Solar Cells, *International Journal of Photoenergy* Volume 2021, Article ID 5530213, 4 pages, <https://doi.org/10.1155/2021/5530213>
- [66] B. Jung, J. Park, D. Seo and N. Park, Sustainable System for Raw-Metal Recovery from Crystalline Silicon Solar Panels: From Noble-Metal Extraction to Lead Removal, *ACS Sustainable Chemistry and Engineering* 4 (2016) 4079–408, <https://doi.org/10.1021/acssuschemeng.6b00894>
- [67] 刘文杰, 文杰, 钟小华, 童培云 and 朱刘, Method for recycling ITO target material waste, CN114409380A, filed 11 January 2022 and issued 29 April 2022, <https://patents.google.com/patent/CN114409380A/en?q=CN114409380A>
- [68] 文宏福, 李鹏 and 叶俊峰, Preparation method for directly crushing ITO waste target to prepare powder and producing ITO target, CN112079627A, filed 16 September 2020 and 15 December 2020, <https://patents.google.com/patent/CN112079627A/en?q=CN112079627A>
- [69] 余芳, 文崇斌, 朱刘 and 童培云, Method for preparing ITO evaporation material from ITO residual target reclaimed material, CN113233871A, filed 25 April 2021 and 10 August 2021, <https://patents.google.com/patent/CN113233871A/en?q=CN113233871A>

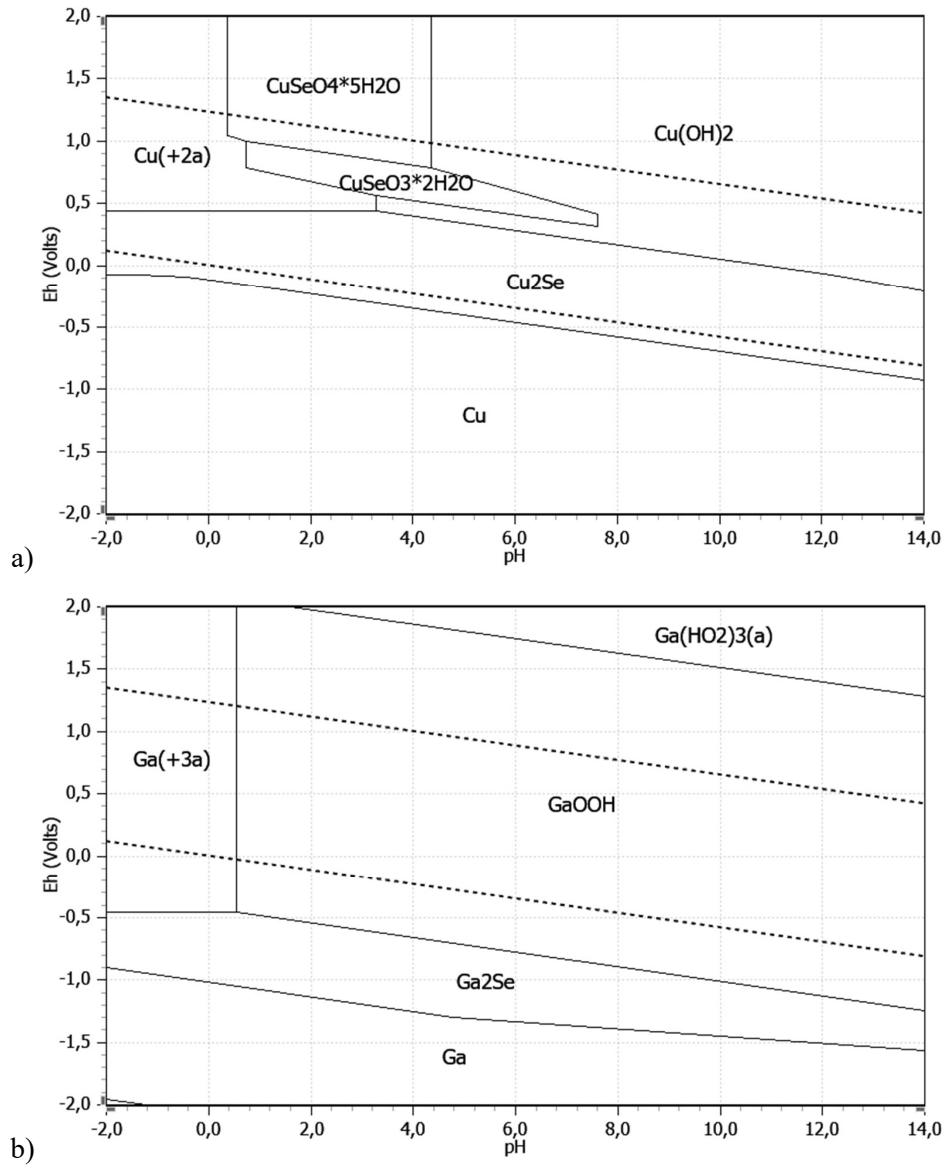
- [70] A. Amato and F. Beolchini, End of life liquid crystal displays recycling: A patent review, *Journal of Environmental Management* 225 (2018) 1-9, <https://doi.org/10.1016/j.jenvman.2018.07.035>
- [71] B. Augustine, K. Remes, G. S. Lorite, J. Varghese, T. Fabritius, Recycling perovskite solar cells through inexpensive quality recovery and reuse of patterned indium tin oxide and substrates from expired devices by single solvent treatment, *Solar Energy Materials and Solar Cells* 194 (2019) 74-82, <https://doi.org/10.1016/j.solmat.2019.01.041>
- [72] R. Hu, X. Su, H. Liu, Y. Liu, M.-M. Huo and W. Zhang, Recycled indium tin oxide transparent conductive electrode for polymer solar cells, *Journal of Material Science* 55 (2020) 11403–11410, <https://doi.org/10.1007/s10853-020-04825-x>
- [73] M. T. Dang, J. Lefebvre and J. D. Wuest, Recycling Indium Tin Oxide (ITO) Electrodes Used in Thin-Film Devices with Adjacent Hole-Transport Layers of Metal Oxides, *ACS Sustainable Chemistry & Engineering* 3 (12) (2015) 3373–3381, <https://doi.org/10.1021/acssuschemeng.5b01080>
- [74] W.J. Gilbert, “Corrosion in Emissions Control Equipment”, in: *ASM Handbook. Volume 13C. Corrosion: Environments and Industries*, edited by S.D. Cramer and B. S. Covino Jr., 251-256, USA: ASM International, 2006
- [75] E. McCafferty, “Getting started on the basics”, in: *Introduction to Corrosion Science*, 15-22, USA: Springer, 2010
- [76] R. Bender, D. Féron, D. Mills, S. Ritter, R. Bäßler, D. Bettge, I. De Graeve, A. Dugstad, S. Grassini, T. Hack, M. Halama, E.-H. Han, T. Harder, G. Hinds, J. Kittel, R. Krieg, C. Leygraf, L. Martinelli, A. Mol, D. Neff, J.-O. Nilsson, I. Odnevall, S. Paterson, S. Paul, T. Prošek, M. Raupach, R.I. Revilla, F. Ropital, H. Schweigart, E. Szala, H. Terry, J. Tidblad, S. Virtanen, P. Volovitch, D. Watkinson, M. Wilms, G. Winning, M. Zheludkevich, Corrosion challenges towards a sustainable society, *Materials and Corrosion* 73 (2022) 1–22, <https://doi.org/10.1002/maco.202213140>
- [77] H. Cui, G. Heath, T. Remo, D. Ravikumar, T. Silverman, M. Deceglie, M. Kempe, J. Engel-Cox, Technoeconomic analysis of high-value, crystalline silicon photovoltaic module recycling processes, *Solar Energy Materials and Solar Cells* 238 (2022) 111592, <https://doi.org/10.1016/j.solmat.2022.111592>
- [78] A. Ravilla, Emily Gullickson, A. Tomes and I. Celik, Economic and environmental sustainability of copper indium gallium selenide (CIGS) solar panels recycling, *Science of the Total Environment* 951 (2024) 175670, <https://doi.org/10.1016/j.scitotenv.2024.175670>
- [79] F. Faraji, A. Alizadeh, F. Rashchi N. Mostouf, Kinetics of leaching: a review, *Reviews in Chemical Engineering* 38 (2) (2020) 113–148, <https://doi.org/10.1515/revce-2019-0073>
- [80] D.D. Ebbing and S.D. Gammon, *General Chemistry*, ninth ed., USA: Houghton Mifflin Company, 2009

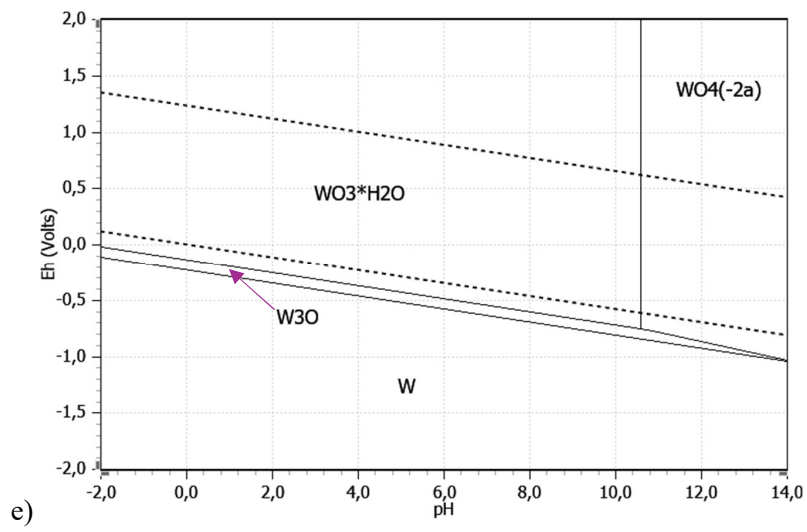
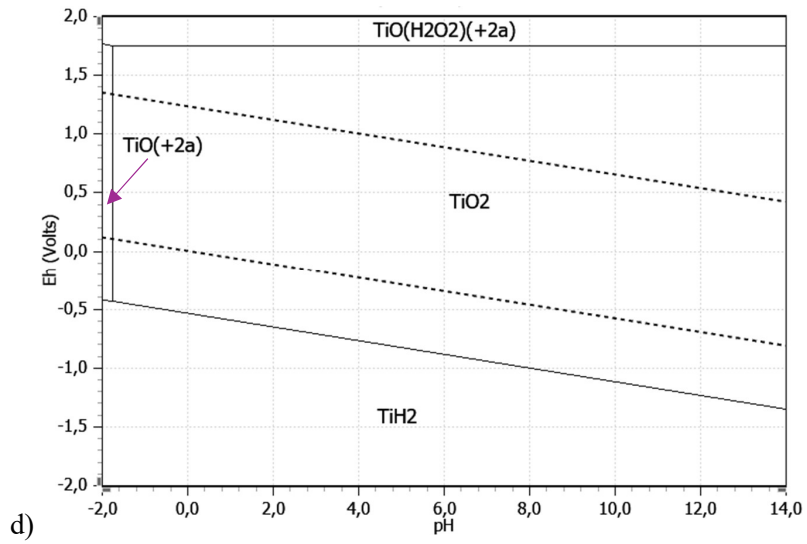
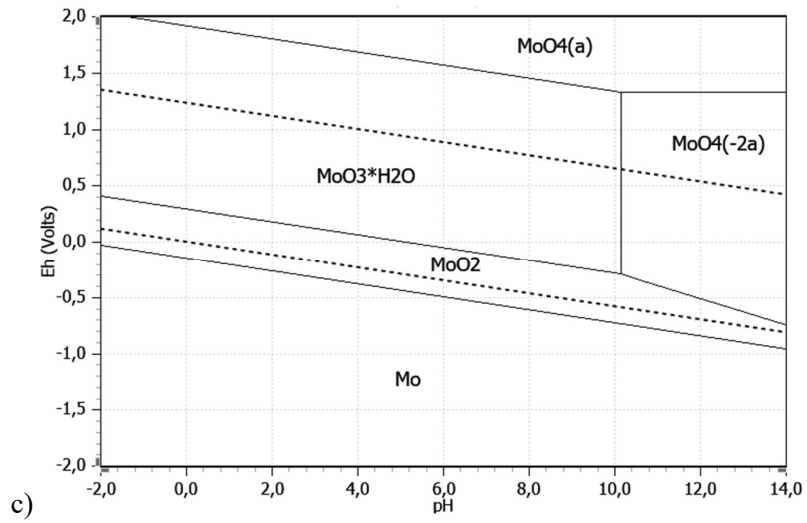
- [81] M. Easson, B. Condon, A. Villalpando, S.-C. Chang, The application of ultrasound and enzymes in textile processing of greige cotton, *Ultrasonics* 84 (2018) 223-233, <https://doi.org/10.1016/j.ultras.2017.11.007>
- [82] Metso Outotec, HSC Chemistry, version 10.1.0.1., Metso, [software] <https://www.hsc-chemistry.com/>
- [83] I. F. Barton and J. B. Hiskey, Chalcopyrite leaching in novel lixivants, *Hydrometallurgy* 207 (2022) 105775, <https://doi.org/10.1016/j.hydromet.2021.105775>
- [84] University of Cambridge, Construction of a Pourbaix Diagram, no date available, DoITPoMS, https://www.doitpoms.ac.uk/tlplib/pourbaix/pourbaix_construction.php (Accessed 3rd March 2025)
- [85] H. M. Kingston and J. P. Walter, “The art and science of microwave sample preparation”, in: *Inductively Coupled Plasma Mass Spectrometry*, edited by A. Montaser, 33-82, USA: Wiley, 1998
- [86] A. Arora, *Textbook of Inorganic Chemistry*, India: Discovery Publishing House, 2005
- [87] B. D. Craig and D. B. Anderson (Editors), “Nitric acid” in: *Handbook of Corrosion Data*, second ed., 541-571, USA: ASM International, 1995
- [88] P. Cannon, The solubility of molybdenum trioxide in various mineral acids, *Journal of Inorganic and Nuclear Chemistry* 11 (1959) 124-127
- [89] L.M. Ferris, Solubility of molybdic oxide and its hydrates in nitric acid, nitric acid ferric nitrate, and nitric acid-uranyl nitrate solutions, *Journal of Chemistry and Engineering Data* 6 (4) (1961) 600–603, <https://doi.org/10.1021/jc60011a035>
- [90] British Stainless Steel Association, Passivation of stainless steels, British Stainless Steel Association, https://bssa.org.uk/bssa_articles/passivation-of-stainless-steels/ (Accessed 10 July 2022)
- [91] F. A. Cotton and G. Wilkinson, *Advanced Inorganic Chemistry: a comprehensive text*, fifth ed., USA: John Wiley & Sons, 1988
- [92] C. Payan, A.-L. Gancel, M. Jourdes, M. Christmann and P.-L. Teissedre, Wine acidification methods: a review, *OENO One* 57 (3) (2023) 113-126, <https://doi.org/10.20870/oeno-one.2023.57.3.7476>
- [93] A. M. V. S. V. Cavaleiro, V. M. S. Gil, J. D. Pedrosa de Jesus, R. D. Gillard and P. A. Williams, N.m.r. Studies of Complexes of Molybdenum(VI) with Tartaric Acid in Aqueous Solution, *Transition Metal Chemistry* 9 (1984) 62-67
- [94] A. M. V. Cavaleiro, J. D. Pedrosa de Jesus, R. D. Gillard and P. A. Williams, Tungsten(VI) and Mixed Tungsten, Molybdenum(VI) Complexes of Tartaric Acid, *Transition Metal Chemistry* 9 (1984) 81-82

- [95] A. M. V. Cavaleiro and J. D. Pedrosa de Jesus, Reactions of Mo(VI) with (2R,3R)-Tartaric Acid in Diluted Aqueous Solutions: A Study by Circular Dichroism Spectrophotometry, *Inorganica Chimica Acta* 166 (1989) 205-212
- [96] Z. Liu, X. Guo, Z. Xu and Q. Tian, Recent advancements in aqueous electrowinning for metal recovery: A comprehensive review, *Minerals Engineering* 216 (2024) 108897, <https://doi.org/10.1016/j.mineng.2024.108897>
- [97] EDAX, Tips & tricks: Optimizing spatial resolution for EDS analysis, no date available, EDAX, https://www.edax.com/-/media/ametekedax/files/resources/tips_tricks/optimizingspatialresolutionforedsanalysis.pdf (Accessed 9 March 2025)
- [98] Z. Gao, M. Zhao, D. Zhuang, E. Fu, X. Li, L. Ouyang, L. Guo, R. Sun, K. Kimura and K. Nakajima, Study on the performance of Tungsten–Titanium alloy film as a diffusion barrier for iron in a flexible CIGS solar cell, *Solar Energy* 120 (2015) 357–362, <http://dx.doi.org/10.1016/j.solener.2015.07.027>
- [99] P. C. Huang, C. C. Sung, J. H. Chen, R. C. Hsiao and C. Y. Hsu, Effect of selenization and sulfurization on the structure and performance of CIGS solar cell, *Journal of Materials Science: Materials in Electronics* 29 (2018) 1444–1450, <https://doi.org/10.1007/s10854-017-8052-6>
- [100] D. C. Montgomery, *Design and Analysis of Experiments*, EMEA edition, 10th ed.; USA: John Wiley & Sons, 2020
- [101] MathWorks, MATLAB, version 9.7. 0.1190202 (R2019b), MathWorks, [software] <https://www.mathworks.com/products/matlab.html>
- [102] R. Sitaram and S. M. Khopkar, Anion-exchange behaviour of indium(III) in citrate and tartrate solutions: separation from mixtures, *Analytica Chimica Acta* 71 (1974) 472-476
- [103] M. Zabiszak, J. Frymark, M. Nowak, J. Grajewski, K. Stachowiak, M. T. Kaczmarek and R. Jastrz, Influence of d-Electron Divalent Metal Ions in Complex Formation with L-Tartaric and L-Malic Acids, *Molecules* 26 (2021) 5290, <https://doi.org/10.3390/molecules26175290>
- [104] Y. Nagoya, K. Kushiya, M. Tachiyuki and O. Yamase, Role of incorporated sulfur into the surface of Cu(InGa)Se₂ thin-film absorber, *Solar Energy Materials & Solar Cells* 67 (2001) 247-253, [https://doi.org/10.1016/S0927-0248\(00\)00288-9](https://doi.org/10.1016/S0927-0248(00)00288-9)

Appendix

A1. Pourbaix (Eh-pH) plots





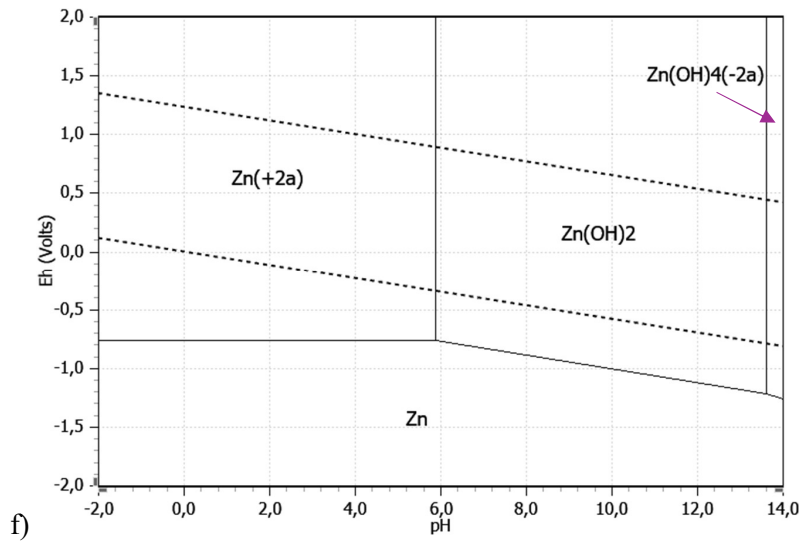


Fig. A1: Pourbaix plot of a) Cu, b) Ga, c) Mo, d) Ti, e) W and f) Zn at 20 °C and molality of each element equal to 1 mol/kg.

A2. Sample division



Fig. A2: Division of the flexible CIGS solar cell ($15.6 \times 15.6 \text{ cm}^2$) into smaller pieces which were used in the experiments: triangular (30.4 cm^2) and square (15.2 cm^2) pieces for the acid and alkaline leaching experiments, respectively.

A3. Design, analysis and assessment of split-plot factorial experiments

Factorial experiments are an experimentation strategy which offers high efficiency in experimentation, because it uses all experimental data in the most efficient way. A type of factorial experiments, which is used when there is at least one factor which is hard to change from one experimental run to the other, is called split-plot factorial. The hard-to-change factor, called whole-plot (WP) factor, imposes a restriction on complete randomization of the experimental runs, which is otherwise the recommended way for performing experiments [100]. For instance, one of the most hard-to-change factors at industrial scale is the temperature of big furnaces, since it is time-consuming to wait until the furnace reaches the desired temperature and stabilize. Because of this reason, in split-plots, all the samples that are to be treated at the same temperature are treated simultaneously (in contrast to completely randomized experiments, which would require every run to be performed separately, its temperature to be selected randomly every time among the temperature levels to investigate, and the furnace to be turned on and off as many times as the runs). The way of performing this experiment in split-plots imposes a restriction on complete randomization of the factor temperature. It must be clarified though, that the order in which the different levels of the factor (i.e. different temperatures) will be tested must still be random. For example, whether all the experiments of high or low temperature will be performed first, should be decided randomly. Each combination of WP factor levels constitutes a different WP, e.g. if there are 3 WP factors, each of them at 2 levels, the total number of WP will be $2^3=8$. When performing experiments, there are also factors which are easy-to-change. These factors in split-plots are called sub-plot (SP) factors. For instance, the treatment time is an easy-to-change factor, since the only requirement is to remove the samples from the furnace at the indicated times. Complete randomization of the easy-to-change factors is possible. Each WP comprises a number of SP, equal to the number of combinations of SP factor levels. For example, if there are 4 SP factors, each at 2 levels, each WP will contain $2^4=16$ SP.

In the particular thesis, split plot factorials were chosen, due to many practical difficulties with changing some of the design factors completely randomly. The used split plots were unreplicated, with all the factors at two levels each. Therefore, the presented analysis methods focus on this specific design. In order to perform the analysis, the sizes called contrasts, Sum of Squares (SS), effects, and parameters should be calculated. Their calculations are based on the following formulas [100], when factors A, B, C, ..., M are the selected design factors of the experiment and their total number is μ :

$$\text{Contrast}_{ABC\dots} = (a \pm 1)(b \pm 1)(c \pm 1) \dots (m \pm 1) \quad (\text{Eq. A1})$$

The sign of 1 is negative for the factors included in the respective contrast and positive for the ones not included. For example, if there are 3 factors in total in the experiment, Contrast_{AB} is calculated as:

$$\text{Contrast}_{AB}=(a-1)(b-1)(c+1)=(ab-a-b+1)(c+1)=abc+ab-ac-a-bc-b+c+1$$

Each of the lowercase letter combination, as well as number 1, represent the name of an experimental run and should be substituted by the response value corresponding to the specific run. The letters show which factors are set at their high level during that run. The rest factors are at their low level. E.g. run ab means that factors A and B were at their high level, while factor C was set at its low level. 1 represents the run in which all factors are at their low level.

As soon as each contrast is calculated, the SS, effect and parameter which correspond to it can be calculated too [100]:

$$SS_{ABC\dots} = \frac{1}{2^\mu} (\text{Contrast}_{ABC\dots})^2 \quad (\text{Eq. A2})$$

$$\text{Effect}_{ABC\dots} = \frac{2}{2^\mu} \text{Contrast}_{ABC\dots} \quad (\text{Eq. A3})$$

$$\text{Parameter}_{ABC\dots} = \frac{1}{2} \text{Effect}_{ABC\dots} \quad (\text{Eq. A4})$$

As soon as these sizes are calculated for all contrasts, normal (or half-normal) probability plots are constructed for the WP and SP effects separately and, through them, the significant main effects and interactions are detected: the effects and interactions which fall away from the straight line of the plots are the significant ones. All main effects and interactions between the WP factors belong to the WP plot, while all those including SP factors belong to the SP plot (even interactions between SP and WP factors) [A1]. The different levels in randomization of split-plots (one randomization between WP and another randomization for each SP) is the reason why two separate plots are needed [A1].

After the significant factors have been detected, a model is proposed. For v number of significant factors and interactions χ , the fitted regression model has the form

$$\hat{y} = \text{Grand average} + \sum_{i=1}^v \left(\frac{\text{parameter}_i}{2} \cdot \chi_i \right) \quad (\text{Eq. A5})$$

Model adequacy checking through examination of the residuals should always follow [100]. In split-plot designs, there are also two types of residuals; the WP and the SP residuals. There are m different WP residuals (one for each of the m WP) and each of them is calculated as [A2]:

$$\text{WP residual}_i = \left(\frac{1}{p} \sum_{j=1}^p e_j \right)_i \quad (\text{Eq. A6})$$

where $i=1, 2, \dots, m$. Moreover, e_j is the ordinary residual of each of the p runs belonging to the i^{th} WP and is calculated as:

$$e_j = \text{response}_j - \text{fitted value}_j \text{ from the proposed model} \quad (\text{Eq. A7})$$

Therefore, all the runs belonging to the same WP have the same WP residual.

Each of the p SP residuals of the SP runs belonging to the same i^{th} WP is calculated as [80]:

$$(\text{SP residual})_i = e_j - \text{WP residual}_i \quad (\text{Eq. A8})$$

where $i=1, 2, \dots, m$ and $j=1, 2, \dots, p$.

Investigation of the residuals usually includes checking (i) their normal probability plots for violations of the normality assumption and (ii) the plots of residuals vs. the run order and/or vs. the fitted values and/or vs. any other factor that may have affected the variance. More specifically, in the prior case, the normal probability plots are satisfactory if all the points fall close to a straight line. In the latter case, the plots should look structureless and with a relatively constant variance per plot [100]. In the case of plots of residuals vs. fitted values, the WP residuals should be plotted against the average fitted value per WP and the SP residuals should be plotted against the fitted values. Finally, in split-plot designs, it is also recommended to plot the WP residuals against the SP residuals, to test for their general level of randomness [A2].

Finally, measures of adequacy of fit of model reveal whether the correct WP and SP effects have been included in the proposed model and describe the predictive performance of each group of effects (i.e. WP and SP). For this purpose, Almimi, Kulahci, and Montgomery [A2] proposed the computation of two R^2 , R^2 -Adjusted, Prediction Error Sums of Squares (PRESS), and R^2 -Prediction statistics; one of each for the WP sub-model and one of each for the SP sub-model.

In order to calculate the measures of adequacy in split-plots, the proposed design and model have to “break” into two sub-designs and two sub-models: the WP sub-design and sub-model and the SP sub-design and sub-model. One can easily understand that in the WP sub-design, only the WP main effects and interactions will be taken into account, while in the SP sub-design, only the SP main effects and interactions. Similar is the case for the sub-models. However, what is not always clear is that the grand average (or intercept) is also a part of the WP sub-model and must be taken into account for some of the calculations, as explained later in the text.

After creating the WP and SP sub-models, Almimi, Kulahci, and Montgomery [A2] suggest calculating the measures of adequacy of fit of the model as follows:

$$R_{\text{WP}}^2 = \frac{SS_{\text{Model(WP)}}}{SS_{\text{Total(WP)}}} \quad (\text{Eq. A9})$$

$$R_{\text{SP}}^2 = \frac{SS_{\text{Model(SP)}}}{SS_{\text{Total(SP)}}} \quad (\text{Eq. A10})$$

$$R_{\text{WP_Adj}}^2 = 1 - \frac{SS_{\text{Residuals(WP)}}/df_{SS_{\text{Residuals(WP)}}}}{SS_{\text{Total(WP)}}/df_{SS_{\text{Total(WP)}}}} \quad (\text{Eq. A11})$$

$$R_{SP_Adj}^2 = 1 - \frac{SS_{Residuals(SP)}/df_{SS_{Residuals(SP)}}}{SS_{Total(SP)}/df_{SS_{Total(SP)}}} \quad (\text{Eq. A12})$$

where df denotes the degrees of freedom of the respective source. According to Montgomery [100], the R^2 statistics is loosely interpreted as the proportion of the variability in the data “explained” by the respective proposed model, while the R^2_{Adj} statistics is a variation of the R^2 , in which the number of factors in the model is reflected. The latter statistics becomes particularly useful as the number of design factors increases and the practitioner wishes to evaluate the impact of increasing or decreasing the number of terms included in the model. High values of R^2 and R^2_{Adj} are desirable.

Regarding PRESS, an easy and fast way to calculate it in general (not specifically for split-plots) for the total n runs is

$$PRESS = \sum_{i=1}^n \left(\frac{e_i}{1-h_{ii}} \right)^2 \quad (\text{Eq. A13})$$

where the term $\frac{e_i}{1-h_{ii}}$ is equal to the i^{th} PRESS residual $e_{(i)}$, as explained by Montgomery [100]. Moreover, h_{ii} are the diagonal elements of the hat matrix, H , of the model and they can be calculated from the formula

$$h_{ii} = \mathbf{x}_i(\mathbf{X}'\mathbf{X})^{-1}\mathbf{x}'_i \quad (\text{Eq. A14})$$

It is worth clarifying here that the \mathbf{x}_i symbolizes the i^{th} row of the design matrix \mathbf{X} .

As previously mentioned, two PRESS statistics should also be computed for split-plots, one for WP and one for SP, using the respective sub-models [A2]. Therefore,

$$PRESS_{WP} = \sum_{i=1}^n \left(\frac{\text{WP residual}_i}{1-h_{ii(WP)}} \right)^2 \quad (\text{Eq. A15})$$

$$PRESS_{SP} = \sum_{i=1}^n \left(\frac{\text{SP residual}_i}{1-h_{ii(SP)}} \right)^2 \quad (\text{Eq. A16})$$

where $h_{ii(WP)}$ and $h_{ii(SP)}$ are the diagonal elements of the H matrix of the WP and SP sub-models, respectively. In order to calculate the $h_{ii(WP)}$ correctly, the intercept must also be taken into account in the WP sub-model. According to Montgomery [100], the PRESS statistics is a measure of how well the respective proposed model is likely to predict the response in a new experiment. Since PRESS stands for “PRediction Error Sum of Squares”, small values of PRESS are desirable.

Finally, the two R^2 -Prediction statistics are calculated as

$$R_{WP_Pred}^2 = 1 - \frac{PRESS_{WP}}{SS_{Total(WP)}} \quad (\text{Eq. A17})$$

$$R_{SP_Pred}^2 = 1 - \frac{PRESS_{SP}}{SS_{Total(SP)}} \quad (\text{Eq. A18})$$

As the R^2_{Pred} statistics is based on the PRESS statistics, it gives some indication of the predictive capability of the respective proposed model [100]. High R^2_{Pred} values are desirable.

A4. Calculations of leached mass, % yield and wt% purity

The leaching yield of an element i at time t [mg/cell], is calculated in this thesis as:

$$\frac{mass_i}{cell} = (C_{ICP})_i \cdot DF \cdot V_{solution} \cdot \frac{A_{cell}}{A_{sample}} \quad (\text{Eq. A19})$$

where C_{ICP} is the concentration of the element in the sample measured with the ICP [ppm or mg/l], DF the dilution factor of the ICP-measured sample, $V_{solution}$ the volume of the leaching solution at the time of sampling [l] and A_i the geometrical surface area of i .

The % leaching efficiency of an element i at time t is calculated based on the formula:

$$\% \text{ leaching efficiency } i = \frac{100 \cdot (mass_i/cell)}{(mass/cell)_{total}} \quad (\text{Eq. A20})$$

where $(mass/cell)_{total}$ is the total mass of that element present in a cell and was determined by digestion experiments.

The wt% purity of the Ag-rich particles, is calculated according to the formula:

$$\text{wt\% Ag purity} = \frac{(C_{ICP})_{Ag} \cdot DF \cdot V_{dig}}{m_{particles}} \quad (\text{Eq. A21})$$

where $m_{particles}$ is the total mass [mg] of the digested recovered particles and V_{dig} the volume of the digestate [l].

The wt% purity of ITO in ITO-rich particles was determined from (Eq. A22), considering that ITO consists of In_2O_3 and SnO_2 :

$$\text{wt\% ITO purity} = 100 \frac{0.5 \cdot \left(\frac{C_{ICP}}{MW}\right)_{In} \cdot DF \cdot V_{dig} \cdot MW_{In_2O_3} + \left(\frac{C_{ICP}}{MW}\right)_{Sn} \cdot DF \cdot V_{dig} \cdot MW_{SnO_2}}{m_{particles}} \quad (\text{Eq. A22})$$

where MW is the molar mass [g/mol].

The % recovery of Ag achieved through the recovery of the Ag-rich particles was calculated according to the formula:

$$\text{wt\% Ag recovery} = \frac{100 \cdot (\text{mass/cell})_{\text{recovered Ag}}}{(\text{mass/cell})_{\text{total}}} \quad (\text{Eq. A23})$$

where the $(\text{mass/cell})_{\text{recovered Ag}}$ was determined with the ICP-OES, after digestion of the recovered particles.

Finally, the content of an impurity *i* in the recovered particles from the US-leaching steps was calculated as:

$$\text{wt\% impurity } i = \frac{(C_{\text{ICP}})_i \cdot \text{DF} \cdot V_{\text{dig}}}{m_{\text{particles}}} \quad (\text{Eq. A24})$$

A5. Leaching results

Table A1: The highest leaching yields achieved for each element when leaching with A:L equal to 1:3 cm²/ml and different acid concentrations (mechanical stirring at 200 rpm, 20 °C).

Element	Maximum Mass/cell leached (mg/cell)		
	0.1 M	0.5 M	2 M
Ag	0.27 -0.27 +0.47	56.31 ± 11.04	65.27 -4.43 +3.54
Cr	0.45 ± 0.10	0.86 ± 0.06	2.02 ± 1.34
Cu	0.13 -0.13 +0.23	0.94 ± 0.13	10.68 ± 2.28
Fe	5.32 ± 0.17	7.40 ± 0.87	13.00 ± 8.03
Ga	0.22 ± 0.04	0.35 ± 0.10	3.12 ± 0.67
In	9.25 ± 1.36	12.67 ± 1.69	37.03 ± 3.80
Mo	9.59 ± 3.28	43.09 ± 7.42	58.63 ± 8.88
Se	n.d.	0.50 ± 0.19	32.22 ± 5.66
Sn	0.30 ± 0.04	0.41 ± 0.17	1.20 ± 0.06
Ti	0.12 ± 0.03	1.22 ± 0.56	1.85 ± 0.37
W	0.81 ± 0.22	6.62 ± 3.03	10.49 ± 2.58
Zn	12.32 ± 2.53	11.84 ± 2.24	9.63 ± 0.41

n.d.: not detected

Table A2: % Leaching efficiencies of Mo and W when leaching with a NaOH of pH=11 at 50 °C and with or without addition of 0.25 M sodium tartrate.

Time (h)	Only NaOH		NaOH and sodium tartrate	
	Mo	W	Mo	W
1	8.30	0.48	26.20	1.26
2	21.33	1.34	43.99	7.70
4	47.65	4.18	68.32	42.03
6	70.86	15.56	87.30	75.69
8	81.34	34.69	95.63	98.98
16	88.14	54.63	90.52	93.84
18	88.18	66.86	89.44	92.63
20	88.59	75.31	88.96	92.19
22	88.54	80.76	88.55	91.48
24	87.65	83.58	88.27	91.07

[A1] S. Bisgaard, H. T. Fuller and E. Barrios, Quality Quandaries: Two-Level Factorials Run as Split-Plot Experiments, *Quality Engineering* 8 (1996) 705–708
<https://doi.org/10.1080/08982119608904682>

[A2] A.A. Almimi, M. Kulaheci and D.C. Montgomery, Checking the Adequacy of Fit of Models from Split-Plot Designs, *Journal of Quality Technology* 41 (2009) 272–284,
<https://doi.org/10.1080/00224065.2009.11917782>